INFLUENCE OF ADAPTATION ON SINGLE NEURON AND POPULATION CODING IN MOUSE PRIMARY VISUAL CORTEX

Rachael Houlton

A dissertation submitted in partial fulfilment of

the requirements for the degree of

Doctor of Philosophy

Department of Neuroscience, Physiology and Pharmacology

University College London

2013

I, Rachael Houlton, confirm that the work presented in this thesis is my own. Where information has been derived from other sources, or data has been collected by collaborators, I confirm that this has been indicated in the thesis.

Rachael Houlton, 14 July 2013

Acknowledgements

I would firstly like to thank my supervisor, Prof. Thomas Mrsic-Flogel for accepting me into his lab, supporting me during my PhD, and most importantly for his patience and encouragement throughout. I would also like to thank Dr Sonja Hofer who collected the calcium imaging data that I analysed in Chapter 3, which became the inspiration for this project. Dr. Nicholas Lesica not only hosted me in his laboratory for the extracellular recordings described in Chapter 2, but also spent a large amount of time instructing me and assisting with data pre-processing.

I am further indebted to the other members of the Mrsic-Flogel lab, who offered advice and support and have become valued friends. I would particularly like to thank Elie Sader for contributing to the patch clamp recordings and Yunyun Han for assisting with the extracellular recordings. Abdellatif Nemri and Alessandro Coatti also provided invaluable assistance with proof reading.

I would also like to thank my friends and family for all of their support.

Finally, I extremely grateful to both the Wellcome Trust and Four-Year PhD Course Committee, for having given me this fantastic opportunity.

Author contributions:

Chapter 2

All extracellular recordings were carried out by the author. Dr Nicholas Lesica provided assistance with initial spike extraction. All subsequent analysis was carried out by the author.

Chapter 3

Two-photon calcium imaging and spike extraction was performed by Dr Sonja Hofer. All subsequent analysis was performed by the author.

Chapter 4

Whole-cell recordings were performed by the author. A subset of cells (n= 8) were recorded by Eli Sader, a research assistant in the Mrsic-Flogel laboratory. All analysis was performed by the author.

ABSTRACT

In the visual system, prolonged exposure to a high contrast stimulus leads to a decrease in neuronal responsiveness, referred to as contrast adaptation. Contrast adaptation has been extensively studied in carnivores and primates, but has so far received little attention in mice. This thesis explores contrast adaptation and its mechanisms in mouse primary visual cortex (V1).

Using extracellular tetrode recordings in mouse V1, I found contrast adaptation to be orientation unspecific. While this finding differs from reports in carnivores and primates, it is consistent with the notion that responsiveness of individual neurons is influenced by the activity history of the local network. Adaptation was also found to be cell-type specific, as putative parvalbumin (PV) expressing interneurons underwent less adaptation than other cell types.

There is debate whether adaptation arises within the cortex or is inherited from the earlier stages in the visual pathway (e.g. visual thalamus or retina). In order to assess the relative contributions of cortical/subcortical mechanisms towards adaptation in mouse V1, I used optogenetic methods to suppress cortical activity (via activation of Channelrhodopsin-2 in PV interneurons) during an adapting stimulus. Suppressing cortical activity, and hence any activity-dependent cortical mechanisms, largely counteracted the effects of adaptation on neuronal responsiveness, consistent with a substantial cortical component of adaptation. Interestingly, whilst adaptation reduced both contrast and response gain, only the latter effect was influenced by cortical suppression. This suggests that the mechanisms mediating adaptation-induced alterations in contrast and response gain are different, and possibly occur at different loci within the visual pathway.

The consequences of adaptation on V1 population responses were explored with two-photon calcium imaging. Adaptation to dynamic stimuli of multiple orientations caused a divisive scaling of responses, consistent with a reduction in response gain. Adaptation also decorrelated neuronal activity, leading to sparser and more distributed stimulus representations across the population. Whole-cell recordings further revealed that these effects were associated with decreased membrane depolarisation, and an increase in membrane potential variability.

TABLE OF CONTENTS

CHAPTER 1: GENERAL INTRODUCTION

Motivation:

Why vision?

The primary visual cortex (V1) is probably the best studied cortical area. This extensive knowledge base makes it an ideal region in which to address the nature and mechanisms of cortical processing. V1 neurons have well defined response properties that can be precisely measured, yet it is still unclear how some of these properties arise and to what extent they are fixed, or stimulus/context dependent.

Why adaptation?

No stimulus is an island; sensory processing is dependent on exposure to preceding stimuli, behavioural state (Niell and Stryker, 2010; Ayaz et al., 2013), reward association (Stanisor et al., 2013) and multisensory integration (Wang et al., 2008). Visual adaptation, as discussed in this thesis, refers to the change in neuronal response to a visual stimulus, which results from visual experience during the preceding tens of milliseconds to minutes. This is a dynamic process, by which the visual system adjusts to the properties of the current visual environment. The short-term and reversible nature of adaptation makes it possible to relate physiology and perception, and adaptation has also been used as an experimental tool to selectively suppress specific neuronal populations (Winston, 2004; Priebe et al., 2010). However, while several mechanisms of adaptation have been reported, their relative contributions to the response adaptation observed in V1 neurons remains uncertain.

Why mouse?

The key advantage of the mouse as an experimental model is the availability of genetic tools, which make it possible to label, monitor and manipulate specific cell types and circuits (O'Connor et al., 2009). Such approaches offer unprecedented opportunities to explore neuronal circuitry and function, and hence the mouse is quickly becoming the preferred model in sensory processing. With a wealth of data about the organisation and function of the mouse visual cortex, it is becoming apparent that despite a limited spatial acuity, many properties of mouse V1 neurons resemble those observed in V1 of higher mammals (reviewed by Huberman and Niell, 2011). However, the circuit mechanisms of visual adaptation in the mouse remain relatively unexplored (Stroud et al., 2012; Jeyabalaratnam et al., 2013).

Visual processing in the mammalian geniculostriate pathway:

Retina

Light enters the eye and is transduced into neural signals by photoreceptors. Photoreceptor responses are processed within the retinal circuitry, giving rise to the receptive field properties of retinal ganglion cells that form the output of the retina. Within visual neuroscience, a neuron's receptive field refers to the region of visual space that can elicit responses when stimulated. In primates and carnivores the majority of retinal ganglion cells (RGCs) exhibit antagonistic centre-surround receptive fields (reviewed by Meister and Berry, 1999; see Figure 1.1).

The main subclasses of RGCs in primates are described as 'midget' or 'parasol' cells, based on their dendritic morphology. Midget cells are small, receiving input from only a limited number of photoreceptors and provide chromatic information. They respond with a slow conduction velocity but have greater spatial resolution than parasol cells. Midget cells project to the parvocellular regions of the lateral geniculate nucleus of the thalamus, and are considered to form part of the 'What' visual stream (Wässle, 2004). Parasol cells have larger dendritic trees (and hence receptive fields), receive inputs from many photoreceptors, and are not sensitive to colour. They give rapid, transient responses and show greater sensitivity to low contrast stimuli than midget cells. Parasol cells project to the magnocellular regions of the lateral geniculate nucleus and are considered to form part of the 'Where' visual stream. In carnivores, morphological homologues of midget and parasol cells are called beta and alpha cells respectively, and are also referred to by their physiological classifications as 'X' and 'Y' cells (Shapley and Hugh Perry, 1986). However, in addition to these well characterised subtypes, a diversity of other RGC subtypes have been identified in both primates (Field and Chichilnisky, 2007) and other species (Rockhill et al., 2002). In rabbits and rodents, some RGCs exhibit selectivity for the direction of stimulus movement (Barlow and Hill, 1963; Jeon et al., 1998, see below).

The mouse retina differs from that of primates in several ways. The mouse possesses mainly rod photoreceptors, which are suited for scotopic (low light) conditions (Jeon et al., 1998). Mouse cone photoreceptors express one, or a combination of two, photopigments that are sensitive to short (ultraviolet) or medium (green) wavelengths of light (Calderone and Jacobs, 1995). Therefore, like cats, mice are dichromats and cannot differentiate red and green. As mice lack a fovea,

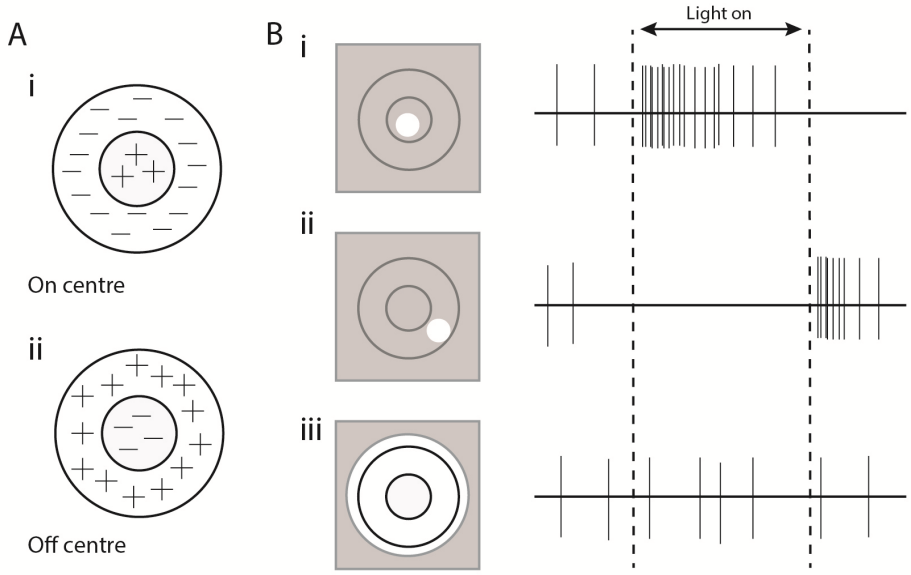

Figure 1.1. Schematic of antagonistic centre-surround organisation of RGC receptive fields.
A.) Receptive field structure of an On (i) and Off (ii) centre-surround receptive field. B.) Responses of a On-centre RGC to light stimuli (shading indicates darkness). i) A light stimulus in the centre of the receptive field causes excitation. ii). A light stimulus in the surround region of receptive field suppresses activity, while its removal triggers an offset response. iii) Diffuse lighting covering the entire receptive field is relatively ineffective in eliciting a response, due to the antagonistic effects of the centre and surround regions. Adapted from Frisby and Stone, 2010.

the entire retina is similar to the peripheral retina of the primate. Whilst the density of photoreceptors per unit area is greater in mice than some primates, due to the considerable difference in retinal size, this still corresponds to far fewer receptors per degree of visual space, and hence lower visual acuity.

As in other species, mouse retinal ganglion cells appear to span a variety of subtypes (Völgyi et al., 2009). While RGCs have been observed with physiological response properties similar to the X and Y (midget and parasol) subtypes reported in other species, up to 50% of mouse RGCs appear to exhibit direction selectivity (Huberman et al., 2009). The role of these direction-selective RGCs (DSRGCs) in higher visual processing is not clear.

Lateral geniculate nucleus

The lateral genticulate nucleus (LGN) of the thalamus receives direct input from RGCs (Figure 1.2). The LGN is classically considered as a relay station between the retina and visual cortex, with magnocellular and parvocellular LGN neurons exhibiting similar On-Off receptive fields to their RGC inputs (Kaplan and Shapley,

Figure 1.2. Schematic of mouse visual pathways.
Solid lines indicate direct retinal projections to the superior colliculus (SC) and dorsal lateral geniculate nucleus (dLGN) in the thalamus. Dashed lines indicate thalamocortical projections. Grey shading in retina/LGN indicates the location of ipsilaterally projecting RGCs and their projection site. Binocular and monocular regions of V1 are indicated by 'B' and 'M" respectively. Reproduced from Huberman and Niell, 2011.

1982). However, the LGN also receives substantial feedback projections from the cortex (Guillery and Sherman, 2002), which may shape its responses.

While in primates and carnivores the LGN is segregated by parvo/magnocellular cell types and divided into bands of inputs from the ipsilateral and contralateral retina, there are no clear layers in mouse LGN. Despite these structural differences, the majority of mouse LGN neurons exhibit centre-surround receptive fields, and sustained or transient responses, resembling those of parvocellular/magnocellular (or X/Y) neurons observed in other species (Grubb and Thompson, 2003; Piscopo et al., 2013). Mouse LGN neurons have large receptive fields (approximately 11° diameter) and correspondingly poor spatial selectivity (approximately 0.2 cycles/degree- Grubb and Thompson, 2003). In addition to these centre-surround units, a small subpopulation of mouse LGN neurons also appear to show direction (and orientation) selectivity, likely inherited from DSRGCs (Piscopo et al., 2013).

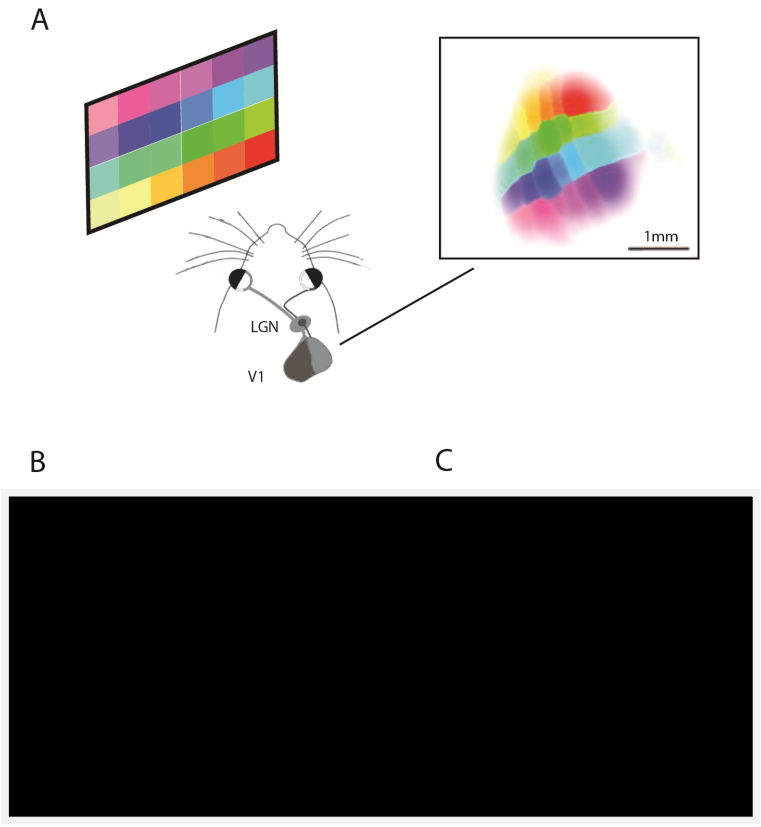

Figure 1.3. V1 functional architecture.
A.) Intrinsic imaging of retinotopic organisation of mouse V1. The color of each pixel indicates the location of the stimulus in monocular visual space which elicited the strongest response on the cortical surface. B.) Two-photon calcium imaging in cat V1 showing iso-orientation domains. Reproduced from Ohki et al., 2006. Colour coding of each cell represents its preferred stimulus orientation. C.) Calcium imaging in rat V1 reveals lack of iso-orienation domains in rodents. Reproduced from Ohki et al., 2005. Scale bars indicate 100 µm.

Primary visual cortex

The primary visual cortex (V1) receives direct thalamic input from the LGN. The primary thalamorecipient layer is layer 4 (which in turn provides inputs to layers 2/3), although the mouse LGN also projects directly to layers 3, 5 and 6. Rodent V1 exhibits similar cross-layer circuitry and contains similar inhibitory/excitatory cell types to those seen in carnivores and primates (Burkhalter, 1989; Olivas et al., 2012).

In V1, the receptive fields of individual neurons, which are elongated relative to those in the LGN (see below), form a continuous representation of contralateral visual space. (Figure 1.3A) In carnivores and primates, neurons with similar orientation preferences are spatially grouped into iso-orientation domains. However, in mouse, neurons of different orientation preference are intermingled in a ‘salt and

pepper' fashion (Ohki et al., 2005; Figure 1.3B&C). This lack of orientation columns is common to all rodents, including the highly visual grey squirrel (Van Hooser et al., 2005), suggesting that this large scale cortical organisation is not a prerequisite for either selective receptive fields or visual performance. Species differences are similarly observed in the binocular region of V1 (which in mice occupies the lateral portion of V1). Primates and cats exhibit 'ocular dominance columns', in which neurons driven by the contra and ipsilateral eye are spatially grouped (Hubel and Wiesel, 1969). Ocular dominance columns are, however, absent in mouse V1, where neurons with differing degrees of input from each eye are interspersed (Mrsic-Flogel et al., 2007).

Despite these differences in large-scale organisation, the receptive fields of individual neurons in mouse V1 are remarkably similar (although larger) to those seen in higher mammals (Niell and Stryker, 2008). This suggests that mouse V1 carries out similar computations to that in other species, albeit at lower spatial resolution (Van Hooser et al., 2005; Huberman and Niell, 2011).

Having reviewed the similarities (and differences) between V1 of mice and higher mammals, I will now briefly introduce some of the basic response properties of V1 neurons which are of relevance to contrast adaptation

V1 response properties

Orientation tuning of simple and complex cells.

V1 receptive fields are elongated relative to those in the LGN, giving rise to orientation selectivity (Hubel and Wiesel, 1962). Similar to the centre-surround receptive fields of RGCs and LGN neurons, V1 'simple' cells have antagonistic 'On' and 'Off' subfields. A neuron is depolarised by light stimuli in its On subfield(s) and dark stimuli in its Off subfield(s), responding most strongly to those visual features that match its receptive field structure. This receptive field structure explains a neuron's orientation selectivity: neurons respond with the highest firing rates to bar stimuli whose orientation is aligned with its receptive field, and exhibit a modulated response to drifting or contrast-reversing gratings (Figure 1.4A). The receptive fields of V1 'complex' cells are similarly elongated but have overlapping On and Off subfields. This means that, while still orientation selective, complex cells are depolarised by both light or dark oriented stimuli, and in contrast to the modulated response of simple cells, produce a sustained (non-modulated) response during

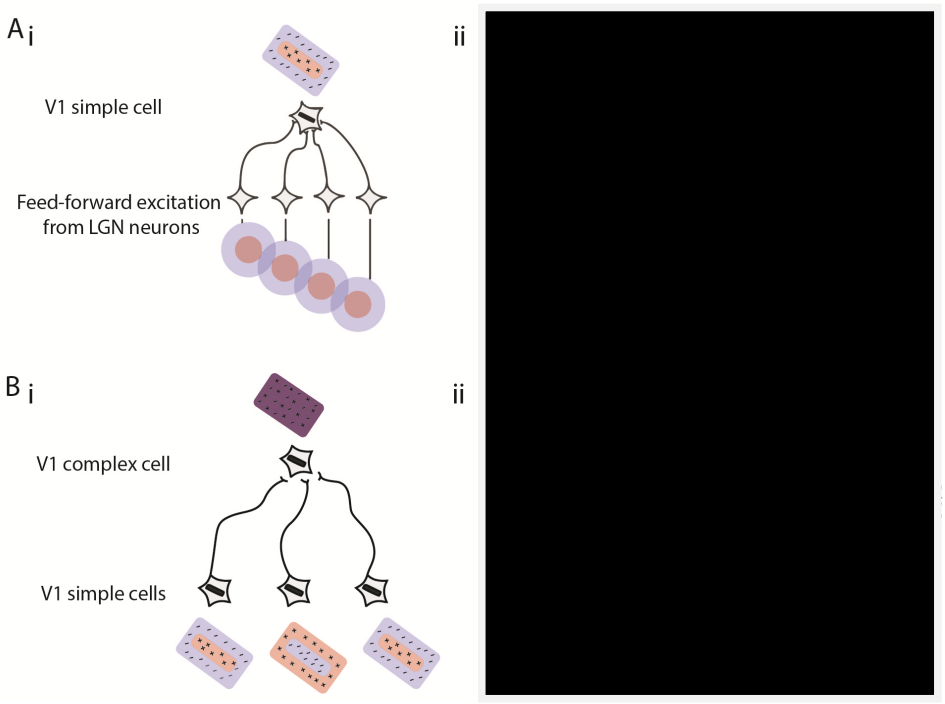

Figure 1.4. V1 simple and complex cells.
A.) i) The feedforward model proposed by Hubel and Wiesel (Hubel and Wiesel, 1962) suggests that the On-Off receptive field of a simple cell is conferred by the spatial alignment of the receptive fields of presynaptic LGN neurons. ii.) The spiking and subthreshold responses of a simple cell in cat V1 during a drifting grating of its preferred orientation. The receptive field organisation produces a stimulus phase preference. The neuron is maximally excited by the simultaneous presentation of light bars in its On region and dark bars in its Off region, and shows minimal activity when the phase is reversed. This produces highly modulated responses as the grating moves through the receptive field. Modulation depth is measured by the F1/F0 ratio, where F1 is the amplitude of the response (firing rate or membrane potential) at the stimulus temporal frequency, and F0 is the mean response throughout the stimulus cycle, as measured by the Fourier transformation (Skottun et al., 1991). B.) i) Feedforward model suggests that the overlapping On and Off subfields of a complex cell receptive field is produced by a convergence of inputs from multiple simple cells with different On-Off configurations. ii.) Due to the overlap of On and Off domains complex cells exhibit less preference for stimulus phase and the response to drifting grating stimuli is less modulated than that of simple cells. Aii and Bii are reproduced from Priebe et al., 2004.

drifting/contrast-reversing gratings (Figure 1.4B). Hence neurons can be classified as simple or complex according to the depth of modulation of their responses during drifting grating stimuli (Skottun et al., 1991; Priebe et al., 2004).

As the centre-surround receptive fields of LGN neurons are not orientation selective, this feature is thought to arise de novo in V1. (While a small fraction of mouse LGN neurons exhibit orientation/direction selectivity, it is not clear if they project to V1 and how they contribute the responses of neurons therein; Piscopo et al., 2013). According to the feedforward model originally suggested by Hubel and Wiesel, simple cells inherit their receptive field properties from spatially aligned

inputs of centre-surround LGN neurons (Figure 1.4Ai). The receptive fields of complex cells are in turn postulated to arise from the convergent intracortical inputs of multiple simple cells (Figure 1.4Bi). However, whether there is a clear distinction between simple and complex cells remains debated in all species (Carandini and Ferster, 2000; Priebe et al., 2004)

Contrast saturation

Contrast describes the maximum difference in luminance within a region of visual space and is therefore considered a measure of stimulus 'intensity'. The firing rate and subthreshold responses of V1 neurons increase with stimulus contrast in a sigmoidal fashion, exhibiting saturation at high contrasts (Figure 1.5A). Contrast response functions can be parameterised by the midpoint of the contrast response function ('C50'- the contrast at which responses are half maximal), and the response range ('Rmax').

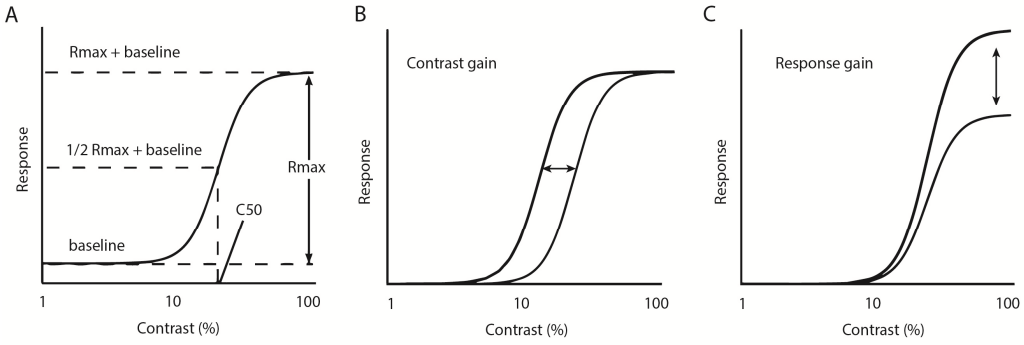

Figure 1.5. The contrast response function
A.) The firing rate of V1 neurons increases with stimulus contrast in a sigmoidal function, saturating at high contrasts. The shape of this function can be described by the half maximal contrast (C50) and response range (Rmax). B.) A horizontal shift along the X axis (reflected by a change in C50) is referred to as a change in 'contrast gain'. C.) A vertical expansion/compression of the function (reflected by a change in Rmax) is referred to as a change in 'response gain'. Adapted from Soma et al., 2013.

The contrast response function can be used to differentiate between alterations in either the inputs that a neuron receives or the integration that produces its output. If there is a constant reduction in input drive, this will result in a rightward shift in the contrast response function, as the neuron will require a greater stimulus intensity (contrast) in order to achieve the same level of output (output can refer to either firing rate or membrane depolarisation). This will cause an increase in the C50 value, and is described as a decrease in contrast or input gain (Figure 1.5B). If, however, the inputs remain unchanged, but there is a proportional decrease in responsiveness, such that output is scaled by a constant factor, this will result in a

vertical compression of the contrast response function and a corresponding decrease in Rmax (Figure 1.5C). This is referred to as a decrease in response gain.

Contrast invariance of tuning

As discussed above, the firing rates of V1 neurons vary with stimulus contrast. This is also seen in the responses of LGN neurons (Cheng et al., 1995). The feedforward model predicts that, for simple cells, a neuron's membrane potential should reflect a linear combination of the thalamic inputs it receives and hence should scale with contrast (Figure 1.6A). When assuming a threshold-linear relationship between membrane potential and spike rate (Figure 1.6B), a contrast dependent scaling of membrane potential should cause the width of the spike rate tuning curve to increase with contrast (Figure 1.6C). However this is not observed experimentally. Instead, spiking responses are proportionally scaled with stimulus contrast, preserving a relatively constant tuning width.

A key mechanism for this contrast invariance of tuning appears to be subthreshold trial-to-trial variability, which decreases with increasing contrast. Although the mean membrane potential is comparatively lower during a low contrast preferred stimulus than during a high contrast non-preferred stimulus, high trial-to-trial variability during the low contrast condition increases the probability of crossing spike threshold (Figure 1.6D-F). This effect can be seen when comparing mean membrane potential versus firing rate: the threshold-linear relationship is smoothed into a power law by the trial-to-trial variability (Figure 1.6H). Increasing variability increases the steepness of this relationship, and hence responsiveness to weak (low contrast) stimuli is increased (Anderson et al., 2000; Finn et al., 2007). The combination of contrast dependent scaling of membrane potential responses (Figure 1.6G) and a contrast dependent relationship between membrane potential and spike rate (Figure 1.6H) is able to account for the observed contrast invariance of the spike rate tuning width (Figure 1.6I). Although the origin of increased variability during low-contrast stimuli is not completely understood, one study has suggested it may arise subcortically, and is related to the correlated activity of LGN neurons (Sadagopan and Ferster, 2012).

Figure 1.6. Contrast invariance of tuning
A-C.) Decreasing contrast leads to a divisive scaling of subthreshold responses (A) which, if assuming a threshold-linear relationship between membrane potential and spike rate (B), would result in a decrease in tuning width at low frequencies (C). However this is not observed experimentally. Instead, tuning width is found to be constant across contrasts. D-F.) Although the average membrane potential across trials is equal or lower during the low contrast preferred stimulus than the high contrast null (non-preferred) stimulus, higher trial-to-trial variability at low contrasts increases the probability of threshold crossing, leading to a higher average firing rate. G-I.) Subthreshold variability converts the theshold-linear relationship between membrane potential and firing rate into a power-law (Anderson et al., 2000). Increasing membrane potential variability at low contrasts increases the steepness of this relationship (H). The scaled membrane potential combined with contrast dependent variability accurately predicts the observed contrast invariance of firing rate responses (I). Reproduced from Priebe and Ferster, 2012.

Contrast adaptation

Contrast adaptation was first described with human psychophysics. Prolonged exposure to a high contrast adapting stimulus is accompanied by a gradual decline in the perceived contrast of both the adapting stimulus itself and subsequent test stimuli (Blakemore and Campbell, 1969; Blakemore et al., 1973). These perceptual effects were found to be limited to test stimuli of the same orientation and spatial/temporal properties as the adapting stimulus. Furthermore, the effects could be transferred between the eyes; when the adapting stimulus was presented to one eye, the perceived contrast of test stimuli subsequently presented to the other eye was also reduced. As orientation tuning first arises in V1 (at least in primates), and

this is also the first site of binocular integration, these findings suggested that contrast adaptation to patterned stimuli originates within the cortex, either in V1 or higher visual areas.

Adaptation in V1 neurons

Neuronal correlates of contrast adaptation can be observed in V1, where neuronal responsiveness declines during/after the presentation of a high contrast stimulus (Maffei et al., 1973; Vautin and Berkley, 1977; Albrecht et al., 1984; Figure 1.7A). As described above, the responses of V1 neurons increase with stimulus contrast in a sigmoidal function known as the contrast response function. Following a high contrast adapting stimulus, this function is usually both compressed and shifted to the right (Albrecht et al., 1984; Figure 1.7B), indicating a decrease in both response and contrast gain. Although both effects are evident in V1 responses, changes in contrast gain appear to dominate (Ohzawa et al., 1982; 1985; Sclar et al., 1989; Bonds, 1991; Carandini and Ferster, 1997).

Although the strength of adaptation tends to be greater following adapting stimuli of longer duration (Dragoi et al., 2000), adaptation has also been observed after adapting brief stimuli of several tens to hundreds of milliseconds (Bonds, 1991; Muller et al., 1999; Dragoi et al., 2002). Adaptation is strongest following adapting stimuli that drive the neuron most effectively (Movshon and Lennie, 1979; Albrecht et al., 1984; Crowder, 2005), suggesting the involvement of activity-dependent mechanisms. At a subthreshold level, contrast adaptation is associated with a hyperpolarisation of the membrane potential (Carandini and Ferster, 1997; Sanchez-Vives et al., 2000a; Figure 1.7Aii), the magnitude of which also varies with adapter contrast.

As observed in human psychophysics, in cat and primate V1 contrast adaptation is orientation specific— responsiveness is most reduced for test stimuli of the same orientation and spatial/temporal frequency as the adapting stimulus (Movshon and Lennie, 1979; Albrecht et al., 1984; Hammond et al., 1989). In some cases adaptation has also been reported to alter a neuron's stimulus preferences, causing a shift in its tuning curve (Saul and Cynader, 1989; Muller et al., 1999; Dragoi et al., 2000; Ibbotson, 2005), although these effects become more apparent after longer duration adapting stimuli (Dragoi et al., 2002).

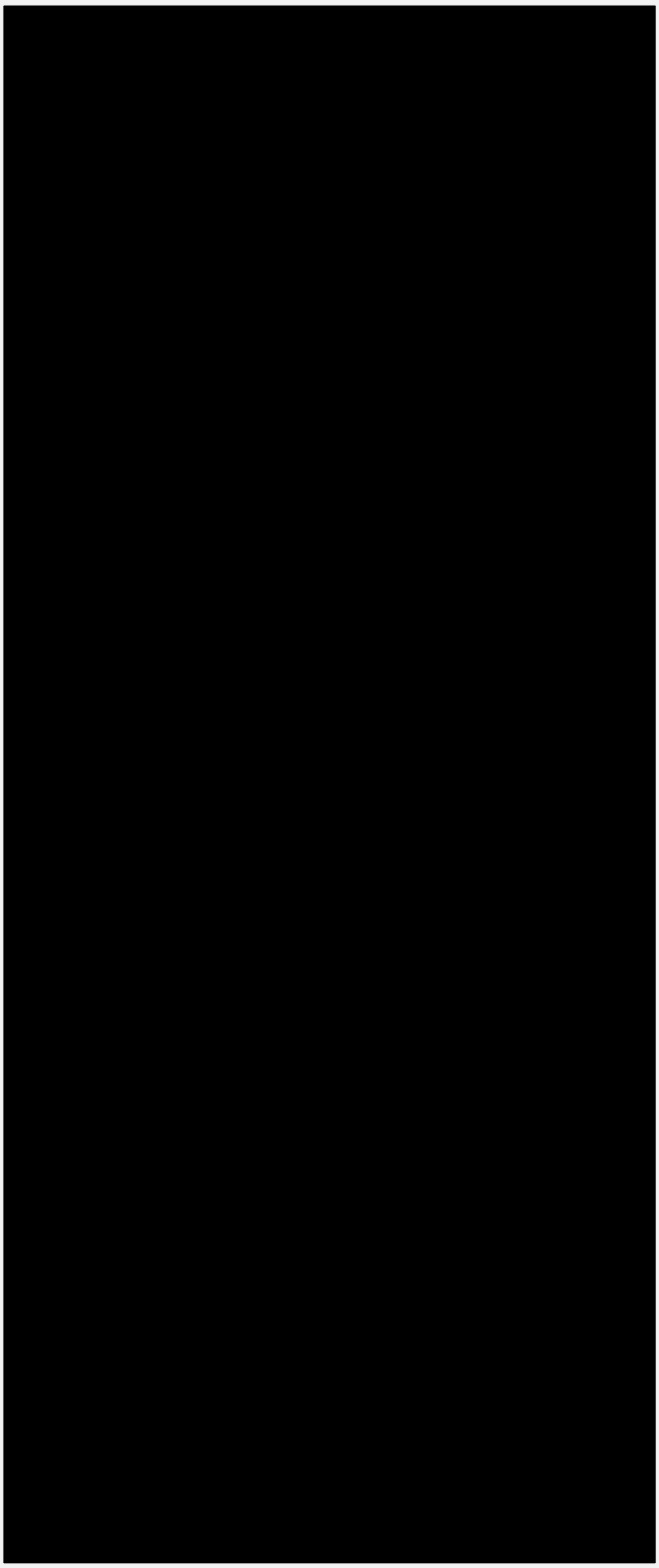

Figure 1.7. V1 Adaptation
A.) Spiking, mean membrane potential (F0) and membrane modulation amplitude (F1) of a cat V1 neuron before, during and after prolonged exposure (60 seconds) to a high contrast grating stimulus. Ai) The high contrast grating is associated with a decline in firing rate, followed by a period of reduced activity during the subsequent low contrast stimulus. Aii) Membrane potential hyperpolarises during the high contrast stimulus, giving rise to a prominent after hyperpolarisation that gradually recovers during the subsequent low contrast stimulus. Aiii) The amplitude of membrane modulations decrease during the high contrast stimulus, but to a lesser extent than the mean membrane potential. B.) The contrast response functions of two V1 neurons (for stimuli of the preferred orientation/direction and spatial/temporal frequency), before/after adaptation to high contrast stimuli of differing orientations. Bi) A neuron which showed equal adaptation following adapting stimuli of different orientations. Bii) A neuron for which adaptation was orientation specific, being greatest following adaptation to the preferred stimulus. Both neurons exhibited a high degree of orientation tuning in their unadapted responses (not shown). C.) Effects of adaptation on the contrast response functions of magnocellular (Ci) and parvocellular (Cii) neurons in primate LGN (open and closed circles indicate non-adapted and adaptated conditions respectively.) Adapting stimulus temporal frequency= 5.5 Hz. D.) Average contrast response function of 12 cat V1 neurons before (closed circles) and during hyperpolarisation (open circles) by intracellular injection of current. A and D reproduced from Sanchez-Vives et al., 2000a; B reproduced from Crowder, 2005; C reproduced from Camp et al., 2009.

However, although numerous studies have explored potential mechanisms of visual adaptation within V1, evidence of contrast adaptation in the LGN and retina suggests that some degree of the adaptation observed in V1 is also be inherited from the early visual system (see below).

Subcortical adaptation

Contrast adaptation can be observed in magnocellular (M) cells of the primate LGN (Solomon et al., 2004; Camp et al., 2009; Figure 1.7C), where it is predominately expressed as a rightward shift in the contrast response function (reflecting a change in contrast gain). A similar increase in C50 is also visible in the LGN 'S potentials' which reflect the driving inputs from RGCs (Bishop et al., 1962; Kaplan and Shapley, 1984), suggesting these effects may in turn be inherited from the retina. Indeed, high contrast stimulation within the receptive field centre of mammalian Y-type RGCs leads to both a fast reduction in response gain and slow membrane hyperpolarisation (Zaghloul et al., 2005; Manookin and Demb, 2006; Solomon et al., 2006). Interestingly, Y-type RGCs and magnocellular LGN neurons are also both subject to 'centre-surround' suppression; responses to stimuli in the receptive field centre are suppressed by the simultaneous presentation of stimuli in the receptive field periphery, which are themselves incapable of evoking a response. As with contrast adaptation, centre-surround suppression is also generally considered to be cortically mediated (Ozeki et al., 2009), however the evidence of these effects within the LGN suggests that precortical mechanisms are also likely to contribute (Camp et al., 2009).

While adaptation is evident in LGN neurons, the responses of these cells are reduced to a lesser extent than that typically seen in V1 (Shou et al., 1996; Sanchez-Vives et al., 2000a), suggesting additional adaptation must occur either intracortically or at the thalamocortical synapse.

Mechanisms of adaptation

There are two potential sources of adaptation; either responsiveness is calibrated independently by each neuron, based on its own activity history (Ullman and Schechtman, 1982), or alternatively a neuron 's gain may be determined from the pooled responses of a number of neurons (Bonds, 1991). Note that these two sources of adaptation are not mutually exclusive, but are rather thought to act in concert, each contributing to varying degrees. I will initially discuss the first option.

Intrinsic adaptation of the recorded neuron

Intrinsic adaptation has been demonstrated via direct current injection in V1 neurons (Sanchez-Vives et al., 2000a). Neurons driven by current injection undergo membrane hyperpolarisation with a similar time constant to that seen during visual adaptation, and are subsequently less responsive to visual stimuli. Conversely, adaptation to high contrast visual stimuli reduces a neuron's responsiveness to subsequent current injection. These results suggest that the reduced responsivness induced by visual adaptation and current injection are mediated by a common mechanism. As the rest of the network is presumed to be unaffected by the intrcellular current injection, the observed hyperpolarisation must be intrinsic to the recorded neuron, and is thought to result from an increase in membrane conductance, mediated by sodium and calcium activated potassium currents (Sanchez-Vives et al., 2000a; 2000b). These findings are consistent with the deleterious fatigue hypothesis, whereby a neuron's responsiveness is inversely related to its preceding activity levels (Vautin and Berkeley, 1977; Swift and Smith, 1982; Georgeson and Harris, 1984).

However, the response reduction elicited by current injection was markedly less than that induced by visual adaptation (the relative firing rate was 87.1 ± 13.8% of control levels following current injection, vs. 41.6 ± 24.01% following visual adaptation; Sanchez-Vives et al., 2000a). Furthermore, adaptation still occurs when spiking activity has been prevented (Vidyasagar, 1990) Sanchez-Vives et al., 2000a), and can also be observed, albeit to a lesser extent, following adapting stimuli which themselves do not elicit a spiking response (Crowder, 2005). This suggests that the effects of adaptation extend beyond the intrinsic adaptation of the recorded neuron. However, a neuron does not function in isolation and the magnitude of its responses will naturally be dependent upon the inputs it receives.

Intrinsic adaptation of presynaptic partners

As discussed above, the hyperpolarisation evoked by current injection was smaller than that associated with visual adaptation, however this discrepancy can potentially be explained by the reduced excitatory drive from other neurons in the network. During visual stimulation all active neurons will adapt and therefore the synaptic inputs each neuron receives will also be reduced. Such network interactions can also account for adaptation to stimuli that fail to evoke a response in the recorded cell (Bonds, 1991; Crowder, 2005). Any presynaptic neuron that is

driven and hence adapted by the stimulus (and whose stimulus selectivity may differ from that of the recorded cell) will provide reduced drive to the postsynaptic neuron, regardless of any change in the intrinsic properties of the postsynaptic neuron. A neuron's sensitivity to a given adapter should therefore also depend on the stimulus selectivity of its presynaptic partners.

Synaptic depression

Additionally, the synaptic inputs a neuron receives may be subject to short term synaptic depression. Theoretical studies have shown that synaptic depression can account for several aspects of cortical adaptation (Chance et al., 1998; Freeman et al., 2002), and significant thalamocortical synaptic depression has been found to occur in the barrel cortex (Chung et al., 2002). However, when Boudreau et al. (Boudreau and Ferster, 2005) recorded post synaptic potentials (PSPs) in V1 whilst electrically stimulating the LGN, they observed only a minimal decrease in PSP amplitude even during high frequency stimuli trains. They concluded that high spontaneous firing rates within the LGN cause thalamocortical synaptic depression to be near saturation even in the absence of an adapting stimulus, leaving little room for further change. Thalamocortical depression therefore seems unlikely to be a predominant mechanism of contrast adaptation during drifting gratings of low temporal frequency. Similarly, it is not clear what degree of intracortical synaptic depression is likely to occur during the levels of spontaneous activity observed in vivo (Reig et al., 2006). As for intrinsic adaptation of presynaptic neurons, any adaptation caused by synaptic depression should follow the selectivity of these presynaptic cells.

So far I have discussed the combined effects of independent adaptation of individual neurons, however, as mentioned above, it is also possible that adaptation is mediated via dynamic interactions between pools of neurons.

Divisive normalisation and gain control

In divisive normalisation models, a neuron's squared response is divided by the sum of squared responses of all neurons within the 'normalisation pool' (Bonds, 1991; Heeger, 1992; Carandini and Heeger, 2011). Theoretical studies suggest that enhanced inhibition between simultaneously active neurons would improve coding efficiency by reducing redundancy (Barlow and Foldiak, 1989). When multiple stimuli are presented simultaneously, normalisation models have been shown to

reproduce several V1 response properties, including contrast saturation, contrast invariant orientation tuning, cross-orientation suppression and surround suppression (Carandini and Heeger, 2011).

During adaptation, neurons are subject to gain control (as discussed above). Gain control, is hypothesized to be equivalent to normalisation, albeit over a longer time course (Bonds, 1991; Heeger, 1992). This would imply that a neuron's responsiveness is dependent, not just on its own activity history and that of its presynaptic partners, but also upon the activity of the other neurons in the normalisation pool. As a result, the selectivity of adaptation that the neuron experiences will be determined by the composite stimulus selectivity of this neuronal pool. If the normalisation pool consists of a neuron's immediate neighbours, the stimulus selectivity of adaptation a neuron experiences will vary depending on the composition of the local network. In species that possess orientation columns, the range of orientation preferences observed within the local network varies dramatically between pinwheel centres and iso-orientation domains. Sengpiel and Bonhoeffer therefore predicted that adaptation should show greater orientation specificity in neurons within iso-orientation domains (where the surrounding normalisation pool is also biased toward a given orientation), than in those neurons at pinwheel centres (Sengpiel and Bonhoeffer, 2002). Although their data failed to reveal any significant correlation between network location and the orientation specificity of adaptation, the findings of a later study using different anaesthesia (Crowder, 2005), supported their hypothesis. Neurons in iso-orientation domains tended to undergo stronger adaptation in response to their preferred stimulus, while those at pinwheel centers underwent similar degrees of adaptation in response to preferred, null or orthogonal adapting stimuli (Figure 1.7B). This supports the notion that the orientation specificity of adaptation is dependent, not only on the activity history of the recorded neuron, but also on that of the local normalisation pool.

A key question remains as to the biophysical mechanism of normalisation. A popular candidate has been shunting inhibition, as, due to Ohm's Law (V=IR), an increase in membrane conductance will cause a divisive scaling of synaptic inputs.

Inhibition

The primary argument against a role of inhibition in visual adaptation is that several studies have shown that iontophoretic application of the $GABA_A$ antagonist bicuculline within V1, does not affect adaptation (DeBruyn and Bonds, 1986; Vidyasagar, 1990; Nelson, 1991; McLean and Palmer, 1996). However, bicuculline has substantial side effects, and is no longer recommended for studying inhibition (Debarbieux 1998). Furthermore, the elevation of excitatory activity that results from GABA blockade may be evoking compensatory mechanisms of adaptation, making these results difficult to interpret.

In area MT, inhibition appears to decrease during adaptation, suggesting that inhibitory neurons, like principal cells, undergo contrast adaptation (Kohn and Movshon, 2003). However, the relative decrease in excitation and inhibition was not established. In rat somatosensory cortex, inhibitory conductances appear to undergo greater adaptation than excitation (Heiss et al., 2008). Although it is not clear whether the same is true in the visual cortex, theoretical models suggest a reduction in the relative inhibitory-excitatory drive could underlie observed effects of adaptation on neuronal tuning curves (Teich and Qian, 2003).

Normalisation without inhibition

Alternatively, rather than increasing intracortical inhibition, gain control could also be achieved by a reduction of excitation. The V1 circuitry has been suggested to amplify responses inherited from the LGN through a combination of recurrent excitatory connectivity and balanced inhibition (Murphy and Miller, 2009). Normalisation could therefore also result from a reduction in this tonic amplification.

In summary, the adaptation observed in V1 neurons can arise from a number of sources. Moreover, at least in primates, some adaptation will additionally be inherited from the retina and/or LGN. The degree to which these different mechanisms contribute to adaptation in V1 has not yet been fully resolved, especially as these mechanisms may differentially contribute to contrast and response gain during adaptation.

Consequences of adaptation

As described above, adaptation to high contrast stimuli is associated with a rightward shift in the contrast response function, reflecting a decrease in contrast

gain. This serves to adjust the neuron's dynamic range and maximise its sensitivity to the prevailing contrast levels. However, despite these proposed benefits for individual neurons, the perceptual consequences are less clear; there have been mixed results regarding improvements in discrimination performance (for review see Clifford, 2002), and only weak evidence of improvements in novelty detection (Graham, 2001).

The dissociation between perceptual performance and the sensitivities of individual neurons may result from associated changes in population coding. Changes in trial-to-trial variability and correlations between neurons may have a greater influence on perception than the sensitivity of single neurons. However, relatively few studies have explored the effects of adaptation on population coding.

If adaptation does not improve performance, what benefit does it provide? An obvious advantage of adaptation is reduced energy expenditure. Action potentials are energetically expensive (Levy and Baxter, 1996; Attwell and Laughlin, 2001; Laughlin, 2001; Lennie, 2003). By reducing correlations between neurons, and hence redundancy, adaptation may enable the network to represent the same information with fewer spikes (Olshausen and Field, 2004), and hence improve metabolic efficiency. It is therefore important to investigate how adaptation influences sensory represention, not only in single neurons, but also across neural populations as a whole, in order to assess the informational and metabolic consequences of adaptation.

Contrast adaptation in mouse visual system

To our knowledge only two studies have explored contrast adaptation in the mouse visual cortex (Stroud et al., 2012; Jeyabalaratnam et al., 2013). Using long duration (1 min) and contrast-ramping adapting stimuli, Stroud et al. reported that the effects of adaptation on the contrast and response gain of mouse V1 neurons was similar to that seen in cats. Interestingly, they also found that, in the majority of neurons, the strength of adaptation was independent of the orientation of adapting stimulus. This is consistent with the findings of Crower et al. who found that adaptation was less orientation specific at pinwheel centres (as discussed above). Similarly to cat pinwheels, mouse V1 neurons are surrounded by neighbours with a mixture of orientation preferences (Ohki et al., 2005; Mrsic-Flogel et al., 2007). Therefore, the

normalisation model predicts that neurons should be similarly adapted following stimuli of a range of orientations.

In the both the studies of Stroud et al., and Crowder the orientation specificity of adaptation was assessed by varying the orientation of the adapting stimulus while keeping the test stimulus constant. However these results are therefore difficult to interpret, as by varying the adapter one is varying the activity levels during the adapting stimulus in addition to the relative configuration of adapting-test stimuli, and hence evoking different degrees of intrinsic adaptation in the recorded neuron and its presynaptic partners. In order to disambiguate the contributions of intrinsic adaptation and dynamic network interactions, an alternative strategy is to vary the test stimulus while keeping the orientation of (and hence the activity evoked by) the adapting stimulus constant. Studies using this approach have also found evidence of orientation specific adaptation in cat V1 that is independent of the recorded neuron's activity history (Hammond et al., 1989; Saul and Cynader, 1989; Dragoi et al., 2001). In their 1991 study, Dragoi et al. investigated how adaptation to adapting stimuli of different orientations influenced a neuron's tuning curve. They too found evidence of orientation specificity- when the neuron was adapted to a stimulus that fell on one flank of its orientation tuning curve, the curve was displaced away from the adapting orientation (i.e. the responses to stimuli on the same flank of the tuning curve as the adapting stimulus were depressed, while the responses to stimuli on the far flank of the orientation curve were facilitated). Interestingly, they found that the change in orientation preference was greatest in neurons at pinwheel centres, suggesting the adaptation is more orientation specific at these locations. This result is a direct contradiction of the findings of Crowder et al., and is difficult to reconcile with the normalisation hypothesis. Given these uncertainties we wished to compare the orientation specificity of short term adaptation in the mouse, by varying the orientation of both the adapting and test stimuli.

While orientation specificity of adaptation is seen as evidence for its cortical locus, a lack of orientation specific adaptation in the mouse V1, could suggest that, in this species, a significant proportion of adaptation is inherited from subcortical neurons with non-oriented centre-surround receptive fields. Since there are no studies thus far of contrast adaptation in mouse LGN, it is hard to speculate the degree to which subcortical contrast adaptation may contribute to that observed in V1. In comparison to the primate, mouse LGN neurons appear to prefer stimuli of lower

temporal frequencies (c.f. Solomon et al., 2004; Piscopo et al., 2013). Therefore if, as seen in the primate, adaptation is strongest following those stimuli that drive the neuron most effectively (Solomon et al., 2004), it would likely be most pronounced following exposure to low frequency stimuli. We therefore also sought to explore the relative contributions of cortical/subcortical adaptation in the mouse.

Aims and approaches

The primary aims of this thesis consisted of the following:

1. To characterise adaptation during short duration stimuli in mouse V1, including orientation specificity, effects on contrast/response gain and dependence on cell type (Chapter 2).

2. To compare the relative contributions of cortical/subcortical mechanisms to adaptation in mouse V1 (Chapter 2).

3. To explore the effects of adaptation on population coding in mouse V1 (Chapter 3).

4. To explore the subthreshold mechanisms of adaptation in mouse V1 (Chapter 4).

To characterise adaptation during visual stimulation in mouse V1 (including orientation specificity, the effects on contrast/response gain, and the dependence on cell type) we used multichannel extracellular tetrode recordings. These recordings provide improved single-unit sorting and isolation compared to that obtainable with single-tip extracellular electrodes (Gray et al., 1995; Harris et al., 2000), by taking advantage of the temporal coherence of spikes from closely-spaced recording sites (McNaughton et al., 1983). As a result, it is possible to simultaneously record from multiple neurons with high temporal resolution. This not only increases data yield but also allows assessment of the correlations between co-active neurons with high temporal precision.

Multichannel tetrode recordings were carried out in mice expressing the optogenetic protein Channelrhodopsin-2 (Chr2; Fenno et al., 2011) in a population of inhibitory interneurons expressing parvalbumin (PV; Markram et al., 2004). By using blue light

stimulation, which depolarises Chr2-expressing neurons, we could isolate ('tag') PV interneurons from the rest of the V1 population, allowing us to quantify adaptation in putative excitatory and PV inhibitory neurons. By optogenetically activating PV interneurons we could additionally suppress cortical activity, and hence dissociate the contribution of subcortical and cortical components of contrast adaptation. The methods and results of these experiments are described in Chapter 2.

Extracellular recordings only provide a poor estimate of neuronal location, and spike sorting algorithms typically introduce biases towards highly active neurons. To provide a more unbiased description of adaptation and its effects on population coding in a densely sampled ensemble of V1 neurons, we used two-photon calcium imaging (Stosiek et al., 2003; Mrsic-Flogel et al., 2007). The methods and results of these experiments are described in Chapter 3.

Neither extracellular recordings nor two-photon calcium imaging can provide estimates of synaptically-driven subthreshold activity in cortical neurons. To explore the subthreshold mechanisms of adaptation in mouse V1, we therefore used in vivo whole-cell patch clamp recordings (Margrie et al., 2002). The methods and results of these experiments are presented in Chapter 4.

CHAPTER 2: CHARACTERISATION OF CONTRAST ADAPTATION IN MOUSE VISUAL CORTEX

INTRODUCTION

Contrast adaptation, the decline in neuronal responsiveness during or after exposure to a high contrast visual stimulus, is well documented in V1 neurons (Movshon and Lennie, 1979; Ohzawa et al., 1982; Albrecht et al., 1984; Ohzawa et al., 1985; Kohn, 2007). However it is unclear the extent to which this effect arises within the cortex or is inherited from the earlier stages of visual processing (LGN or retina) (Baccus and Meister, 2004). While intracortical mechanisms have been suggested to explain a large proportion of the adaptation observed in V1 neurons, contrast adaptation has also been observed in the LGN of primates (Solomon et al., 2004; Camp et al., 2009) and to a lesser extent cats (Shou et al., 1996; Sanchez-Vives et al., 2000a).

The aim of this study was to explore contrast adaptation in mouse V1, where it has so far received limited attention (Stroud et al., 2012; Jeyabalaratnam et al., 2013). Additionally, taking advantage of the optogenetic tools available in this species, we aimed to assess the relative influence of cortical and subcortical mechanisms of contrast adaptation. Cortical activity was suppressed during the adapting stimulus (via the optical activation of ChR2 expressed in parvalbumin positive interneurons) in order to disrupt activity-dependent adaptation within the cortex, while leaving any subcortical mechanisms of adaptation intact.

METHODS

Animals and surgical procedures

All experimental procedures were carried out in accordance with institutional animal welfare guidelines and licensed by the UK Home Office. Transgenic mice selectively expressing ChR2 in parvalbumin positive neurons were generated by crossing PV-Cre (Jackson #008069) and flexed-ChR2 animals (Jackson #012569).

Animals were anesthetized with a mixture of Fentanyl (Sublimaze, 0.05mg/kg), Midazolam (5.0mg/kg) and Medetomidim (Domitor, 0.5mg/kg) injected IP. An

adequate depth of anaesthesia was indicated by lack of response to toe pinch. Eye cream (Isoptomax) was applied to the eyes to prevent dehydration during surgery. Atropine Sulphate (Hameln Pharmaceuticals, 20 ng/kg) and Dexamethasone Sodium Phosphate (Hospira, 0.8µg/kg) were injected SC in the neck in order to widen the pupils and prevent brain swelling respectively. Cortex buffer solution (125 mM NaCl, 5 mM KCl, 10 mM glucose, 10 mM HEPES, 2 mM $MgSO_4$, and 2 mM $CaCl_2$ [pH 7.4]), 50µl) was also injected SC to prevent systemic dehydration. Throughout the experiment body temperature was maintained at 38°C, measured with a rectal probe and controlled with a heating blanket.

Fur was trimmed and an incision was made at the rear of the head, approximately level with the ears. The skull was cleared of tissue and immobilized by affixation to a metal head plate using dental cement. The plate was then secured in a frame with the head in a horizontal position. A small craniotomy (~2mm diameter) was made above the right monocular visual cortex, determined by stereotaxic coordinates, using a high-speed foot-operated drill (Foredom). The exposed cortical surface was kept moist with cortex buffer solution (see above). The dura was removed and the cortex was covered with 2% agarose prior to electrode array insertion. After surgery the eye cream was removed except for a thin layer, keeping the eye moist whilst minimizing any visual disturbance.

Extracellular recordings

Extracellular recordings were made using a multi-tetrode array (Neuronexus, A4x2-tet-5mm-150-200-121) that was inserted into the brain with a computer controlled micromanipulator (Scientifica). The probe consisted of 4 evenly spaced shanks, spanning 600 µm of visual cortex in a medial-lateral plane. Each shank contained 8 electrode sites, split between two tetrode configurations that were separated by a vertical distance of 150 µm. A reference electrode was also inserted into the cortex, away from the recording site, via a separate craniotomy. In order to target superficial cortical layers, the array was slowly lowered until visually responsive neurons were first encountered. Visual responsiveness was assessed online from multi-unit PSTHs obtained during full-field flash stimuli. Signals were digitised at a sampling frequency of 25kHz (Tucker Davis Technologies, RZ2 Bioamp processor).

Spike sorting

The procedure for the isolation of single-unit spikes consisted of: 1) bandpass filtering each channel between 500 and 5000 Hz, 2) whitening each tetrode, 3) identifying potential spikes as snippets with energy (Choi et al., 2006) that exceeded a threshold, 4) projecting each of the snippets into the space defined by the first three principal components for each channel, 5) identifying clusters of snippets within this space using KlustaKwik, and 6) quantifying the likelihood that each cluster represented a single unit using isolation distance (Schmitzer-Torbert et al., 2005). The number of snippets in the 'noise' cluster (poorly isolated multi-unit activity) for each tetrode was always at least as large as the number of spikes in any single-unit cluster. Only clusters with an isolation distance greater than 20 were analysed. For each isolated cluster/neuron spike times were stored at a 1 ms resolution.

Visual stimuli

Visual stimuli were generated using MATLAB Psychophysics Toolbox (Brainard, 1997; Pelli, 1997). All stimuli consisted of square wave gratings with a spatial frequency of 0.04 cycles per degree of visual space, drifting at a temporal frequency of 3 cycles per second. Stimuli were presented at full contrast (unless otherwise specified) on an LCD monitor (mean luminance 82 cd/m2). Data were collected during the following 3 experimental protocols:

Protocol 1: Stimulus Selectivity (Figure 2.1A)

Stimuli consisted of 1.6 second, full contrast gratings of 4 different orientations (increasing in 45 degree increments) each drifting in two directions. Stimuli were presented in a pseudo-randomised order and interspersed with 400 ms grey screens. The full set of stimuli was repeated 20 times. No LED illumination was used during this protocol.

Protocol 2: Orientation specificity of adaptation (Figure 2.1C)

Stimuli consisted of a 3.5 second adapting stimulus ('adapter'), immediately followed by a 3.5 second testing stimulus ('tester'). The resulting 7 second blocks were interspersed with 3 second grey screens. Possible adapters included: a horizontally orientated full contrast grating drifting in a downward direction; a vertically orientated full contrast grating drifting in a rightward direction; a grey screen of mean luminance (non-adapted condition). Possible test stimuli included a

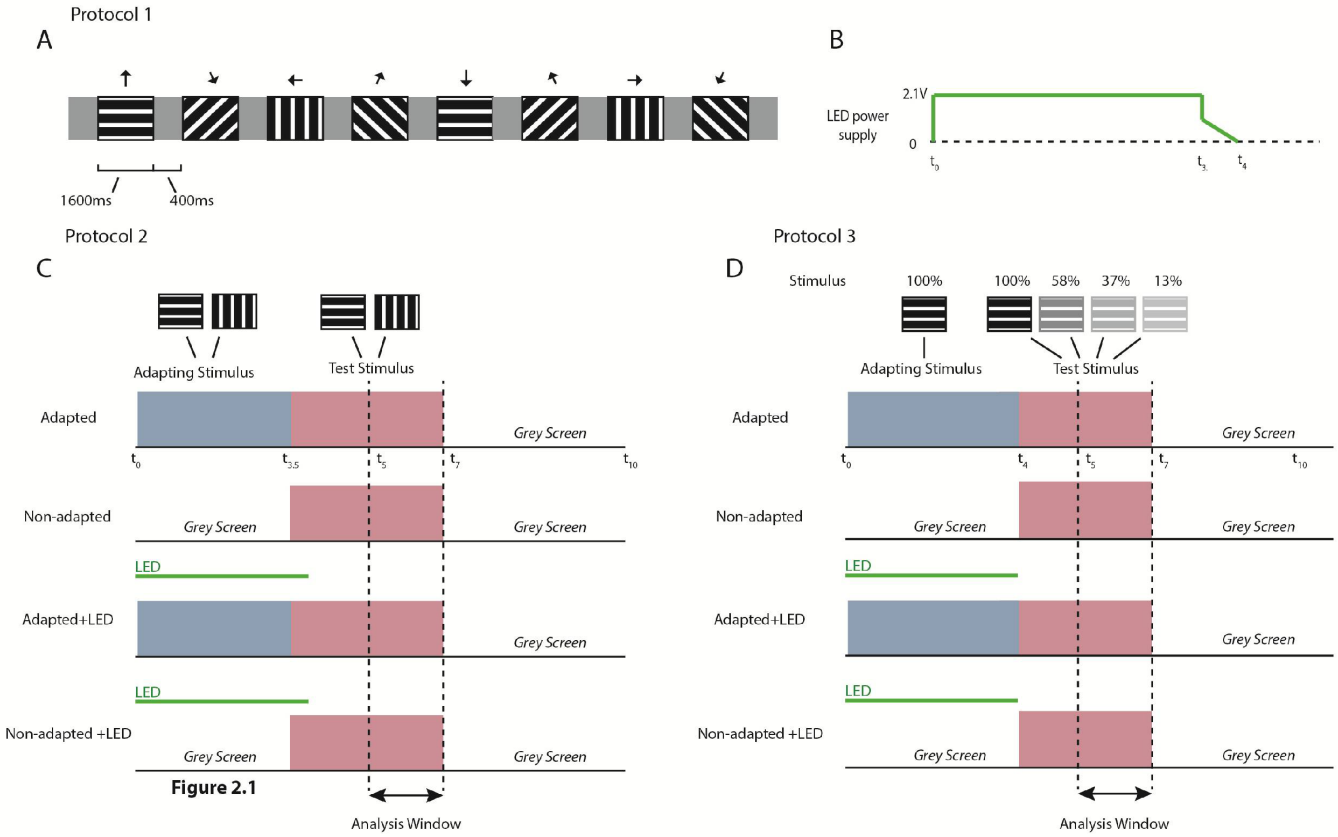

Figure 2.1 Stimulus schematics

A.) Stimulus selectivity protocol, consisting of grating stimuli (1600 ms duration) drifting in 8 directions, interspersed with grey screens (400 ms duration). The stimulus set was repeated 20 times (the same stimulus order was maintained throughout). B.) LED intensity profile. The LED was switched on at t_0 and remained constant for 3.5 seconds. At $t_{3.5}$ it was reduced to 50%, and then ramped down over the following 500ms before ceasing at t_4. C.) Stimulus Protocol 2 (orientation specificity of adaptation). Adapting stimuli of two different orientations were followed by test stimuli of the same or orthogonal orientation (see text). D.) Stimulus Protocol 3 (the effect of adaptation on contrast response functions). A 100% contrast adapting stimulus was followed test stimuli of varying contrasts (orientation was fixed throughout).

horizontally orientated full contrast grating drifting in a downward direction, and a vertically orientated full contrast grating drifting in a rightward direction.

For approximately half of the neurons (85/163) only the horizontal test stimulus was used. All other neurons were additionally recorded using vertical test stimuli, resulting in either 3 or 6 possible adapting-test stimulus combinations. Each of these combinations was additionally shown in the presence/absence of LED stimulation (resulting in a total of 6 or 12 stimulus conditions). LED illumination was provided on alternate trials, during the presentation of the adapting stimulus (see below).

Protocol 3: Contrast specificity of adaptation (Figure 2.1D)

During this protocol stimuli consisted of a 4 second adapting stimulus, immediately followed by a 3 second testing stimulus. As for Protocol 2, the resulting 7 second stimulus blocks were interspersed with 3 second grey screens. Possible adapters included a horizontally orientated full contrast grating drifting in a downward direction and a grey screen of mean luminance (non-adapted condition). Test stimuli consisted of horizontally orientated downward drifting gratings, displayed at a one of 4 possible contrasts (13, 38, 57 or 100%). This resulted in 8 stimulus combinations. As for Protocol 2, these stimulus combinations were additionally shown in the presence/absence of LED stimulation (resulting in a total of 16 stimulus conditions).

LED illumination

Illumination (470 nm) was provided by a high power LED light source (Thorlabs), and directed via a fibre optic cable (400 μm, Thorlabs) which was positioned 3-4 mm from the surface of the cortex, where it dispersed to cover an area approximately 3 mm in diameter. During Protocols 2 and 3, continuous LED illumination was provided on alternate trials, during which it began at t_0, remained constant until $t_{3.5}$, decreased in intensity over 500 ms, and ceased at t_4 (Figure 2.1B).

Data analysis

Analysis was carried out in Matlab (Mathworks) using custom code.

Analysis window

While the responses during Protocol 1 were averaged over the entire stimulus duration (1.6s), for Protocols 2 and 3 the responses were averaged over an analysis window spanning from t_5 to t_7. This window was chosen to avoid any rebound of activity following the offset of the LED.

Exclusion criteria

Neurons were excluded from analysis if they failed to consistently respond (spike) across multiple trials. The exclusion criteria used were specific to the individual stimulus protocols:

Protocol 1 (Stimulus selectivity):

Neurons were excluded if they failed to respond on at least 50% of the trials of their preferred stimulus direction (54/245 neurons).

Protocol 2 (Orientation specificity of adaptation)

Neurons were excluded if they failed to respond during the analysis window on at least 50% of the trials of their preferred test stimulus, leaving a population of 139 neurons. When comparing the orientation specificity of adaptation, analysis was further restricted to those neurons which showed a significant preference for one of the two orientations of adapting stimuli (Figures 2.6J and 2.10A-C). This was assessed by performing a Wilcoxon rank sum test on the firing rates during each adapting stimulus across all repetitions. 58/139 Pyr neurons and 11/24 PV neurons exhibited a significant preference between the two orientations of adapting stimuli and were used to compare the orientation specificity of early adaptation during the adapting stimulus (Figure 2.6J). Of these neurons, 27 Pyr neurons (and 5 PV neurons) were additionally recorded during test stimuli of both orientations, and hence were used to compare the orientation specificity of the effects of adaptation on subsequent test stimuli (Figure 2.10A-C).

Protocol 3 (Contrast specificity of adaptation)

Neurons were excluded if they failed to respond during the analysis window on at least 50% of the trials of the full contrast test stimulus (66/129 neurons).

Identification of cell types

Putative PV neurons were identified based on their responses during 4 seconds of LED illumination. For each stimulus condition the firing rate during trials with/without

LED illumination was compared by a Wilcoxon rank sum test. A neuron was deemed to be ChR2 positive, and hence PV positive if LED illumination was associated with a significant increase in firing rate during at least one of these conditions AND the mean firing rate across all conditions was greater during LED illumination than in its absence.

Stimulus selectivity indices

The neurons' preferred stimulus was defined as the orientation/direction which elicited the greatest mean firing rate. Orientation and direction selectivity indices were defined as follows:

$OSI = (R_{pref} - R_{orthog})/(R_{pref} + R_{orthog})$

$DSI = (R_{pref} - R_{null})/(R_{pref} + R_{null})$

Where R_{pref} is the response to the preferred stimulus orientation, R_{orthog} is the mean response to stimuli with an orientation ± 90 degrees from the preferred, and R_{null} is the response to stimuli moving in the opposite direction to the preferred.

F1/F0 ratios

As discussed in the introduction, the degree of response modulation a neuron exhibits during a drifting grating provides an indication of their receptive field structure and can be used as a means to classify them as simple and complex cells (Skottun et al., 1991). While simple cells sum inputs across their receptive fields in a roughly linear manner, spatial summation is nonlinear in complex cells. Modulation depth is measured by Fourier analysis of the response (either firing rate or membrane potential). 'F1' refers to the amplitude of the response at the stimulus temporal frequency (ie the component of the response that is phase locked to the grating), whilst 'F0' refers to the mean response per unit time. The ratio of F1:F0 therefore provides a measure of modulation depth, and hence response linearity. In the current study F1/F0 ratios were obtained by Fourier analysis of the average firing rate response across trials.

Reliability

Across trial reliability was quantified as the mean correlation coefficient between pairs of spike trains from all repetitions of a given stimulus. Spike count variability was quantified by the Fano factor (variance in spike count over trials/mean spike count over trials).

Adaptation indices

In order to quantify the reduction in responsiveness during adapting stimuli, each response was averaged over stimulus cycles (333ms time bins) and across repetitions, to give that neuron's mean response. The adaptation index was defined as the response 2 seconds (6 stimulus cycles) after stimulus onset, expressed as a percentage of the peak value.

Firing rate dependency of adaptation

In order to assess the relationship between the preceding activity levels and the degree of adaptation during the t5-t7 analysis window, both measures were normalised as follows:

The firing rate during the preferred adapting stimulus was normalised relative to the spontaneous firing rate during a grey screen stimulus:

$$R_{Adapter} = \frac{(R_{Preferred\ adapter} - R_{Spontaneous})}{(R_{Preferred\ adapter} + R_{Spontaneous})}$$

The degree of adaptation was quantified as the normalised difference in firing rate when the preferred test stimulus was preceded by either the preferred adapting stimulus or a grey screen (non-adapted condition).

$$R_{Tester\ adaptation} = \frac{R_{Tester\ following\ preferred\ adapter} - R_{Tester\ following\ grey\ screen}}{R_{Tester\ following\ preferred\ adapter} + R_{Tester\ following\ grey\ screen}}$$

When comparing the difference in firing rate during the two adapting stimuli ($\Delta R_{Adapter}$) to the difference in firing rate during the subsequent test stimulus (ΔR_{Tester}), the measures were similarly normalised:

$$\Delta R_{Adapter} = \frac{(R_{Preferred\ adapter} - R_{Non\text{-}preferred\ adapter})}{(R_{Preferred\ adapter} + R_{Non\text{-}preferred\ adapter})}$$

$$\Delta R_{Tester} = \frac{R_{Tester\ following\ preferred\ adapter} - R_{Tester\ following\ non\text{-}preferred\ adapter}}{R_{Tester\ following\ preferred\ adapter} + R_{Tester\ following\ non\text{-}preferred\ adapter}}$$

Contrast response functions

For each neuron, contrast response functions were fitted with the following sigmoidal function:

$$y = \frac{(Rmin + Rmax)}{(1 + e^{S(C50-x)})}$$

Where Rmin is the baseline response (spontaneous firing rate during the grey screen), Rmax is the baseline subtracted maximum (i.e. response range), C50 is the half maximal contrast and S is measure of the slope of the function.

Fitting was achieved by the least-squares method. For those neurons for which the coefficient of determination exceeded 0.7, C50, Rmax and S values were compared across conditions.

Adapter strength

'Adapter strength' (Stroud et al., 2012) was calculated as follows:

$$\text{Adapter strength} = \frac{(\text{Adapting contrast} - C50_{\text{Non-adapted}})}{(\text{Adapting contrast} + C50_{\text{Non-adapted}})}$$

As the same full contrast adapter was used in all cases, the adapting contrast was always 100%.

Normalisation of C50 and Rmax values

In order to compare the change in C50 and Rmax values to the adapter strength (Figure 2.15F-I), the normalised difference between the measures was calculated as their difference divided by their sum. For example for C50 values:

$$\text{Normalised change in C50} = \frac{(C50_{\text{Adapted}} - C50_{\text{Non-adapted}})}{(C50_{\text{Adapted}} + C50_{\text{Non-adapted}})}$$

Effect of cortical silencing on adapted response

The 'effect of cortical silencing on adapted response', and the 'degree of adaptation' correspond to the normalised differences in firing rates during the analysis window (t_5 -t_7):

$$\text{Effect of cortical silencing on adapted response} = \frac{(R_{\text{Adapt+LED}} - R_{\text{Adapt}})}{(R_{\text{Adapt+LED}} + R_{\text{Adapt}})}$$

$$\text{Degree of adaptation} = \frac{(R_{\text{Adapt}} - R_{\text{Non-adapted}})}{(R_{\text{Adapt}} + R_{\text{Non-adapted}})}$$

The degree of suppression refers to the difference in firing during the LED illumination period (t_0 -t_4):

$$\text{Degree of suppression} = \frac{(R_{Adapt+LED} - R_{Adapt})}{(R_{Adapt+LED} + R_{Adapt})}$$

Pairwise correlations between neurons

Correlations between pairs of simultaneously recorded neurons were quantified as the integral under the central ±100 ms of their spike train cross correlogram. These correlation functions were made analogous to Pearson's correlation coefficient by (i) subtracting the product of the average firing rates, and (ii) dividing by $\sqrt{(A_1 + A_2)}$, where A_1 and A_2 are the heights of each neuron's autocorrelation function before normalisation, such that correlation could take values between -1 and +1. (This was achieved using the Matlab using the 'xcorr' function in 'coeff' mode). Cross-correlograms were additionally smoothed with a 11ms running average prior to integration.

For total correlation the spike trains for each neuron were obtained by concatenation of responses during all trials of a given stimulus condition. In order to calculate signal correlation, the spike trains of the two neurons were offset by one trial, so that $trial_n$ for neuron A was aligned to $trial_{n+1}$ for neuron B. This created a 'shifted' spike train, in which any remaining correlation between the neurons is related to similarities in their stimulus-triggered response (Figure 2.2). Noise correlation was calculated by subtracting signal correlation from total correlation.

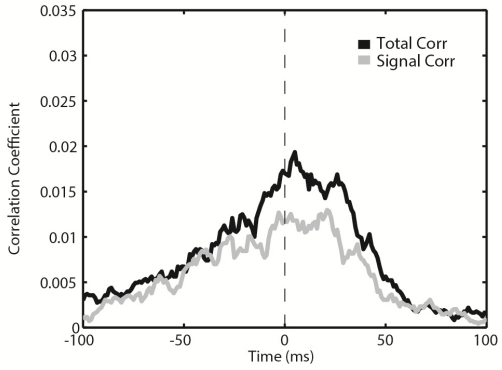

Figure 2.2 Example cross correlogram
Black line indicates the cross correlogram obtained from the concatenated spiking responses of a pair of neurons during the non-adapted condition. The integral under this curve was used to quantify 'total' correlation. Grey line indicates the cross correlogram obtained from a temporally shifted version of the same spike trains, in which the responses evoked by neuron A during a given trial are aligned to those evoked by neuron B during a subsequent trial. This removes any real-time correlation, leaving only the correlation between the neurons' stimulus evoked responses. The integral under this curve was used to quantify signal correlation. Noise correlation was inferred as total correlation minus signal correlation.

Statistics

For all statistical comparisons normality was tested using a 2-sided Shapiro-Wilk test. If data was Leptokurtic, the Shapiro-Francia test was performed. Otherwise (if data was platykurtic) the Shapiro-Wilk test was performed. When assessing group effects, the normality of the entire sample was tested. When assessing condition effects (repeated measures) for a single population, the normality of the differences between all combinations of conditions was tested. Where the assumption of normality was violated, non-parametric analysis was used.

When comparing the responses of the same neurons across multiple conditions, where the number of conditions was greater than two, the effect of conditions was first assessed by a repeated measures ANOVA (or Friedman's non-parametric repeated measures ANOVA). If significant ($p<0.05$), this was followed by pairwise t-tests (or Wilcoxon signed-rank paired comparisons).

When comparing responses across multiple groups of neurons, the effect of group was first assessed by an ANOVA (or the Kruskal-Wallis non parametric ANOVA). If significant ($p<0.05$), this was followed by pairwise t-tests (or Wilcoxon rank-sum comparisons).

Where applicable multiple comparisons were corrected for using the sequential Holm-Sidak correction (reviewed by Abdi, 2010). Unless otherwise specified error bars indicate mean ± standard error of the mean (S.E.M).

RESULTS

The aim of the study was to characterise contrast adaptation in mouse V1 and to assess the relative cortical and subcortical contributions to this phenomenon. In vivo extracellular recordings were made using a silicon tetrode array in the superficial layers of primary visual cortex, in mice expressing ChR2 in PV positive neurons (see Methods). ChR2 expressing neurons were selectively activated by light stimulation (Nagel et al., 2003; Boyden et al., 2005). This light sensitivity was used to both delineate the response properties of this neuronal population (Lima et al., 2009; Cardin, 2012) and to suppress the activity of nearby principal neurons (Atallah et al., 2012; Lien and Scanziani, 2012; Olsen et al., 2012).

Data were collected from a total of 8 animals (3 males and 5 females, P31-83). Two hundred and seventy neurons were included in the analysis (see Methods for exclusion criteria), recorded during 3 stimulation protocols: 191 during Protocol 1; 163 during Protocol 2; and 63 during Protocol 3. Note that 94/163 of neurons recorded during Protocol 2 and 53/63 of neurons recorded during Protocol 3 were also recorded during Protocol 1.

Responses of PV and non-PV expressing neurons

Several computational models have predicted differential adaptation of excitatory and inhibitory neurons within V1 (Chelaru and Dragoi, 2007; Levy et al., 2013), however this has not yet been explored experimentally. By comparing their responses in the presence/absence of LED illumination we were able to identify PV positive neurons, and characterise adaptation in this inhibitory cell type.

Spiking responses were recorded during visual stimulation with either drifting grating stimuli (as shown in Figure 2.3A-C) or a grey screen (data not shown), and LED illumination was provided on alternate trials (see Methods). On these trials illumination began at $t_{0,}$ remained constant until $t_{3.5}$, and ramped down in intensity until ceasing at t_4 (see Methods).

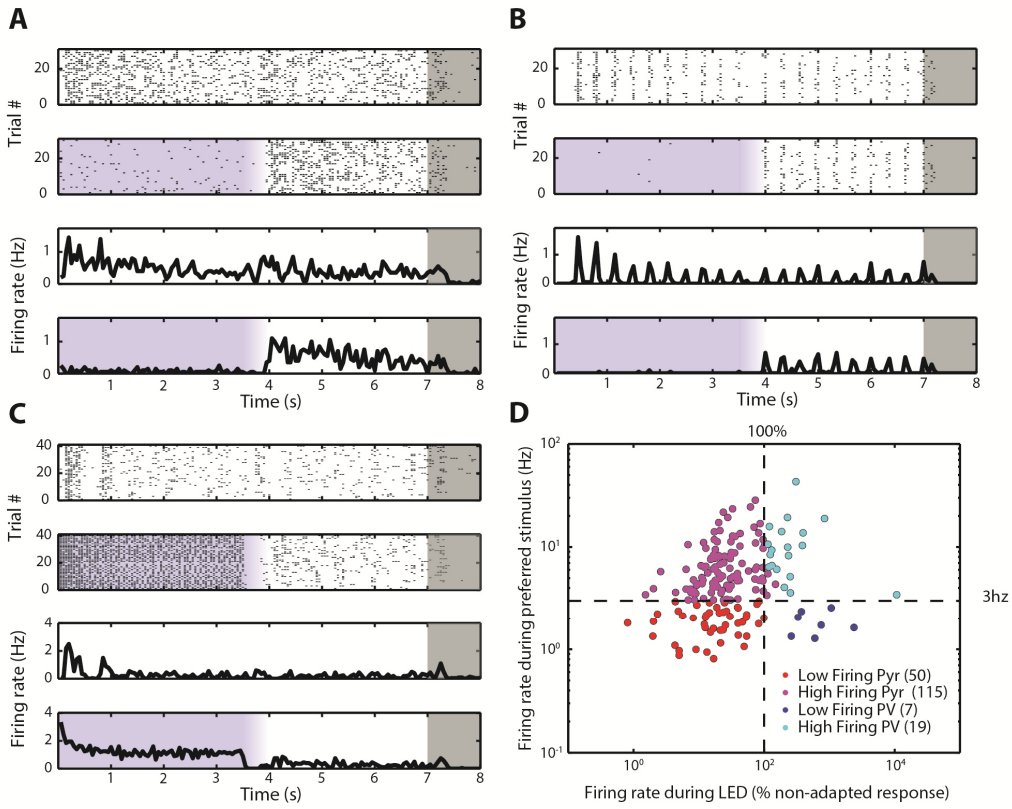

Figure 2.3 Classification of cell types
A, B & C) Raster plots and PSTHs of 2 putative pyramidal neurons whose visually evoked responses were suppressed during LED illumination (A & B) and a putative PV expressing neuron (C), whose response was enhanced during LED illumination. Drifting grating stimuli were displayed for 7 seconds from t_0, followed by a grey screen (as indicated by grey boxes). LED illumination (indicated by blue boxes) was provided on alternate trials. On these trials illumination began at t_0, remained constant for 3.5 seconds, before ramping down in intensity over a 500 ms period and ceasing at t_4. D.) Putative PV expressing neurons (shown in blue/cyan) were identified as those which exhibited a significant increase in firing rate during LED illumination (see Methods). Neurons whose responses were not significantly enhanced by LED illumination were classified as putative pyramidal (Pyr) cells (shown in red/magenta). Both cell types were additionally subdivided according to their firing rate during their preferred stimulus direction (see Methods). This resulted in 4 categories: low/high firing Pyr neurons (red/magenta) and low/high firing PV neurons (blue/cyan).

A neuron was deemed to be ChR2 positive, and hence PV positive, if two criteria were met: 1) there was a significant increase in firing rate during LED illumination for at least one of the stimulus conditions (either drifting gratings or grey screen), and 2) the mean firing rate across both conditions was greater during LED illumination trials than during trials in which no illumination was provided. Of the 270 neurons included in the dataset, 40 (17.4%) met this criteria and were classified as PV neurons. This proportion is slightly higher than previously reported (Markram et al., 2004; Gonchar et al., 2007; see Discussion).

Those neurons which failed to meet the above criteria were considered to be PV negative and were classified as putative pyramidal (Pyr) neurons. The majority of the Pyr neurons were suppressed during LED illumination; the average firing rate during the adapting stimulus (t_0-t_4) during LED trials was 32 ± 2 % (mean ± SEM) of that during the non-adapted condition. Note that the possible inclusion of non-PV expressing interneurons within the Pyr population, and potential false positives within the PV population (see Discussion) is likely to cause any cell type differences to be underestimated.

Stimulus selectivity (Protocol 1)

Pyr and PV populations were initially compared based on their responses during the stimulus selectivity protocol, which consisted of episodically presented gratings drifting in 8 different directions (see Methods).

The Pyr and PV populations (165 Pyr and 26 PV neurons) recorded during this protocol were additionally split according to their firing rate. Neurons whose firing rate during their preferred stimulus direction exceeded 3 Hz were considered to be 'high firing' (115/165 Pyr neurons, 19/26 PV neurons) whilst those with a maximum firing less than or equal to 3Hz were considered to be 'low firing' (Figure 2.3D). Whilst 3Hz is an arbitrary value, equivalent cell type effects were obtained using a 5 Hz threshold (data not shown).

Figure 2.4 (A-C) shows the responses of example Pyr/PV neurons during stimuli moving in different directions (stimulus orientation is always perpendicular to direction of movement). The orientation and direction selectivity of individual neurons was quantified by the relative difference in firing rate evoked by the preferred and orthogonal/null stimuli (see Methods). Orientation and directional selectivity varied significantly between different cell types (Figure 2.4D-G, cell type effects: OSI $p= 8.2\times10^{-4}$; DSI $p= 2.0\times10^{-4}$), with high firing PV neurons exhibiting the lowest selectivity for both orientation and direction. This is consistent with previous calcium imaging (Sohya et al., 2007; Kerlin et al., 2010; Hofer et al., 2011) and electrophysiological (Ma et al., 2010) studies in mouse V1.

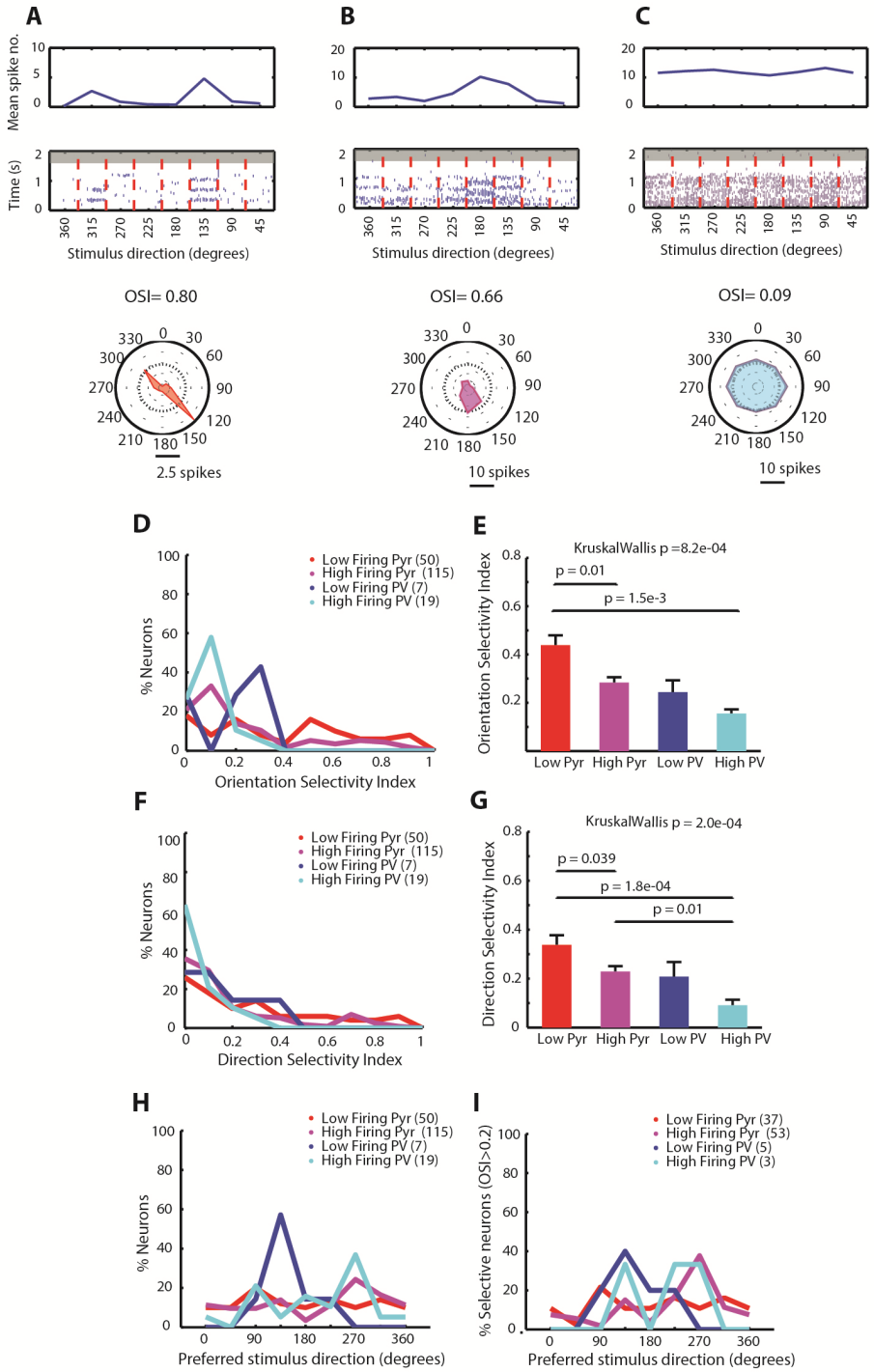

Figure 2.4. Stimulus selectivity of different cell types.
A-C.) Example responses of a low and high firing Pyr neuron (A and B respectively) and a high firing PV neuron (C), across 8 stimulus directions. D&E) Orientation Selectivity Indices (OSI) for Pyr and PV cells of different firing rates. F&G) Direction Selectivity Indices (DSI) for Pyr and PV cells of different firing rates. H.) Direction preferences of neurons of different cell types (all neurons). I.) Direction preferences of orientation selective neurons of different cell types (neurons with OSI>0.2). Error bars indicate mean ± S.E.M. Cell type classifications as introduced in Figure 2.3D.

Selectivity also seems to vary within Pyr/PV populations as a function of firing rate, with high firing neurons exhibiting lower selectivity. Indeed, across the population, firing rate and OSI were negatively correlated ($p= 2.7\times10^{-4}$, r= -0.33, data not shown). A similar trend was also observed by Niell and Stryker (2008); neurons in cortical layer 5 exhibited both the highest firing rates and the lowest stimulus selectivity.

Neurons of all cell types showed a range of orientation preferences (Figure 2.4H&I), and there was little evidence of the bias for cardinal orientations previously reported in V1 in other species (De Valois et al., 1982; Chapman and Bonhoeffer, 1998; Li et al., 2003), and in mouse LGN (Piscopo et al., 2013). However, in their comprehensive study of mouse V1, Niell and Stryker also failed to find evidence of cardinal bias (Niell and Stryker, 2008).

The depth of stimulus locked modulations (F1/F0 ratio, see Methods) was calculated for each neuron during their preferred stimulus direction. Of the Pyr neurons, 66 had an F1/F0 ratio greater than 1 and were classified as simple cells whilst the remaining

99 (F1/F0<1) were classified as complex cells. F1/F0 ratios also appeared to vary across cell types, with PV neurons (and high firing Pyr neurons) exhibiting the least modulated (i.e. least linear) responses (Figure 2.5A&B, $p= 2.0\times10^{-5}$). This is consistent with the dense and relatively non-specific local connectivity of PV neurons (Hofer et al., 2011) and is in agreement with other studies (Niell and Stryker, 2008; Ma et al., 2010). The difference in linearity between low and high firing Pyr neurons is again compatible with reports of low linearity (and selectivity) in relatively high firing layer 5 neurons (Niell and Stryker, 2008).

Intriguingly, some PV neurons appear to exhibit high F1/F0 ratios yet low orientation selectivity (see Supplementary Figure 2.1A for an example PV neuron with an F1/F0 ratio of 1.50 and OSI of 0.05). Such ‘linear non-orientated’ neurons have been reported previously in mouse V1 (Mangini and Pearlman, 1980; Métin et al., 1988; Niell and Stryker, 2008) and are reminiscent of centre-surround LGN neurons, which are sensitive to stimulus phase but insensitive to direction of motion (Wiesel and Hubel, 1966; Piscopo et al., 2013).

Trial to trial reliability, quantified as the average correlation coefficient between pairs of spike trains in different trials, was also calculated for responses to the neurons’

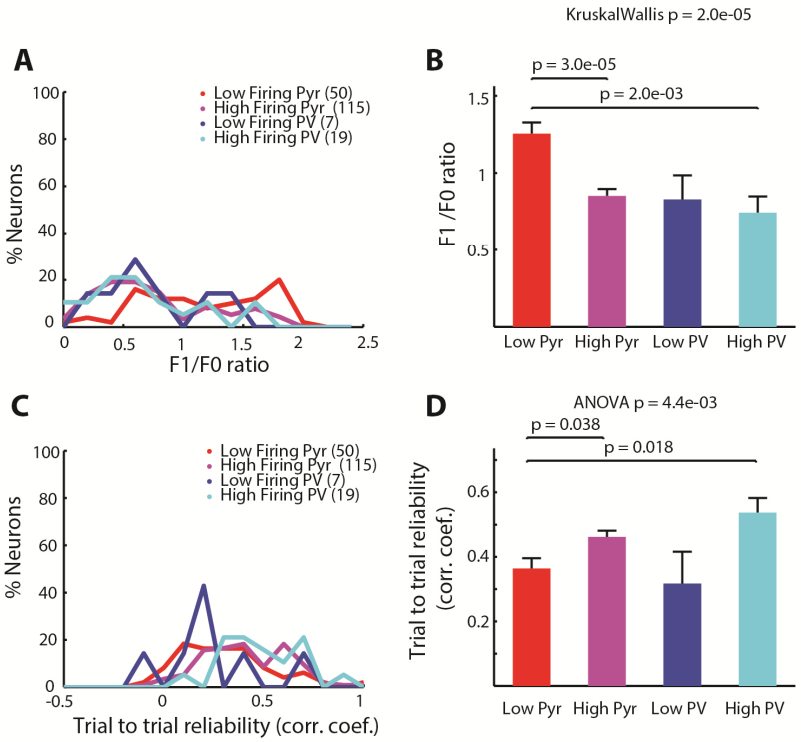

Figure 2.5. Linearity and reliability of different cell types.
A&B) F1/F0 ratios (i.e modulation depth) of different cell types during their preferred stimulus direction.C&D) Trial-to-trial reliability (mean correlation coefficient between spike trains) of different cell types during their preferred stimulus direction. Error bars indicate mean ± S.E.M.

preferred stimulus direction. Reliability varied significantly across cell type (Figure 2.5C&D, p= 4.4 $\times 10^{-3}$), with high firing PV neurons showing greatest consistency over trials. However, this effect may primarily reflect the difference in firing rate. Reliability tends to increase with firing rate (La Rocha et al., 2007), as can be observed in the difference between high/low firing Pyr cell populations.

Overall, the response properties of PV and Pyr neurons appear consistent with previous reports, with high firing PV neurons showing less stimulus selectivity (orientation/direction and phase), but greater trial to trial reliability than low firing Pyr neurons. However, the differences between low firing PV and high firing Pyr neurons were far less pronounced. The diversity of response properties within the Pyr population, and their dependency on firing rate may partly reflect the inclusion of non-PV expressing interneurons, which have also been reported to exhibit higher firing rates and lower selectivity than excitatory neurons (Ma et al., 2010).

Adaptation timecourses (Protocol 2)

Having characterised the basic response properties of PV and Pyr populations, we next compared their adaptation during prolonged high contrast stimuli. Within Protocol 2 (see above), neurons were recorded during the presentation of high contrast gratings of two different orientations/directions (see Methods). For each stimulus, spiking responses were summed over 333ms time bins (equivalent to one stimulus cycle) and averaged across trials, to give the mean response that was then normalised to its peak (Figure 2.6A-C).

For each neuron the initial adaptation during its preferred stimulus (preferred being defined as whichever of the two stimuli evoked the highest mean firing rate) was quantified by the response after 2 seconds of stimulation (expressed as a percentage of the peak response). Although the extent of adaptation varied between individual neurons, there was a significant difference between cell types (Figure 2.6D&E, $p= 1.3 \times 10^{-4}$). Whilst the responses of Pyr neurons reduced to approximately 40-50% after 2 seconds, high firing PV neurons were still responding at 70% of their maximum rate. To our knowledge contrast adaptation has not previously been compared in inhibitory and excitatory neurons. However, fast spiking PV neurons (Kawaguchi and Kubota, 1993) have also been found to undergo less firing rate adaptation during current pulse injection than regular spiking putative excitatory neurons (Nowak et al., 2003). The differences in visual adaptation may therefore, at least in part, reflect the intrinsic properties of the different cell types (Cardin et al., 2007).

Interestingly, the later stages of adaptation did not appear to differ between cell types (see Figure 2.6H). Although high firing PV neurons undergo less initial adaptation within 2 seconds than the other cell types, subsequent decline in firing appears similar. Indeed, when comparing responses within the analysis window (t_5-t_7), the difference in responsiveness between adapted and non-adapted trials did not significantly vary across cell types (Supplementary Figure 2.1B).

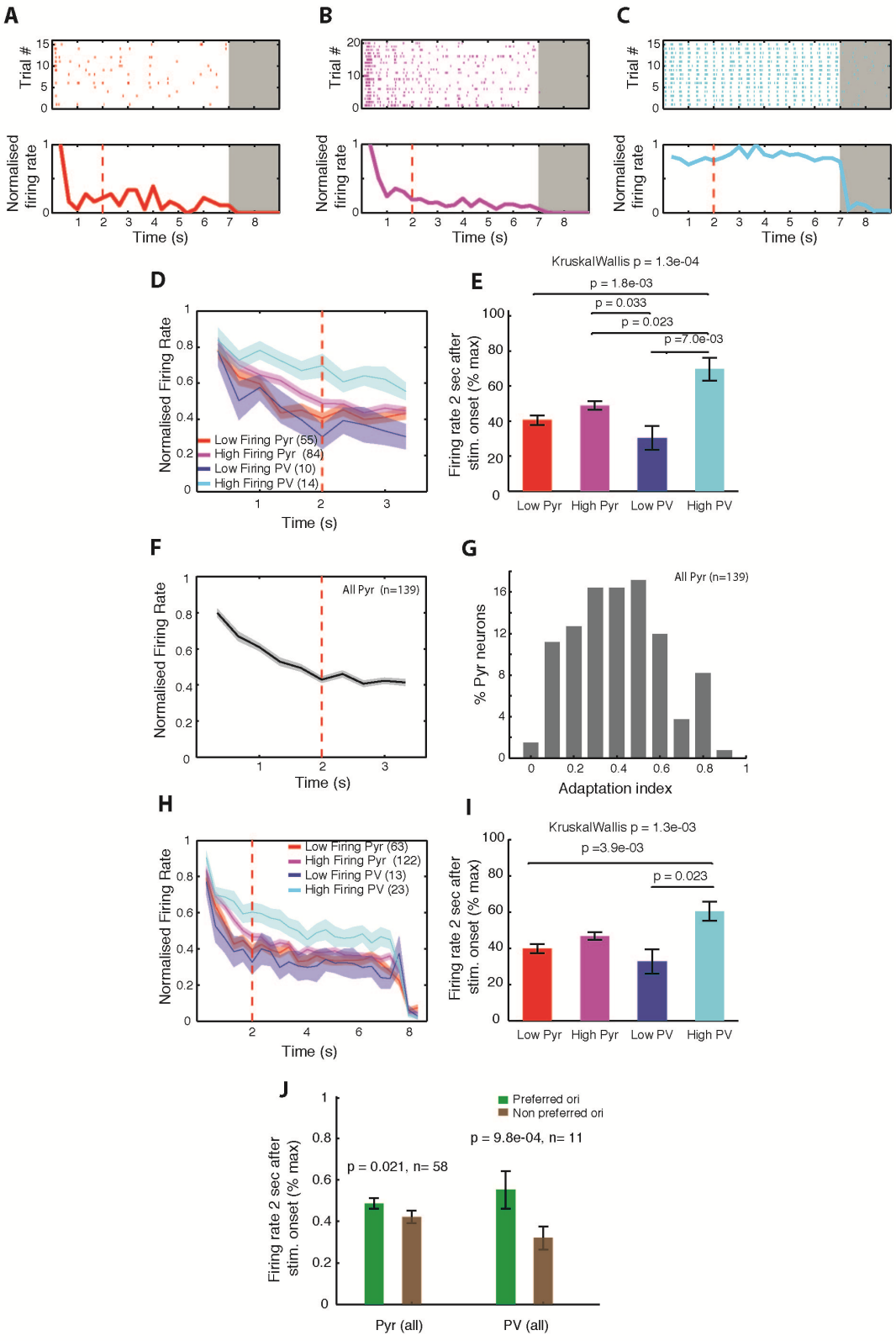
A
B
C
Trial #
Normalised firing rate
Time (s)
D
E
Normalised Firing Rate
Low Firing Pyr (55)
High Firing Pyr (84)
Low Firing PV (10)
High Firing PV (14)
KruskalWallis p = 1.3e-04
p = 1.8e-03
p = 0.033
p = 0.023
p =7.0e-03
Firing rate 2 sec after stim. onset (% max)
Low Pyr
High Pyr
Low PV
High PV
F
G
All Pyr (n=139)
% Pyr neurons
Adaptation index
H
I
Low Firing Pyr (63)
High Firing Pyr (122)
Low Firing PV (13)
High Firing PV (23)
KruskalWallis p = 1.3e-03
p =3.9e-03
p = 0.023
J
Preferred ori
Non preferred ori
p = 0.021, n= 58
p = 9.8e-04, n= 11
Pyr (all)
PV (all)

Figure 2.6. Adaptation of different cell types during drifting gratings.
A-D) Raster plots and PSTHs of low firing (A) and high firing (B) Pyr neurons and a high firing PV neurons (C) during a high contrast grating. Drifting gratings were presented for 7 seconds, followed a grey screen (as indicated by grey boxes). D) Average adaptation timecouse for different cell types during their preferred stimulus direction (of the two orientations presented). (Time bins = 333ms, equivalent to one stimulus cycle.) Line and shading indicate mean ± S.E.M. E) Adaptation indices of data shown in D. (Adaptation index was quantified for each cell as the average firing rate 2 secs after stimulus onset, expressed as a percentage of the peak rate- see main text). Error bars indicate mean ± S.E.M. F.) Average response adaptation for all Pyr neurons (both low and high firing units). G) Distribution of adaptation indices for all Pyr neurons. H) Average adaptation timecouse for different cell types during horizontal gratings (data combined over Protocols 1 & 2) Line and shading indicate mean ± S.E.M. I.) Adaptation indices of data shown in H. J.) Comparison of adaptation indices during preferred/non preferred stimuli, for those neurons which exhibited a significant preference for one stimulus orientation.

Therefore, in addition to the differences in stimulus selectivity, modulation strength and reliability, PV neurons appear to undergo less early adaptation than Pyr neurons during high contrast stimuli. Such differential adaptation across cell types would be expected to shift the balance between excitation and inhibition towards inhibition, and may contribute to the early decline of Pyr neuron responsiveness. This is in keeping with the predictions of Fregnac and colleagues (Levy et al., 2013), who found evidence of increased inhibition during high contrast stimulus conditions.

We also examined the stimulus dependency of adaptation by comparing the adaptation to 'preferred' and 'non-preferred' stimuli. For neurons that exhibited a significant difference in firing rate during the two stimulus orientations (58 Pyr neurons and 11 PV neurons), the preferred stimulus was defined as that which evoked the highest mean firing rate. Both Pyr and PV neurons displayed smaller adaptation indices (indicating a greater extent of adaptation) during their non-preferred stimulus, however this stimulus dependency was most obvious for PV neurons (Figure 2.6J).

The theory of 'deleterious fatigue' suggests that stimuli that drive a neuron most effectively should elicit the greatest degree of adaptation (Sekuler and Pantle, 1967; Swift and Smith, 1982; Georgeson and Harris, 1984). Paradoxically, in terms of initial adaptation the opposite appears to be true; neurons undergo weaker initial adaptation during their preferred stimulus.

Adaptation during stimuli of different contrasts (Protocol 3)

Stimulus dependent adaptation was further explored by comparing the degree of adaptation exhibited during stimuli of different contrasts. As higher contrasts evoke stronger responses, the fatigue hypothesis predicts that they should undergo

greater adaptation. (N.B. for this and for all subsequent analysis Pyr/PV populations include the pooled responses of both high and low firing neurons.)

For Pyr neurons, stimulus contrast did not appear to affect the degree of adaptation exhibited within 2 seconds of stimulus onset (Figure 2.7A&B). However, response latency (defined as the stimulus cycle in which the responses reached their peak) showed a clear effect of contrast, with responses to highest contrast stimuli eliciting the shortest latencies (Figure 2.7C, $p= 5.3 \times 10^{-5}$). The contrast dependency of response latency is consistent with previous reports (Dean and Tolhurst, 1986; Carandini and Heeger, 1994; Albrecht, 1995; Reich et al., 2001), however, it could potentially mask differences in adaptation; if the responses to different contrasts peak at different latencies, the response at 2 seconds after stimulus onset will correspond to different delays from the peak response. In order to account for any influence of latency, responses were therefore also plotted relative to their peak (Figure 2.7D). However, there was similarly no effect of stimulus contrast on the degree of adaptation exhibited 2 seconds after the response reached its peak (Figure 2.7E). These results do not support the deleterious fatigue hypothesis, as the degree of initial adaptation appears to be relatively independent of stimulus contrast.

In order to further clarify any relationship between stimulus drive and the degree of adaptation, the response 2 seconds post stimulus onset was normalised across contrasts and plotted against the normalised maximum firing rates for each neuron (Figure 2.7F). If adaptation were stronger for those contrasts that elicited the strongest responses, there should be a negative relationship between these variables (N.B. the smallest response after 2 seconds corresponds to the greatest degree of adaptation), however, there was no apparent correlation.

The same analysis was also carried out for PV neurons (n= 12). As for the Pyr neurons there was no difference in the degree of adaptation 2 seconds after either the stimulus onset or the peak response for stimuli of different contrasts (Figure 2.7G&H, J&K).

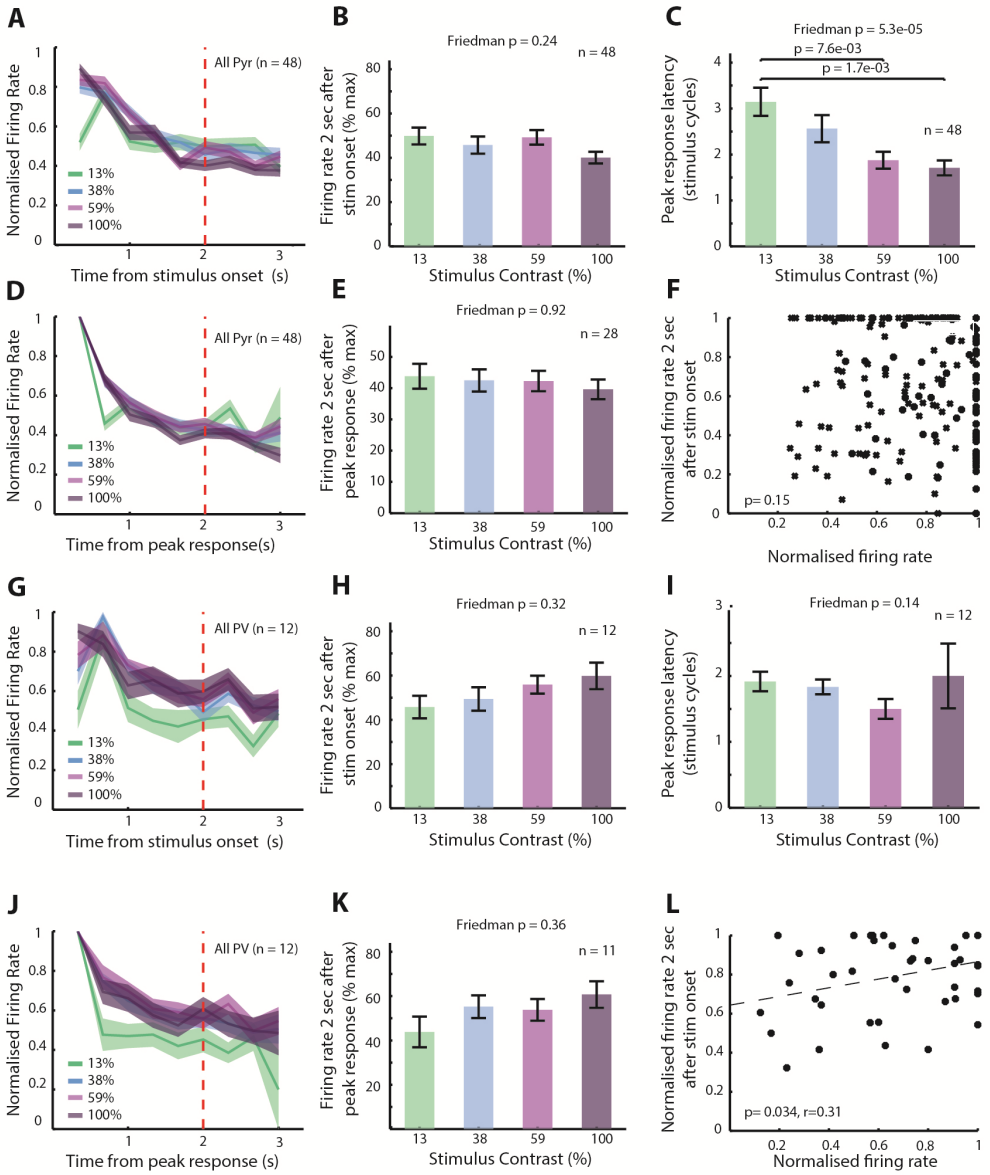

Figure 2.7. Adaptation during stimuli of different contrasts.
A.) Average adaptation of Pyr neurons (both high and low firing) during stimuli of different contrasts. Line and shading indicate mean ± S.E.M. B.) Adaptation of Pyr neurons during stimuli of different contrasts (defined as the response 2 s after stimulus onset, expressed as a percentage of the peak response). C.) Latency (in stimulus cycles) of peak response following stimulus onset. Error bars indicate mean ± S.E.M. D.) As in A, with responses of each neuron aligned to their respective peaks. E.) As in B, with adaptation defined as the response 2 s after peak response, expressed as a percentage of that peak. F.) Normalised peak firing rate for each stimulus contrast versus corresponding normalised adaptation (relative to stimulus onset), for all Pyr neurons (see text for details). G-L) As for A-F, for PV neurons (both high and low firing).

Interestingly, however, the response latency of these neurons also appeared to be independent of contrast (Figure 2.7I). Response latencies are reported to be shorter for PV neurons than both excitatory cells and SOM interneurons (Ma et al., 2010). In the current data, response latencies also appeared to be shorter for PV than Pyr

neurons, however, when averaged over all stimulus contrasts, there was no significant difference between cell type (data not shown). This discrepancy may indicate that the current measure (based on peak stimulus cycle) lacks sufficient temporal resolution to adequately capture PV neuron latencies.

As for Pyr neurons, the normalised response 2 seconds after the stimulus onset was plotted against normalised maximum firing rates for each PV neuron (Figure 2.7L). Interestingly this revealed a positive, albeit weak, correlation between these variables ($p= 0.034$, $r= 0.31$). Therefore, as seen during adapting stimuli of preferred/non preferred orientations (Figure 2.6J), those stimuli which elicit the greatest responses also tended to cause least adaptation in PV cells.

Quantification of adaptation (Protocol 2)

In order to minimise the influence of any non-stimulus related fluctuations in baseline responsiveness, the effect of adaptation was quantified by comparing responses during adapted and non-adapted trials, which were randomly interleaved (see Methods for details of Protocol 2). During this protocol, individual trials lasted 7 seconds in duration and consisted of an adapting stimulus of 3.5 s duration, followed by a test stimulus of 3.5 s duration (see Methods). The test stimulus consisted of either a horizontal or vertical drifting grating, and was preceded by one of 3 possible adapting stimuli: a horizontal drifting grating, a vertical drifting grating, or a grey screen (non-adapted condition).

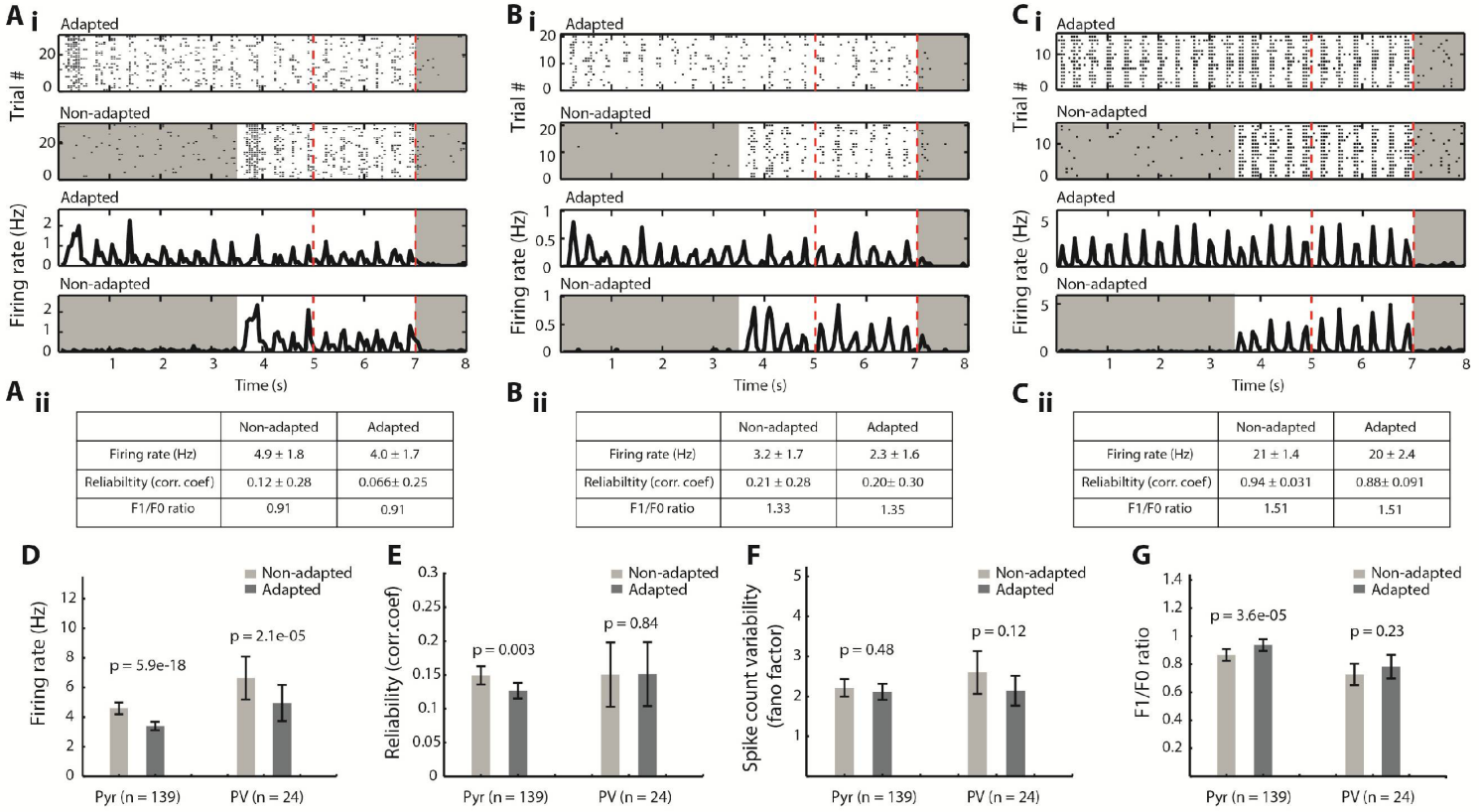

Figure 2.8. Quantification of adaptation following high contrast stimuli.
A-C.) Responses of 2 example Pyr neurons (A & B) and 1 PV neuron (C) during adapted trials, in which the test stimulus was preceded by an identical adapting stimulus, and non-adapted trials in which the test stimulus, was preceded by a grey screen. Responses within the 2 second analysis window between t=5 and t=7 (indicated by dashed lines) were compared across conditions. Mean firing rate, across trial reliability and F1/F0 ratios during adapted and non-adapted conditions are reported for each example neuron. D.) Mean firing rate of Pyr and PV neurons during non-adapted (grey) and adapted (black) conditions. E). Trial to trial reliability (mean correlation coefficient between spike trains) during non-adapted and adapted conditions. F). Spike count variability (Fano factor) during non-adapted and adapted conditions. G.) F1/F0 ratios during non-adapted and adapted conditions. Error bars indicate mean ± S.E.M.

We first assessed the effects of adaptation when the adapting and test stimuli were of the same orientation. For each neuron, the responses during its preferred test stimulus were compared when preceded by either the grey screen (non-adapted condition), or the adapting grating of the same orientation (adapted condition). (The preferred stimulus orientation was defined as whichever of the two test stimuli evoked the highest mean firing rate during the non-adapted condition). Analysis was restricted to 2 second analysis window between t_5 and t_7 (1.5 seconds after test stimulus onset). (See Methods and Figure 2.8A-C.)

The firing rates of both Pyr and PV neurons were significantly reduced during the adapted condition relative to the non-adapted condition (Figure 2.8D). The average adapted firing rate was 78% of the non-adapted rate for Pyr neurons ($p= 5.9 \times 10^{-18}$) and 74% for PV neurons ($p= 2.1 \times 10^{-5}$).

Adaptation also reduced the trial to trial reliability of Pyr neurons, as assessed by the average correlation coefficient between spike trains across stimulus repetitions (Figure 2.8E; adapted reliability of Pyr neurons was 79% of non-adapted value; p= 0.003). This is in keeping with the reduced reliability of inferred spike trains and membrane potential responses, observed during the continuous stimuli in Chapters 3 & 4 respectively. However, there was no significant change in the reliability of PV neurons, nor the spike count variability/fano factor of either cell type (Figure 2.8F).

Both F1 and F0 components of the firing rate response were reduced in adapted trials. As the F0 component was reduced to a greater extent (data not shown), however, there was a small but significant increase in F1/F0 ratio of Pyr neurons (Figure 2.8G, the average adapted F1/F0 of Pyr neurons was 129% of the non-adapted rate, $p= 3.6 \times 10^{-5}$). Whilst to our knowledge, the influence of adaptation on F1/F0 ratios has not been previously examined in mouse V1, a similar increase in linearity has been observed in subthreshold inputs in cat V1 (Carandini and Ferster, 1997; Sanchez-Vives et al., 2000a). There was no significant change in the F1/F0 ratio of PV neurons.

Putative Pyr neurons likely comprise a relatively heterogeneous population. We therefore asked whether the degree of adaptation exhibited by a neuron was associated with particular stimulus response property. The degree of adaptation (adapted firing rate as a percentage of the non-adapted firing rate) did not show any

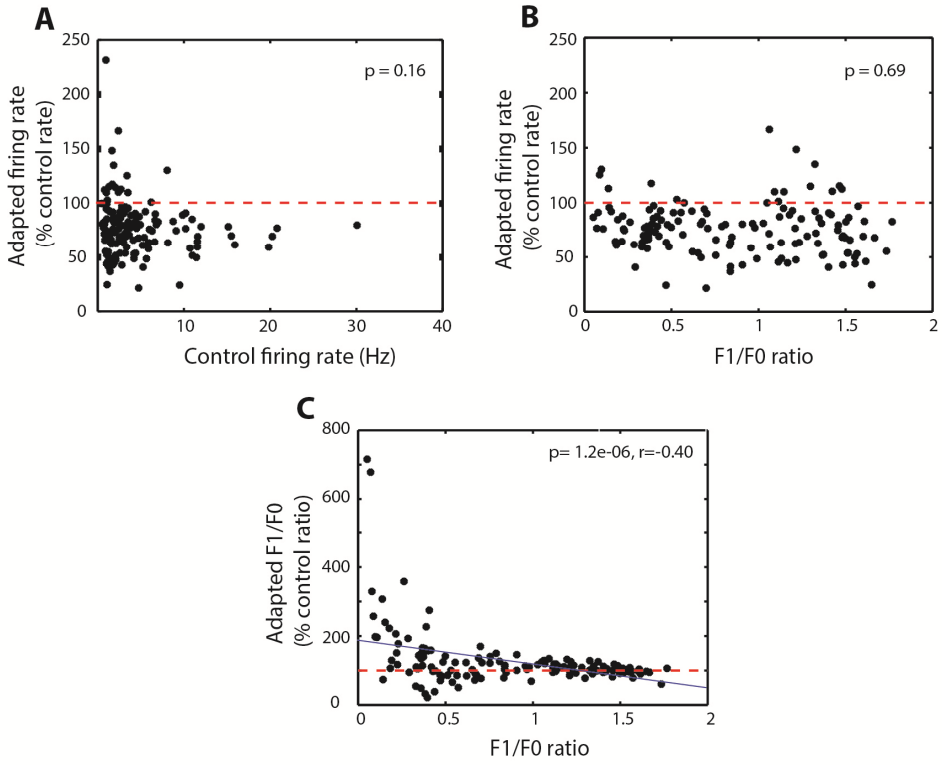

Figure 2.9. Dependence of adaptation effects on Pyr cell properties.
A.) Relative firing rate during the adapted condition, as a function of the firing rate during the non-adapted condition, for all Pyr neurons. B.) Relative firing rate during the adapted condition, as a function of F1/F0 ratio during the non-adapted condition. C.) Relative F1/F0 ratio during the adapted condition, as a function of F1/F0 ratio during the non-adapted condition

dependence on either the neuron's non-adapted firing rate (Figure 2.9A), or its F1/F0 ratio (Figure 2.9B). However, those neurons with the lowest F1/F0 ratios (i.e. the most non-linear or 'complex' responses) during the non-adapted condition appeared to show the greatest increase in linearity during the adapted condition (Figure 2.9C, r=-0.40, p=1.2 ×10-6). This is unlikely to simply reflect a ceiling effect; while F1/F0 ratios ranged up to 1.8, adaptation appeared to have little impact on neurons with F1/F0 ratios greater than 1. Therefore, the influence of adaptation on response linearity appears to differ between simple and complex cells. Interestingly simple and cells also appear to be differentially sensitive to various other contextual effects (Akasaki et al., 2002; Müller et al., 2003; Felsen et al., 2005; Bardy et al., 2006)

Orientation specificity of adaptation (Protocol 2)

In species such as cats and monkeys, in which orientation preference is arranged in a columnar manner, contrast adaption is reported to be orientation specific (i.e. the greatest reduction in responsiveness occurs for test stimuli of the same orientation

as the adapter). A recent study in mouse V1 (in which neurons of different orientation preferences are intermingled) reported that in the majority of neurons adaptation was non-orientation specific, being equally strong following adapting stimuli of different orientation (Stroud et., 2012). This finding is consistent with the normalisation model, which predicts that the responsiveness of a given neuron is influenced, not only its own activity history, but also that of its neighbouring neurons, which constitute the 'normalisation pool'. However the stimulus paradigm used by the aforementioned study (varying the orientation of the adapting stimulus, while holding the test stimulus constant), means the resultant adaptation will be influenced by both the relative orientation of the adapting/ test stimuli and the response strength during the adapting stimulus. We wished to clarify the relative influence of these factors by varying the orientation of both the adapting and test stimuli.

In order to assess the orientation specificity of adaptation within our current dataset, we restricted analysis to those neurons that were recorded during test stimuli of both horizontal and vertical orientations, and additionally exhibited a significant preference between these stimuli (27 Pyr neurons- see methods).

We first compared responses to a given test stimulus when it was preceded by an adapting stimulus of either the same or orthogonal orientation. This comparison is influenced by both the relative orientations of the adapting/test stimuli and the relative response magnitude during the adapting stimulus. We compared responses to the preferred test stimulus when it was preceded by an adapting stimulus of either the same or orthogonal orientation (Figure 2.10Ai, red and yellow traces respectively). We similarly compared the responses to the non-preferred test stimulus when it was preceded by an adapting stimulus of matching or orthogonal orientation (Figure 2.10Aii). For both the preferred and non-preferred test stimulus there was a significant difference in the degree of adaptation induced by either the matched or orthogonal adapting stimulus (Figure 2.10B). Interestingly, this relationship was reversed for the two orientations of test stimuli; for the preferred test stimulus, the firing rate adaptation was greater following the matched adapting stimulus (which was also the preferred orientation), however, for the non-preferred test stimulus, adaptation was greater following the orthogonal adapting stimulus (the neuron's preferred orientation). This disparity suggests that, rather than relative orientations of the adapting and test stimulus, the key factor in determining the

degree of adaptation is the effective drive during the adapting stimulus (i.e. whether or not it is that neuron's preferred orientation).

This lack of orientation specificity was further confirmed by comparing the relative adaptation of the two different test stimuli following a given adapting stimulus. As the same adapting stimulus was used both cases, and each test stimulus was normalised to its own non-adapted response, the only difference between the conditions was the relative orientations of the adapting and test stimuli. For all adapting/test stimuli combinations there was a significant reduction in responsiveness relative to the non-adapted condition. Furthermore, there was no significant difference in the degree of adaptation for test stimuli whose orientation either matched or was orthogonal to that of the adapting stimulus (Figure 2.10C). This lack of orientation specificity is in agreement with the findings of Stroud et al., and is consistent with the normalisation hypothesis, whereby a neuron's responsiveness is influenced by the activity history of its neighbouring neurons (which, in the mouse V1, exhibit a wide range of orientation preferences). Alternatively, non-orientation specific adaptation could also reflect the activity-dependent suppression of presynaptic neurons with low orientation selectivity (or pre-cortical mechanisms of adaptation).

The notion that degree of adaptation is predominantly influenced by the effective drive during the adapting stimulus is in keeping with the 'deleterious fatigue' hypothesis, whereby a neuron's responsiveness is inversely related to its preceding activity levels. Indeed, a significant correlation was observed between the individual neurons' firing rates during the adapting stimulus (relative to spontaneous firing rates), and the degree of adaptation they exhibited during the subsequent test stimulus (Figure 2.10D; $p= 9.5\times10^{-3}$, $r= -0.32$).

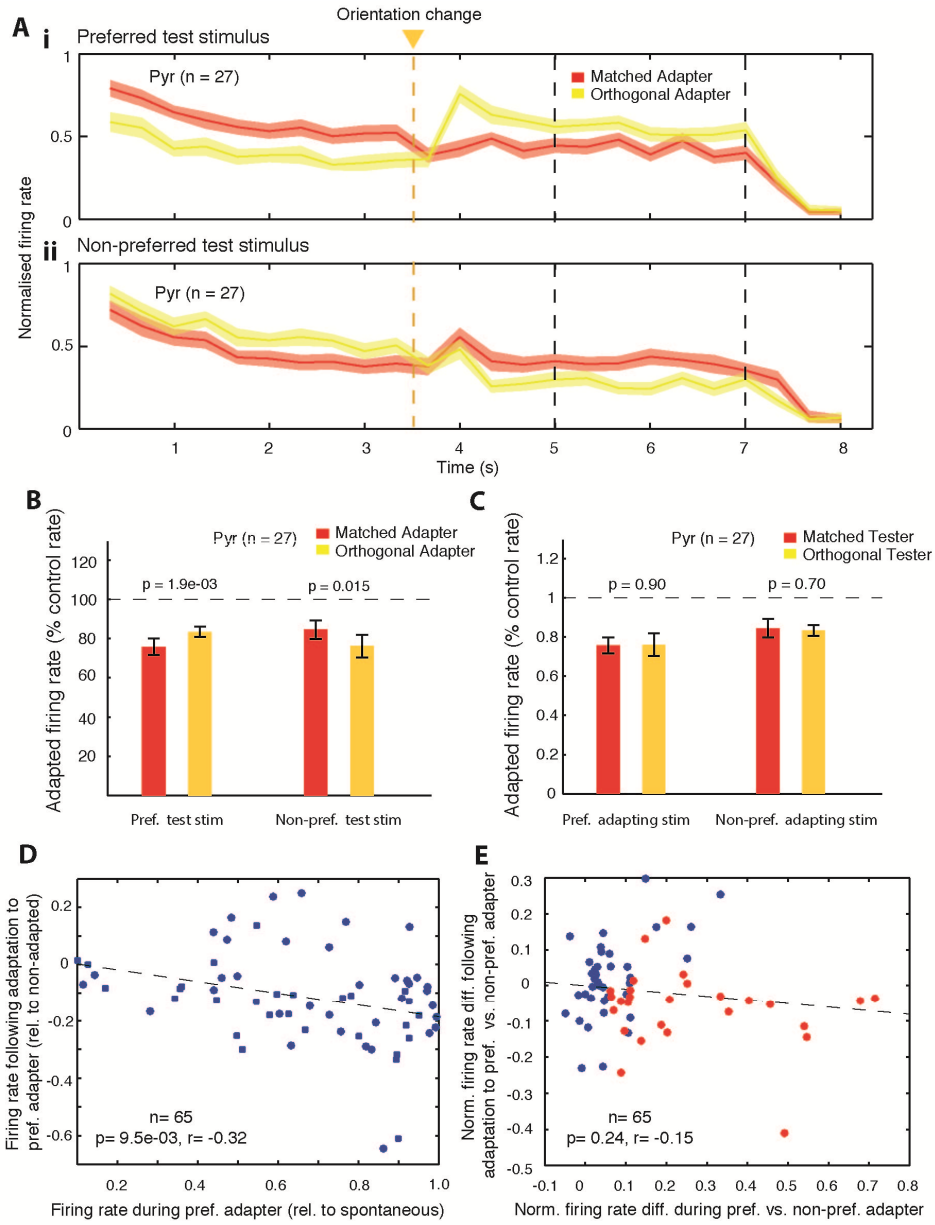

Figure 2.10. Orientation specificity of adaptation

A.) The average responses of Pyr neurons with a significant preference between adapting stimuli (n= 27), when the preferred (Ai) or non-preferred (Aii) test stimulus was preceeded by an adapting stimulus of either a matched (red) or orthogonal (yellow) orientation. Orientation change occurred at $t_{3.5}$. When the orientation of the adapting stimulus matched that of the test stimulus and hence did not change (shown in red), a 180 degree phase shift was introduced at $t_{3.5}$. Lines and shading indicate mean ± S.E.M. The degree of adaptation was compared following matched and orthogonal adapting stimuli, by comparing the response within the analysis window (as indicated by black dashed lines) to that during non-adapted trials. B.) Comparison of the degree of firing rate adaptation during preferred and non-preferred test stimuli, following matched (red) and orthogonal (yellow) adapters (data as in A) C.) The degree of firing rate adaptation exhibited by simple and complex Pyr neurons during the preferred test stimulus, when preceded by either the matched or orthogonal adapting stimulus. D.) Firing rate of Pyr neurons during their preferred test stimulus (relative to the non-adapted condition), plotted as a function of the firing rate during the preceding adapting stimulus (also of the preferred orientation, expressed relative to spontaneous firing rate). Data includes all Pyr neurons for which two orientations test stimuli were presented (n= 65). E.) Normalised difference in firing rate when the preferred test stimulus was preceded by either the preferred or non-preferred adapting stimulus, plotted as a function of the normalized difference in firing rate during these adapting stimuli. Data obtained from same Pyr neurons as shown in D. Red markers indicate those neurons which exhibited a significant preference for a given adapting stimulus (n= 27).

The fatigue hypothesis would also predict that the difference in adaptation following the preferred/non-preferred adapting stimulus should be related to the difference in firing rates evoked during those stimuli. However, no significant correlation was observed between these variables (Figure 2.10E). Instead, neurons that exhibited a marked difference in firing rate during the two orientations of adapting stimuli, exhibited varying degrees of orientation specificity in their adaptation. In some cases adaptation was relatively non-specific, with a significant reduction in responsiveness following adapting stimuli of either orientation (e.g. Supplementary Figure 2D). In other neurons, adaptation was significantly greater following the more effective stimuli (e.g. Supplementary Figure 2E). Furthermore, some neurons failed to show any significant adaptation after either adapting stimulus (data not shown). Additional data is required in order to establish whether these individual differences are related to other physiological characteristics/differences in the local neural network (see Discussion).

Therefore, whilst early adaptation (as quantified by the relative response strength 2 seconds after stimulus onset) did not vary consistently with overall response strength (Figure 2.7F), over a longer time frame, the response during the subsequent test stimulus (as measured here during the t_5-t_7 analysis window) was correlated with activity levels during preceding the adapting stimulus (Figure 2.10D). Furthermore, when controlling for differences in the activity levels during the adapting stimulus, adaptation of mouse V1 Pyr neurons was found to be non-orientation specific, being equally strong for test stimuli whose orientation either matched or was orthogonal to the adapting stimulus. Unfortunately, as few PV neurons exhibited a significant preference between adapting stimuli of different orientations (n= 5), it was not possible to compare orientation specificity of adaptation across cell types.

Adaptation during cortical suppression (Protocol 2)

It is unclear to what extent the adaptation observed in V1 arises intracortically or is inherited from earlier in the visual system. In order to determine the cortical contribution to adaptation in V1, cortical activity was suppressed during the adapting stimulus by optically activating PV neurons expressing ChR2 (see Methods). This manipulation should oppose any intracortical activity-dependent mechanisms of adaptation, whilst leaving any subcortical/thalamocortical mechanisms intact.

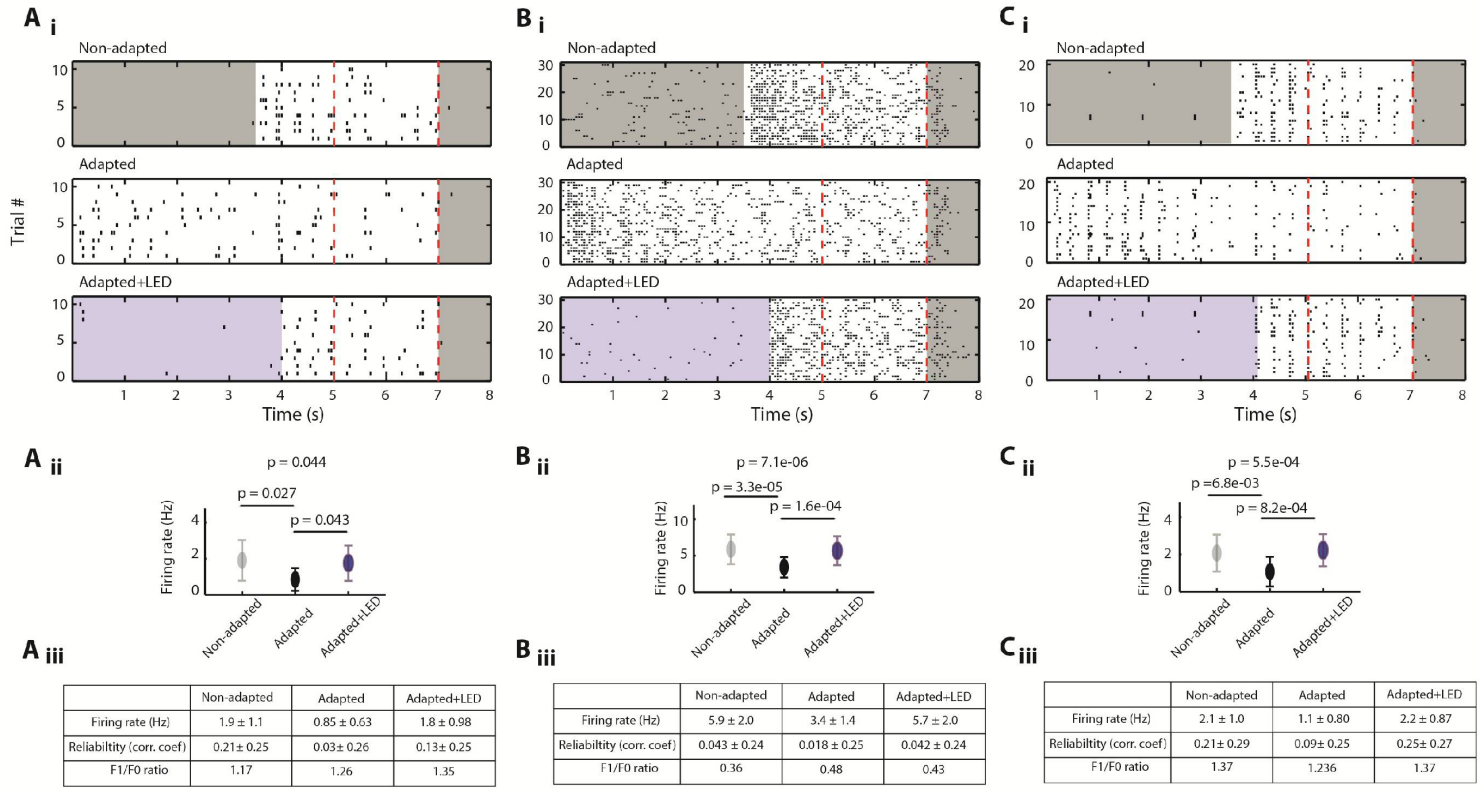

	Non-adapted	Adapted	Adapted+LED
Firing rate (Hz)	1.9 ± 1.1	0.85 ± 0.63	1.8 ± 0.98
Reliabiltity (corr. coef)	0.21± 0.25	0.03± 0.26	0.13± 0.25
F1/F0 ratio	1.17	1.26	1.35

	Non-adapted	Adapted	Adapted+LED
Firing rate (Hz)	5.9 ± 2.0	3.4 ± 1.4	5.7 ± 2.0
Reliabiltity (corr. coef)	0.043 ± 0.24	0.018 ± 0.25	0.042 ± 0.24
F1/F0 ratio	0.36	0.48	0.43

	Non-adapted	Adapted	Adapted+LED
Firing rate (Hz)	2.1 ± 1.0	1.1 ± 0.80	2.2 ± 0.87
Reliabiltity (corr. coef)	0.21± 0.29	0.09± 0.25	0.25± 0.27
F1/F0 ratio	1.37	1.236	1.37

Figure 2.11. Responses of 3 example Pyr neurons during adaptation, in the presence/absence of cortical suppression.
A.i) Raster plots of an example Pyr neuron during non-adapted, adapted and adapted + LED conditions. During both adapted and adapted + LED trials the test stimulus was preceded by an identical adapting grating, while during non-adapted trials the test stimulus was preceded by a grey screen (indicated by grey box). During the LED condition, illumination also began at t=0 and remained constant for 3.5 seconds, before ramping down in intensity over 500 ms and ceasing at t=4 (indicated by blue box). The grating stimulus was shown throughout the LED illumination, although stimulus evoked responses were largely suppressed in majority of neurons recorded. Responses were again quantified during the analysis window, as indicated by the dashed lines. A.ii) Firing rate across conditions (error bars mean ± SD over trials. A.iii) Table of response properties across conditions (mean ± SD over trials). B & C) As for A, for 2 additional Pyr neurons.

On alternate trials, the visual cortex was illuminated with a fibre-coupled 470 nm LED, between t_0 and t_4 (as indicated by the blue boxes in Figure 2.11Ai, Bi and Ci; see Methods for details). The influence of cortical silencing on contrast adaptation was established by comparing response properties during the analysis window (t_5-t_7) of adapted trials with/without LED illumination ('adapted' versus 'adapted + LED'; Figure 2.11Aii, Bii, Cii, Aiii, Biii and Ciii).

As discussed above, the average firing rate of Pyr neurons was reduced to 78% of the non-adapted rate during the adapted condition. However, on trials in which LED illumination was presented during the adapting stimulus (adapted + LED condition), the amount of adaptation was strongly reduced (Figure 2.12A, the average firing rate during the adapted + LED condition was 96% of the non-adapted rate versus 78% during the regular adapted condition, $p= 1.1\times10^{-12}$). Trial-to-trial reliability was also greater during the adapted + LED condition than the adapted condition (Figure 2.12B, the average correlation between adapted + LED trials was 175% of that between non-adapted trials, versus 79% during the regular adapted condition, $p= 2.2\times10^{-3}$). Likewise F1/F0 ratios, which were increased during the adapted condition relative to the non-adapted condition, were reduced after adaptation with LED stimulation (Figure 2.12C, the average Pyr neuron F1/F0 ratio was 129% of its non-adapted value during regular adapted condition and 112% during the adapted + LED condition, $p= 6.9\times10^{-4}$). Neither the degree of firing rate adaptation, nor its sensitivity to LED illumination appeared to differ between simple and complex cells (Figure 2.12D).

Hence, optical activation of PV neurons during the adapting stimulus counteracted the firing rate adaptation of Pyr neurons. Importantly these effects cannot be explained by non-specific effects of the LED illumination/PV neuron activation, as there was no significant difference in firing rate of either Pyr or PV neurons during non-adapted trials with and without LED illumination (Figure 2.12E). Furthermore, the degree to which cortical silencing affected the adapted response (normalised difference in firing rate between adapted + LED and adapted conditions) was significantly correlated to the amount of adaptation observed in each neuron (Figure 2.12F, $p= 5.7\times10^{-14}$, $r= -0.58$). This implies that LED illumination is indeed interacting with cortical mechanisms of adaptation, rather than independently affecting responsiveness or gain.

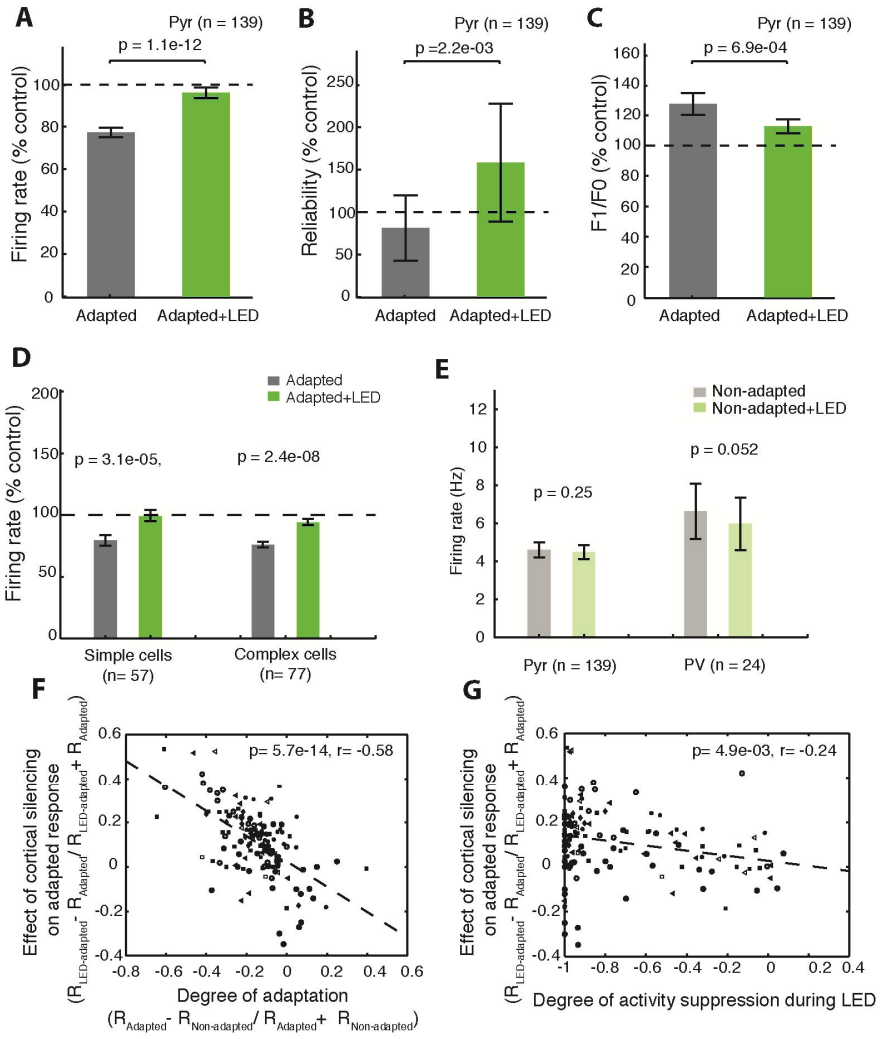

Figure 2.12. Adaptation of Pyr neurons during cortical silencing.
A.) Firing rate of Pyr neurons during the adapted (black) and adapted + LED condition (green), expressed as a percentage of the firing during the non-adapted condition (dashed line). B.) Trial to trial reliability of Pyr neurons during adapted and adapted + LED conditions, expressed as a percentage of reliability during the non-adapted condition. C.) F1/F0 ratio of Pyr neurons during adapted and adapted + LED conditions, expressed as a percentage of F1/F0 ratio during the non-adapted condition. D.) Firing rate of simple and complex Pyr neurons during the adapted and adapted + LED conditions. E.) Effect of LED illumination on the firing rate of Pyr and PV neurons during non-adapted and non-adapted + LED conditions. F.) Normalised difference in firing rate between adapted and adapted + LED conditions, as a function of the nomalised change in firing rate caused by adaptation (see Methods), for all Pyr neurons. Symbols indicate data collected from different animals. G.) Normalised difference in firing rate between adapted and adapted + LED conditions, as a function of the degree of suppression during LED illumination (see Methods). Error bars indicate mean ± S.E.M.

There was also a weak but significant negative correlation between the effect of cortical silencing on the adapted response and the degree of suppression during the illumination itself (Figure 2.12G, $p= 4.9\times10^{-3}$, r= -0.24). This indicates that those neurons whose activity is most suppressed during the LED illumination exhibit the greatest reduction in adaptation, supporting the notion that adaptation is dependent on cortical activity during the adapting stimulus.

During cortical silencing, the suppression that a neuron experiences should directly influence its own intrinsic adaptation (if such effects are assumed to be activity dependent). However, the overall adaptation that a neuron experiences is likely to depend, not only on its own intrinsic adaptation, but also that of its presynaptic partners. In our data, the degree by which cortical silencing affected the adapted response was better predicted by the amount of adaptation that a neuron normally experienced (determined by both intrinsic and network adaptation, Figure 2.12F), than to the extent to which its own responses were suppressed during the LED illumination (which is likely to affect only intrinsic adaptation, Figure 2.12G). This supports the notion that any intrinsic adaptation of the recorded neuron is amplified by network interactions.

Pairwise correlations between neurons (Protocol 2)

In addition to analysing the responses of individual neurons, the use of tetrode arrays also made it possible to compute the correlations between the evoked and spontaneous activities of pairs of Pyr neurons. The stimulus and non-stimulus dependent correlations between neurons were assessed during each condition, from the cross correlograms obtained for each neuron pair (see Methods).

The total pairwise correlation between neurons was significantly lower during the adapted trials than non-adapted trials (Figure 2.13A, $p= 1.6\times10^{-5}$). This finding is in keeping with previous predictions regarding adaptation induced decorrelation (Barlow and Foldiak, 1989; Barlow, 1990), and may be at least partially mediated by the same neuron-intrinsic adaptation proposed to underlie the reduced responsiveness of V1 neurons (Wang et al., 2003). Furthermore, it is also in keeping with the decorrelation of calcium signals observed during the continuous sequences of drifting gratings in Chapter 3.

When 'total' correlation was separated into stimulus dependent 'signal' correlation and non-stimulus dependent 'noise' correlation, signal correlation was found to decrease during adaptation (Figure 2.13B, $p= 6.7\times10^{-11}$), whilst the 'noise' correlation increased (Figure 2.13C, $p = 6.6\times10^{-3}$). A possible explanation for the reduction in stimulus dependent correlations is the increase in F1/F0 ratio, as mentioned above. An increase in this ratio means that a neuron's firing is more tightly locked to a particular phase of the stimulus cycle. Therefore two neurons with different phase preferences will give more disparate responses following adaptation.

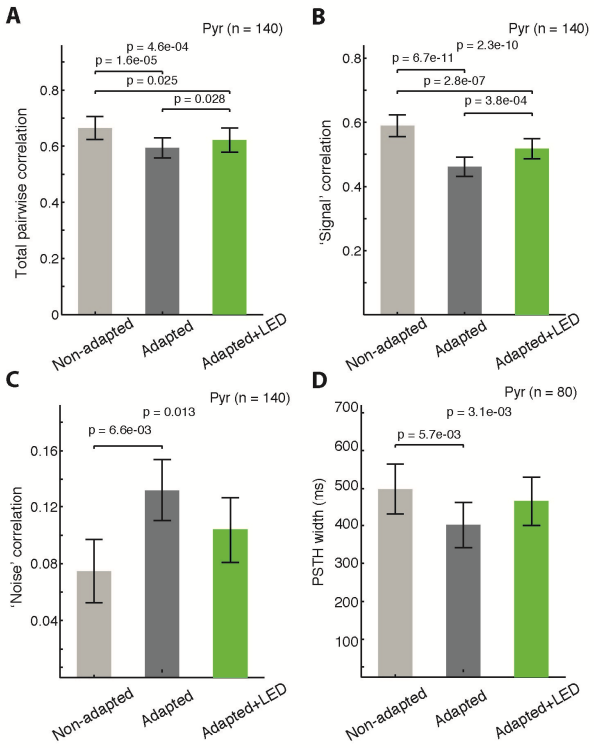

Figure 2.13. The influence of adaptation and cortical silencing on inter-neuronal correlations.
A.) The total correlation between pairs of Pyr neurons (quantified as the integral of the cross correlogram of their spike trains- see Figure 2.2 and Methods) during the non-adapted (grey), adapted (black) and adapted + LED (green) conditions. B.) The stimulus dependent 'signal' correlation between pairs of Pyr neurons (quantified as the integral of the 'shifted' cross correlogram; see text) across conditions. C.) The non-stimulus dependent 'noise' correlation between pairs of Pyr neurons (i.e. total correlation minus signal correlation) across conditions. D.) The width of individual neurons' PSTH auto correlograms (i.e phase selectivity- see text) across conditions. Error bars indicate mean ± S.E.M.

This explanation is supported by the observation that the width of the PSTH auto-correlogram decreases during adaptation, reducing any overlap between neurons with discrepant phase preferences (Figure 2.13D, $p= 5.7\times10^{-3}$).

In all cases, LED illumination appeared to oppose the effects of adaptation. However, the total and signal correlations were still significantly smaller than during non-adapted conditions. This suggests that at least some of the adaptation-induced decorrelation may be mediated subcortically (Dan et al., 1996).

Contrast specificity of adaptation (Protocol 3)

In order to more accurately describe how cortical suppression influences adaptation we additionally obtained contrast response functions using test stimuli of 4 different contrasts, during non-adapted and adapted conditions, with/without LED

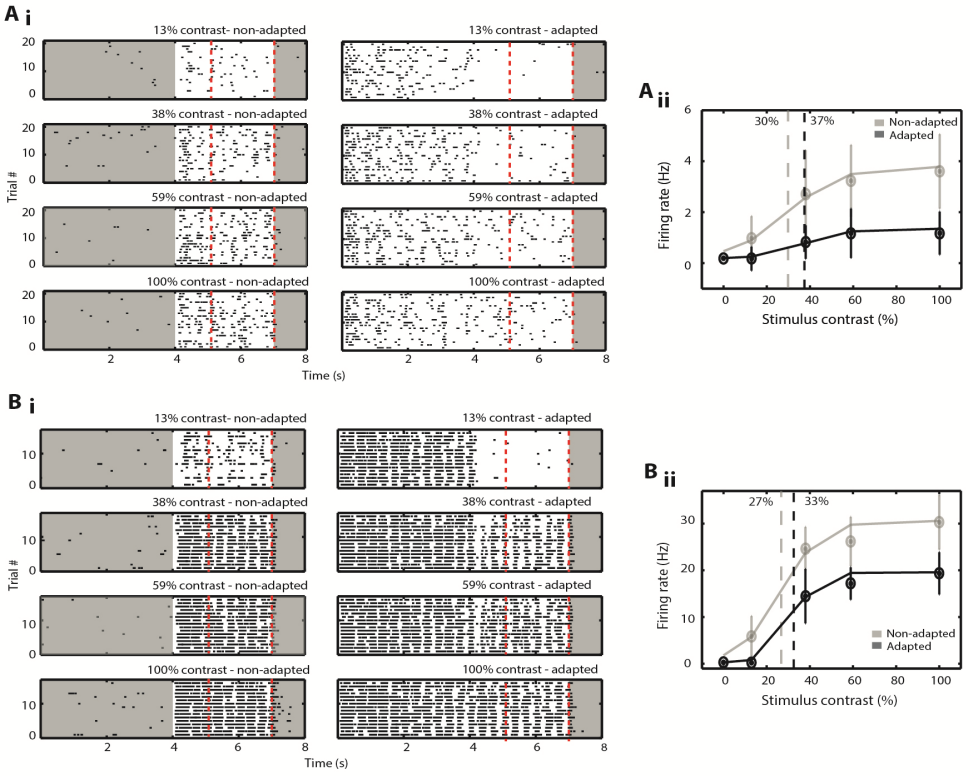

Figure 2.14. Contrast response functions of example neurons.
A.i) Raster plots showing responses of an example Pyr neuron during non-adapted and adapted stimuli of different contrasts. During adapted trials the full contrast adapting stimulus was presented for 4 seconds followed by a 3 second test stimulus of one of 4 different contrasts (see main text). During non-adapted conditions test stimuli were preceded by a grey screen (grey boxes). A.ii) The mean firing rates during the analysis window (dashed red lines in A.i.), plotted as a function of stimulus contrast, during non-adapted (grey) and adapted (black) conditions. Points are joined by the best fitting sigmoidal function. Dotted lines indicate the C50 contrast (the mid-point of the slope of the best fitting sigmoid). Error bars indicate mean ± S.D. across trials. B). As for A for an example PV neuron.

illumination. (See Figure 2.14 Ai and Bi for the responses of two example neurons during stimuli of different contrasts, without LED illumination.)

We initially compared adapted and non-adapted contrast response functions for Pyr and PV populations. Firing rate increased with contrast, and for most cells this relationship was well fit with a sigmoidal function. (The fits of two example neurons are shown in Figure 2.14 Aii and Bii.) For those neurons for which r^2 for the sigmoidal fit exceeded 0.7 (36/51 Pyr neurons and 11/12 PV neurons), the half maximal contrast (C50) and response range (Rmax) were extracted from the fit parameters to give an estimate of the changes in contrast and response gain, respectively.

The average C50 of Pyr neurons during non-adapted conditions (19.6 ± 9.4%) is in close agreement with that reported by a previous study in mouse V1 (median= 19.8;

Niell and Stryker, 2008), although somewhat less than that observed by Stroud et al. (~40%, Stroud et al., 2012). For both Pyr and PV neurons, adaptation led to a rightward and downward shift in the contrast response function, reflected by an increase in C50 (Figure 2.15C, Pyr C50= 20% during the non-adapted condition versus 29% when adapted, $p= 5.4\times10^{-5}$; PV C50= 32% during the non-adapted condition versus 40% when adapted, $p= 6.8\times 10^{-3}$) and a decrease in Rmax (Figure 2.15D, Pyr Rmax= 6.7Hz during the non-adapted condition versus 4.2Hz when adapted, $p= 1.7\times 10^{-7}$; PV Rmax= 10.1Hz during the non-adapted condition versus 6.6Hz when adapted, $p= 9.8\times 10^{-4}$). These data reflect a reduction in both contrast and response gain, consistent with reports in other species (Ohzawa et al., 1982; 1985; Sclar et al., 1989; Bonds, 1991; Carandini and Ferster, 1997) and in the mouse (Stroud et al., 2012).

While there was no difference in the effects of adaptation across cell types, the non-adapted contrast response functions of PV neurons appeared relatively flatter than those of Pyr neurons and had significantly greater C50 values ($p= 1.4\times10^{-3}$; Figure 2.15C). However, cell type differences in Rmax and slope values were not statistically significant (Figure 2.15D&E). Atallah et al. found the contrast response functions of PV neurons in mouse V1 to be shallower than those of Pyr neurons (Atallah et al., 2012), however Contrereas et al., failed to find any such difference between fast and regular spiking neurons in cat V1 (Contreras and Palmer, 2003) . Interestingly, PV neurons in cat V1 have also been reported to show greater orientation selectivity than those in mouse V1 (Cardin et al., 2007), potentially indicating species differences in the response properties of these interneurons.

For each neuron, the ‘adapter strength’ was calculated as the difference between the C50 value during the non-adapted condition and adapter contrast (adapter contrast was always 100%), and provides a measure of response saturation during the adapting stimulus (see Methods). Low ‘adapter strength’ corresponds to a high C50 during the non-adapted condition, whereas high ‘adapter strength’ corresponds to a low C50 during the non-adapted condition. For both Pyr and PV neurons the change in C50 during adaptation was correlated with adapter strength (Figure 2.15F&G, Pyr $p= 0.012$, $r= 0.41$; PV $p= 1.3\times10^{-4}$, $r= 0.90$), supporting the notion that adjustments in contrast gain maximise sensitivity to the prevailing (adapter) contrast. However, consistent with previous studies (Stroud et al., 2012), there was

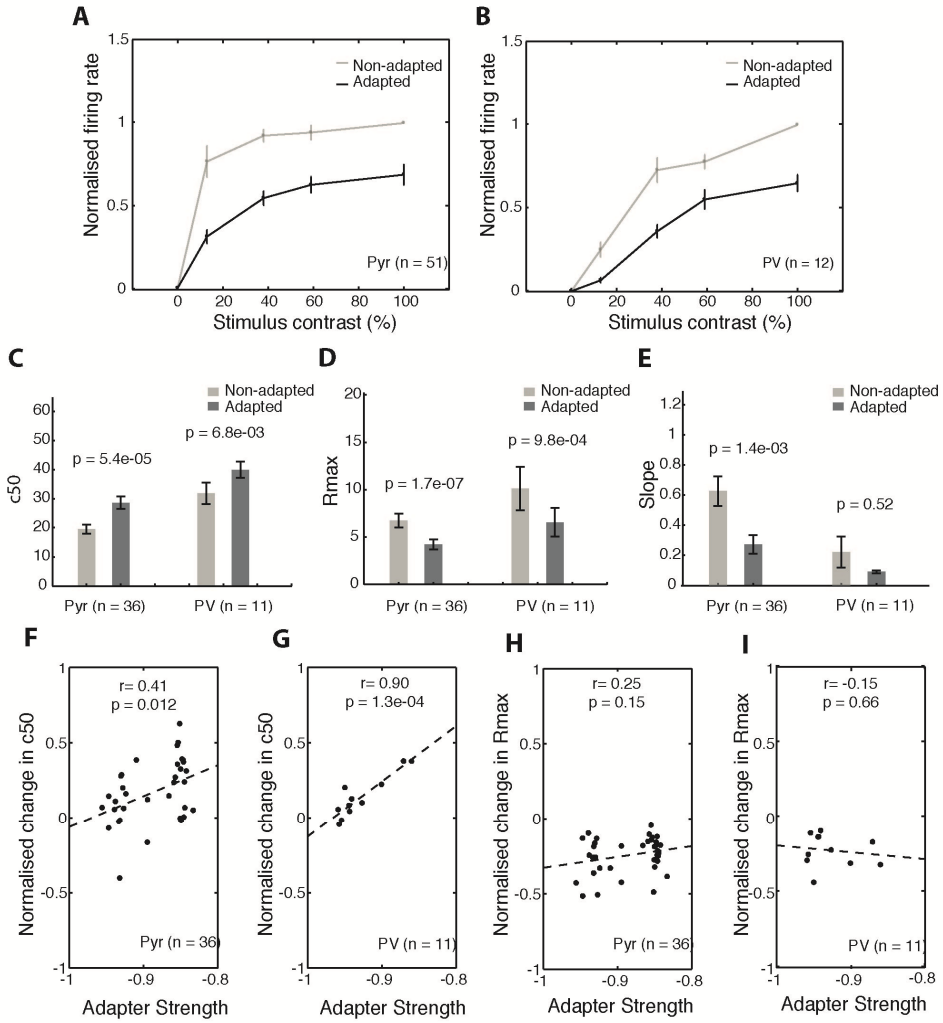

Figure 2.15. Effect of adaptation on contrast response functions.
A.) Normalised firing rates of Pyr neuron population (n= 51), as a function of stimulus contrast during non-adapted (grey) and adapted (black) conditions. B.) As for A, for PV neuron population (n = 12). C.) C50 values (the half maximal contrast) during non-adapted (grey) and adapted (black) conditions for Pyr and PV neurons. D.) Rmax values (response range) during non-adapted and adapted conditions. E.) Slope of sigmoid function during non-adapted and adapted conditions. F.) The difference in C50 values between non-adapted and adapted conditions for Pyr neurons, as a function of the neuron's drive during the non-adapted condition (i.e. the degree of response saturation during the adapting stimulus- see text). G.) As for F for PV neurons. H.) The difference in Rmax values during non-adapted and adapted conditions as a function of the neuron's drive during the non-adapted condition. I.) As in H, for PV neurons. Note that for data in C-I, analysis was restricted to those neurons for which a sigmoid function could be fit with an r^2 value >0.7 (36/51 and 11/12 PV neurons). Error bars indicate mean ± S.E.M.

no significant relationship between adapter strength and the change in Rmax for either cell type (Figure 2.15H&I).

Adaptation therefore appears to be associated with a decrease in both contrast and response gain for both Pyr and PV neurons. In order to determine how cortical

mechanisms contribute to these effects, we next compared contrast response functions of Pyr neurons obtained with and without cortical suppression via optical activation of ChR2-expressing PV interneurons.

As seen during Protocol 2, which tested the orientation specificity of adaptation, the presence of LED illumination during the adapting stimulus caused an increase in firing rate relative to the adapted condition, for test stimuli of all contrasts (Figure 2.16A). However, as evident in Figure 2.16B, the effectiveness of the cortical silencing in counteracting adaptation appeared to vary for the different contrasts. In keeping with Protocol 2, LED illumination was able to largely reverse the effects of adaptation for high contrast stimuli, but it was less effective for lower contrasts. This stimulus dependency can be explained by the differential effects of LED illumination on contrast and response gain (see below).

As shown above, adaptation caused an increase in C50 and a decrease in Rmax, indicating a decrease in both contrast and response gain. The presence of LED illumination significantly increased Rmax relative to the adapted condition, although not to non-adapted levels (Figure 2.16D, $p= 3.7 \times 10^{-10}$). However, cortical silencing during adapting stimulus had no noticeable effect on C50 (Figure 2.16E). This suggests that suppression of cortical activity is able to partially counteract the effects of adaptation on response gain, but it is ineffective against changes in contrast gain.

The differential effects upon contrast and response gain can explain why cortical silencing appears to have greater influence on high contrast test stimuli. At high contrasts, a change in contrast gain has little impact on firing rate, as responses remain saturated despite the shift in C50. A change in response gain however, affects all contrasts equally. Therefore, while the responses to test stimuli of all contrasts are reduced by adaptation, the influence of response gain (relative to contrast gain) is greatest for high contrast test stimuli. By counteracting the decrease in response gain, cortical silencing is therefore able to largely reverse the effects of adaptation at high contrast. However, as cortical silencing is ineffective in opposing changes in contrast gain, it has less influence on the adaptation of responses to low contrast stimuli.

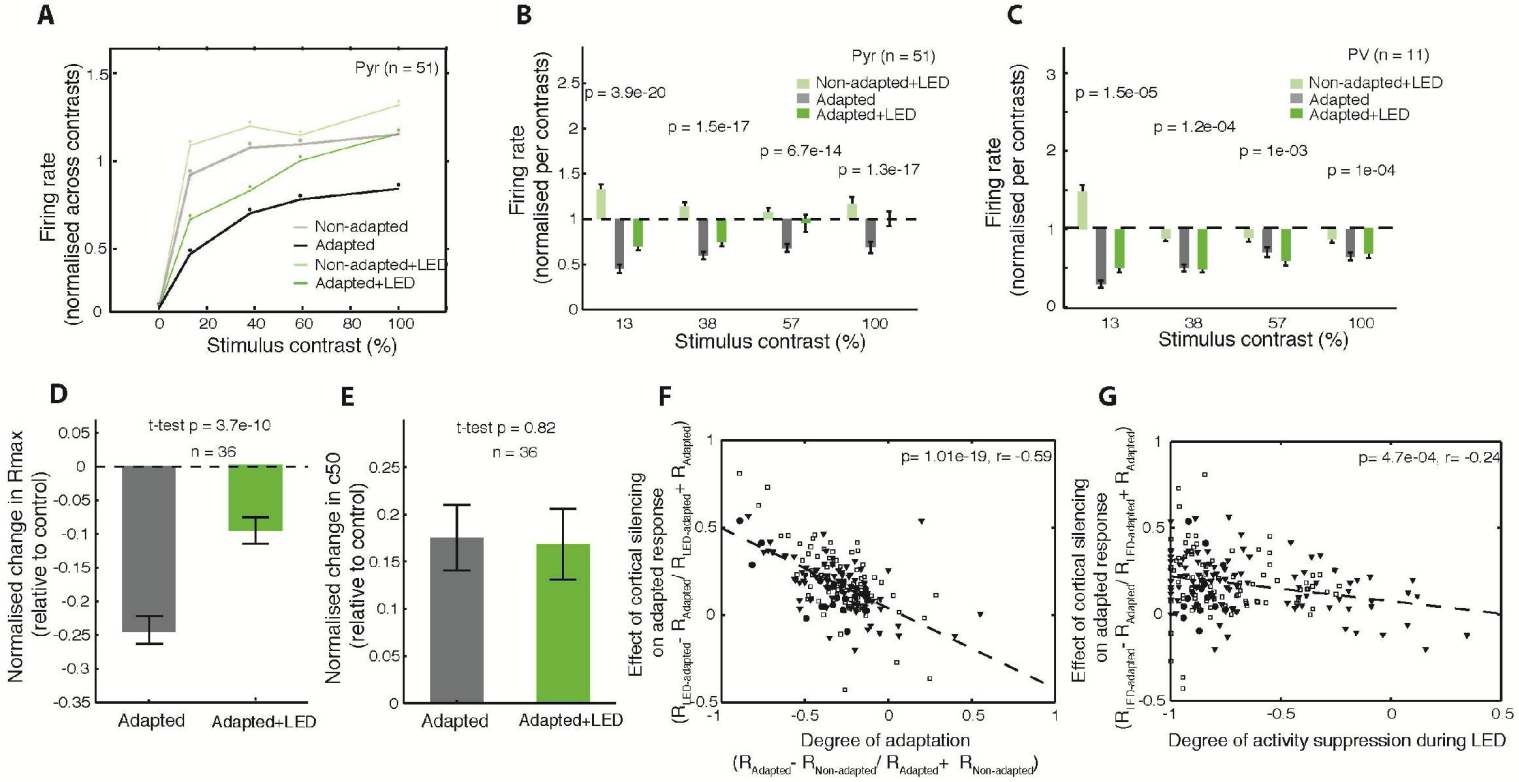

Figure 2.16. The effect of cortical silencing on contrast response functions.
A.) Normalised firing rates of Pyr neuron population (n = 51), as a function of stimulus contrast during non-adapted (grey), adapted (black), adapted + LED (green) and non-adapted + LED (light green) conditions. B.) Mean firing rate during adapted (black), adapted + LED (green) and non-adapted + LED (light green) conditions, normalised to the non-adapted condition for each stimulus contrast. C.) As for B, for PV neurons. D) Normalised difference in Rmax between non-adapted condition and adapted/adapted + LED conditions. E) Normalised difference in C50 between non-adapted condition and adapted/adapted + LED conditions. F.) Normalised difference in firing rate between adapted and adapted + LED conditions , as a function of the nomalised change in firing rate caused by adaptation (see Methods), for all Pyr neurons. Symbols indicate data collected from different animals. G.) Normalised difference in firing rate between adapted and adapted + LED conditions, as a function of the degree of suppression during LED illumination (see Methods). Error bars indicate mean ± S.E.M

The differing sensitivities of response and contrast gain to cortical suppression therefore raise the intriguing possibility that response gain could be mediated cortically, while contrast gain may be primarily mediated subcortically (or at the thalamocortical synapse).

We next determined whether cortical silencing directly interacts with the mechanisms of adaptation, or independently modulates neuronal gain. As seen in the data from Protocol 2, during Protocol 3 the degree to which cortical silencing affected the adapted response was significantly correlated to the amount of adaptation the neuron experienced in the absence of cortical silencing ($p= 1.0\times10^{-19}$, $r= -0.59$ Figure 2.16F). In fact this relationship was remarkably similar across Protocols 2 and 3, despite the fact that these comprised of two independent datasets (see Figure 2.12F). The effect of cortical silencing on the size of the adapted response was also significantly (but weakly) correlated with the degree of suppression that the neuron underwent during the LED illumination (Figure 2.16G, $p= 4.7\times10^{-4}$, $r= 0.24$). Again, this relationship was highly similar to that seen during Protocol 2 (Figure 12.12G) and supports the notion that LED illumination is mediating its effect on adaptation directly via the suppression of cortical activity. Furthermore, as discussed above, the difference in the explanatory power of these two comparisons may reflect the relative role of intrinsic/network interactions in the cortical expression of contrast adaptation.

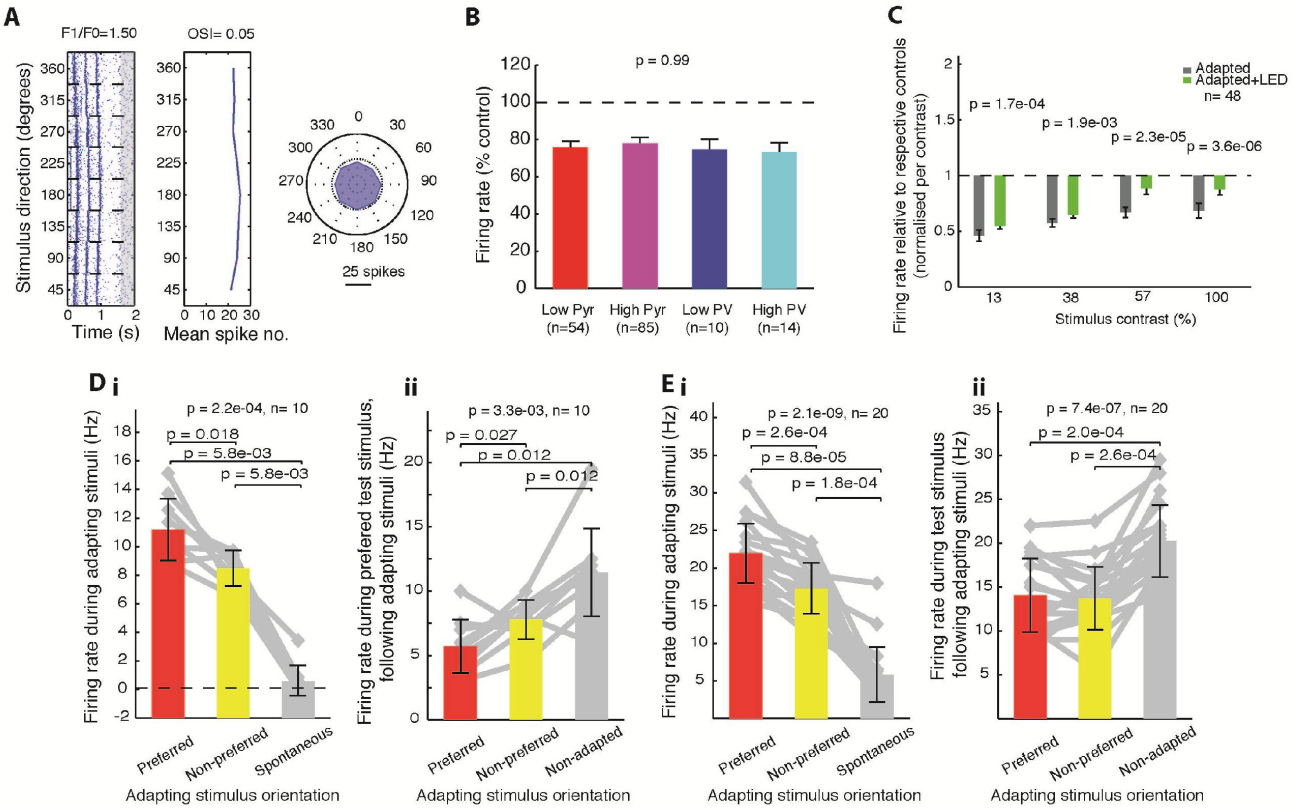

Supplementary Figure 2.1

A.) Responses of an example 'linear non-orientated'PV neuron during grating stimuli drifting in 8 different directions (Stimulus selectivity protocol), over 40 repetitions. B.) Degree of adaptation experienced by different cell types (quantified as the firing rate during the analysis window of the adapted condition, relative to that during the non-adapted condition). C.) Degree of adaptation experienced by Pyr neurons in the presence/absence of LED illumination, across stimulus contrasts. For each stimulus contrast, black bars represent the firing rate during the analysis window of the adapted condition relative to the firing rate during the control condition; Green bars represent the firing rate during the adapted + LED condition relative to the firing rate during the non-adapted + LED condition. Di.) Responses of an example Pyr neuron during adapting stimuli of its preferred (red) and non-preferred (yellow) orientations. Spontaneous activity (grey) is provided for comparison. Dii.) Responses of the same neuron during the preferred test stimulus, when presented after the adapting stimuli shown in Di. Grey bar indicates non-adapted response. E) as for D, for another example Pyr neuron.

DISCUSSION

The aim of this study was to explore contrast adaptation in mouse visual cortex. By suppressing cortical activity via light activation of ChR2-expressing PV interneurons, we were able to assess the relative influence of subcortical and cortical mechanisms of contrast adaptation and compare its effects in PV and non-PV expressing neurons.

Main findings:

1. For a given adapting stimulus, adaptation was non-orientation specific, being equally strong for subsequent test stimuli of either matched or orthogonal orientations.
2. The degree of adaptation varies with the effective drive of the adapting stimulus, but the nature of this relationship reverses between early and later stages of adaptation.
3. The early stage of adaptation is cell type specific, with high firing PV neurons undergoing the greatest reduction in responsiveness.
4. The suppression of cortical activity is able to largely counteract the effects of contrast adaptation in V1 neurons, primarily by influencing response gain.

Orientation specificity of adaptation

For a given adapting stimulus, adaptation was found to be non-orientation specific, being equally strong for subsequent test stimuli whose orientation either matched or was orthogonal to that of the adapting stimulus (Figure 2.10C). This finding is in agreement with a previous study in mouse V1, in which the orientation of the adapting stimulus was varied (Stroud et al., 2012), and supports the normalisation hypothesis (which predicts that the specificity of adaptation is determined by the composite selectivity of neighbouring neurons that form the 'normalisation pool').

The normalisation hypothesis predicts that neurons located in cat iso-orientation domains should exhibit adaptation with a greater degree of orientation specificity (Sengpiel and Bonhoeffer, 2002), than those neurons at pinwheel centres. This is consistent with the findings of Crowder (Crowder, 2005), however the opposite trend has also been reported (Dragoi et al., 2001). One potential explanation for these conflicting results is the different durations of adapting stimuli used in these studies (2 minutes in Dragoi et al., 2001; 1 minute in Crowder, 2005; 3.5 seconds in the current study). Indeed it has been predicted that the relative contribution of divisive normalisation/ neuronal fatigue may vary according to the duration of the adapting stimulus (Bonds, 1991). It would therefore be interesting to assess the orientation specificity of adaptation in mouse V1 over a range adapting durations. If the orientation specificity were found to vary with adapting stimulus duration it would be interesting to examine the perceptual correlates of this effect. Psychophysical studies in humans have shown the effects of adaptation to be orientation specific, being more potent for adapting/test stimuli of matching orientation (Ross and Speed 1996; Snowden and Hammett 1992), but it is unclear how this relates to the adaptation of individual V1 neurons (Boynton and Finney, 2003).

However, while the lack of orientation specific adaptation is consistent with the normalisation model it does not necessitate it. As discussed in Chapter 1, adaptation could also be mediated the activity-dependent suppression of the recorded neuron, its pre-synaptic partners and/or their synaptic connections. In this case the specificity of adaptation will be determined by the selectivity of these presynaptic neurons.

If the pre-synaptic neurons exhibit relatively high orientation selectivity, different neurons are likely to be activated by the different test stimuli. When the adapting stimuli and test stimuli are of the same orientation, the same population of presynaptic neurons will be active in both cases and hence their responses should be reduced during the test stimulus. However, when the orientation of the test stimulus differs from that of the adapting stimulus, this should evoke responses from a distinct population of neurons, which were not active during the adapting stimulus and hence should not have undergone adaptation. The effects of adaptation should therefore be greater for test stimuli of the same orientation as the adapting stimulus (i.e. adaptation will be orientation specific).

Conversely, if the presynaptic neurons are relatively non-orientation selective, the same adaptation mechanisms would lead to non-orientation specific adaptation, as the same population of presynaptic neurons would be activated by adapting/test stimuli of either orientation. Hence the current results could also be explained by adaptation of presynaptic neurons with low orientation selectivity (potentially including those within the LGN).

Deleterious Fatigue Hypothesis

Early adaptation (as assessed by the normalised response strength 2 seconds after stimulus onset) was greater during the non-preferred stimulus orientation than the preferred orientation (Figure 2.6J). This was seen for both Pyr and PV neurons. For PV neurons, this relationship was also seen in the responses to stimuli of different contrasts; high contrast stimuli (which elicited greater average firing rates) underwent less initial adaptation than lower contrast stimuli (Figure 2.7L). These findings appear to contradict the deleterious fatigue hypothesis, which predicts that those stimuli which drive the neuron most effectively will induce the greatest adaptation (Georgeson and Harris, 1984). However, later stages of adaptation (as measured by the response during the t_5-t_7 analysis window) showed the reverse pattern, with a greater decrease in responsiveness following the more effective adapting stimulus (Figure 2.10B). The reversal of this relationship between early and later stages of adaptation may indicate the firing rate during the latter portion of the adapting stimulus has a critical influence on the subsequent response to the following test stimulus.

Further support for the deleterious fatigue hypothesis can be seen when comparing responses across the population of neurons. Those neurons which responded most strongly during the adapting stimulus underwent the greatest reduction in responsiveness during the subsequent test stimulus (Figure 2.10D). However, interestingly, there was no significant correlation between the difference in firing rate during the preferred/non-preferred test stimulus and the difference in adaptation during the subsequent test stimulus (Figure 2.10E). This suggests the relationship between preceding firing rate and subsequent adaptation is subject to individual variation.

Stroud et al., also reported that the adaptation expressed by mouse V1 neurons displayed differing degrees of orientation specificity. They postulate that these differences may arise from variations in the local network, with orientation specific adaptation arising in regions in which the salt and pepper cortical map is biased towards a narrower range of orientations. However, their stimulus paradigm cannot not dissociate the influence of the relative orientation of the adapting/test stimuli from that of the effective drive of the adapting stimulus. Therefore it is difficult to determine if the range of orientation specificities observed are the result of individual differences in the rate-dependent intrinsic adaptation of the recorded neurons, or the synaptic inputs they receive.

Future experiments could attempt to characterise the rate dependency of adaptation in individual neurons over a range of adapting stimuli, and compare the parameters of this relationship to other physiological characteristics, such as orientation selectivity, F1/F0 ratios, response latency or network location. In such experiments it may be preferable to use adapting stimuli of differing contrasts rather than orientations as these stimuli should reduce the influence of network inhomogeneities and will elicit a range of activity levels, even in those neurons which exhibit relatively low orientation selectivity. It would also be interesting to compare adaptation during the test stimulus to the preceding subthreshold activity during the adapting stimulus. In order to establish the individual variability of intrinsic adaptation without the influence of network interactions, one could also compare the adaptation induced by a preceding current injection of different levels (c.f. Sanchez-Vives et al. 2000a).

Adaptation in PV and non-PV expressing neurons

Early adaptation (as assessed by the normalised response strength 2 seconds after stimulus onset) showed a significant dependence on cell type, with high firing PV neurons undergoing the greatest reduction in responsiveness. However, later stages of adaptation (as assessed by the response during the t_5-t_7 analysis window) did not vary across cell types.

The cell-type dependency of early adaptation would be expected to shift the balance of excitation and inhibition towards inhibition, and is in keeping with modelling predictions (Levy et al., 2013). Intriguingly, the inverse situation (greater adaptation of inhibition than excitation) is reported to occur in the barrel cortex (Heiss et al., 2008), potentially reflecting fundamental differences in the

mechanisms of adaptation between cortical areas (Chung et al., 2002). Similar results (the greater adaptation of inhibitory than excitatory conductances) have also been reported in mouse V1 (Tan et al., 2011), seemly in conflict with the current data. However, the accuracy of conductance measurements are limited by the filtering properties of dendritic processes and it is unclear how such conductances relate to the response properties of specific cell types.

A key caveat of these conclusions is the potential inclusion of non-PV expressing neurons within our PV population. Whilst the PV-Cre animals used have been shown to give a high fidelity of co-expression between conditional flexed reporters and parvalbumin in cortical layer 2/3, the labelling appears to be less precise in layer 5 (Hofer et al., 2011). Cortical dimpling during electrode entry creates uncertainty regarding the laminar position of our recordings, and inherent bias in the spike sorting procedure is likely to favour the inclusion of high spiking units from lower cortical layers (K. Harris, personal communication). Therefore, it is possible that some non-PV neurons have been falsely included in our PV population. Indeed, this could explain why the proportion of neurons identified as PV positive in the current study exceeds previous estimates (Markram et al., 2004; Gonchar et al., 2007).

The influence of cortical suppression on the expression of contrast adaptation

Suppression of cortical activity (via activation of PV neurons) was able to largely counteract adaptation for high contrast test stimuli, whilst it appeared relatively less effective for lower contrasts (Figure 2.16A&B). A comparison of the contrast response functions obtained following adaptation with and without LED illumination revealed that, while cortical suppression had a significant effect on response gain, it had little impact on contrast gain (Figure 12.16D&E). This suggests that cortical mechanisms of contrast adaptation primary influence response gain, and conversely that changes in contrast gain may primarily be inherited from the early visual system.

An alternative explanation is that LED illumination is directly altering cortical response gain, independently of any interaction with adaptation. Indeed, ongoing modulation of PV neuron activity and GABAergic transmission has previously been demonstrated to scale the responsiveness of V1 pyramidal neurons (Katzner et al., 2011; Atallah et al., 2012; Wilson et al., 2012). Therefore it is possible that by

driving the PV neurons during LED illumination we are causing them to adapt, and this reduction in inhibitory tone is responsible for the subsequent increase in pyramidal neuron responsiveness. While it is true that this may contribute to the observed change in response gain, there are several reasons to suggest it is unlikely to be the dominant effect. Key evidence that the LED illumination is interacting with the mechanisms of contrast adaptation is given by the fact that the effect of cortical silencing on the adapted response was proportional to the degree of adaptation that the neuron normally experienced (Figures 2.12F and 2.16F).

Furthermore, for the neurons recorded during Protocol 2, which examined the orientation specificity of adaptation, LED illumination was not associated with a significant change in Pyr or PV responsiveness when presented during the grey screen adapter (Figure 2.12E). For neurons recorded during Protocol 3, which tested the contrast specificity of adaptation, the situation is not as clear, as the non-adapted + LED condition was associated with both an increase in Pyr responsiveness and a decrease in PV responsiveness. However, PV activity was not significantly different during the adapted and adapted + LED conditions (Figure 2.16C). To investigate this further, the degree of adaptation experienced with/without LED illumination was compared by plotting both the adapted and adapted + LED conditions relative to their respective non-adapted controls (Supplementary Figure 2.1C). LED illumination significantly reduced the degree of adaptation experienced across all stimulus contrasts, providing further evidence of an interaction between LED-mediated suppression and cortical adaptation mechanisms.

Future directions

In an extension of the current findings, whole cell patch clamp recordings could be carried out in visually targeted V1 neurons. Use of this technique would enable the following experiments:

Comparison of adaptation in different classes of excitatory and inhibitory neurons

Whilst the current data indicate a significant difference in the initial adaptation exhibited by PV and Pyr neurons, the possible inclusion of false positives within both groups may confound results. Targeted patch clamp experiments in transgenic mice expressing fluorescent reporters in different cell types would enable visual and electrophysiological confirmation of cell type. Such visually guided recordings would

also give precise depth information, allowing comparisons of adaptation across cortical layers.

Ideally, voltage clamp recordings could also be made from Pyr neurons, in order to isolate and compare the adaptation of excitatory and inhibitory inputs. However, unfortunately, this method is limited by the cable properties of dendrites which lead to 'space-clamp' errors. The filtering properties of neuronal processes slow and attenuate the appearance of dendritic inputs recorded at the soma, and 'voltage escape' means the holding voltage is either incomplete or absent at the distal dendrites (Williams and Mitchell, 2008). There are two main approaches for separating excitatory and inhibitory conductances. By clamping the neuron at the reversal potential for excitatory/inhibitory currents, one can theoretically isolate the other conductance (e.g. Haider et al., 2010; Olsen et al., 2012). However, 'voltage escape' means that the voltage at the distal dentrites differs significantly from that imposed at the soma, allowing composite conductances at these locations to be mislabelled as solely excitation or inhibition. Alternatively, by recording at multiple voltages one can extrapolate the reversal potential of the measured current (Borg-Graham et al., 1998). This approach is also highly limited in terms of measuring the absolute values and temporal dynamics of conductances, however it may be able to provide an indication of the relative change in conductance during different stimulus conditions (Williams and Mitchell, 2008; Spruston and Johnston, 2008). As such, this method could potentially produce a coarse timecourse of evolution of excitatory and inhibitory conductances during adaptation (Heiss et al., 2008). Nonetheless interpretations may be complicated by differing cellular locations (and hence degrees of temporal filtering) of excitatory and inhibitory inputs.

Contrast adaptation of subcortical/intracortical inputs

Intracellular recordings during cortical silencing would also enable a comparison of contrast adaptation in subcortical and intracortical inputs. Recordings made during cortical silencing (via cortical cooling or optical suppression of Archaerhodopsin expressing neurons) can isolate subcortical inputs. These subcortical inputs can then be subtracted from the total inputs recorded during control conditions, in order to infer the properties of intracortical inputs (Lien and Scanziani, 2012). Using the current stimulus paradigm whilst silencing and recording during the test stimulus (following either a high contrast or grey screen adapter), should therefore enable a comparison of the adaptation of subcortical and intracortical inputs. By acquiring

contrast response functions with and without cortical silencing, one could also compare the contrast and response gain of the subcortical and intracortical inputs. However, it would be necessary to control for any intrinsic adaptation of the recorded neuron (i.e. conductance changes), as such effects would influence the appearance of both subcortical and intracortical inputs.

The same approach could also be used to compare subcortical and intracortical adaptation following stimuli of a longer duration. Studies in cat V1 have revealed shifts in orientation tuning following long term adaptation (Dragoi et al., 2000). Recently similar shifts in tuning preferences have also been observed in a minority of mouse V1 neurons following long term (12 minute) adaptation (Jeyabalaratnam et al., 2013). It would be interesting to establish whether this effect is purely cortical, or if a similar shift is also present in the subcortical inputs.

In order to avoid the potential confounds of activating inhibitory populations, for the aforementioned experiments cortical suppression could be achieved more directly by using transgenic animals expressing either halorhodopsin (Gradinaru et al., 2010) or Archaerhodopsin (Chow et al., 2010) in principal neurons.

CHAPTER 3: EFFECT OF ADAPTATION ON POPULATION CODING IN MOUSE V1

INTRODUCTION

As shown in the previous chapter, visual stimulation with high contrast gratings leads to a reduction in the responsiveness of individual V1 neurons. In this chapter we examined how network-wide adaptation affects population coding in V1. In order to induce widespread adaptation throughout V1, grating stimuli drifting in different directions were presented in a continuous sequence without interruption. By sequentially activating (and adapting) subsets of neurons with different preferred orientations, this protocol was predicted to cause an unbiased reduction in intracortical activity. Using 2-photon imaging of spike-related calcium signals (Hofer et al., 2011), we examined how such adaptation influences stimulus selectivity, reliability and correlations in populations of V1 neurons, and the resultant impact on population coding.

METHODS

Animals and surgical procedures

Experiments were performed on male and female C57Bl/6 mice, between postnatal day 29 and 40. All experimental procedures were carried out in accordance with institutional animal welfare guidelines and licensed by the UK Home Office.

Surgery and anaesthesia was carried out as described in Chapter 2. Briefly, animals were anaesthetised with a mix of fentanyl, metatomidine, and midazolam. The skull was exposed and a metal head plate was attached with dental cement. A craniotomy was made over the contralateral V1, based on stereotaxic coordinates. The dura was left intact and the cortex was kept moist with cortex buffer solution (125 mM NaCl, 5 mM KCl, 10 mM glucose, 10 mM HEPES, 2 mM MgSO4, and 2 mM CaCl2 [pH 7.4]), 50µl). Light anaesthesia was maintained during recordings by isoflurane (0.2–0.5%) in a 60:40% mixture of O2:N2O, delivered via a small nose cone. An adequate depth of anaesthesia was indicated by lack of response to toe pinch.

Dye loading and two-photon calcium imaging in vivo

For bulk loading of cortical neurons (Stosiek et al., 2003), the calcium-sensitive dye Oregon Green Bapta-1 AM (OGB-1 AM; Molecular Probes) was first dissolved in 4 µl DMSO containing 20% Pluronic F-127 (Molecular Probes), and further diluted (1/11) in dye buffer (150 mM NaCl, 2.5 mM KCl and 10 mM HEPES (pH 7.4)) to yield a final concentration of 0.9 mM. Sulphorhodamine 101 (SR101, 50 µM; Molecular Probes) was added to the solution to distinguish astrocytes from neurons (Nimmerjahn et al., 2004). The dye was slowly pressure-injected into the right visual cortex at a depth of 150–200 µm with a micropipette (3–5 MΩ, 3–10 psi, 2–4 min), under visual control by two-photon imaging (×10 water immersion objective, Olympus). After dye injection the cortex was sealed with 2% agarose in cortex buffer and a glass coverslip. Activity of cortical neurons was monitored by imaging fluorescence changes with a custom-built microscope and a mode-locked Ti:sapphire laser (Mai Tai, Spectra-Physics) at 830 nm through a ×40 water immersion objective (0.8 NA, Olympus). Scanning and image acquisition were controlled by custom software written in LabVIEW (National Instruments). The average laser power delivered to the brain was <50 mW.

Visual stimulation

Visual stimuli were generated using MATLAB Psychophysics Toolbox (Brainard, 1997; Pelli, 1997) and displayed on an LCD monitor (60 Hz refresh rate) positioned 20 cm from the left eye, at roughly 45 degrees to the long axis of the animal, covering ~105 × 85 degrees of visual space. At the beginning of each experiment, the appropriate retinotopic position in visual cortex was determined using small grating stimuli at 12 neighbouring positions. Only cortical regions in the monocular region of primary visual cortex were included in the analysis. The monitor was repositioned such that the preferred retinotopic position of most imaged neurons was roughly in the middle of the monitor. Calcium signals were measured in response to sequences of full-field grating stimuli.

Test stimuli consisted of square-wave gratings (0.035 cycles per degree, 2 cycles per second, 100% contrast) drifting in eight different directions, for a duration of 2 seconds each. Grating orientation was perpendicular to the direction of drift. Drift direction was sequentially increased in 225° steps, covering the full range from 0° (vertical ascending drift) to 360° (vertical ascending drift). During the continuous presentation condition, drifting stimuli of different orientations were

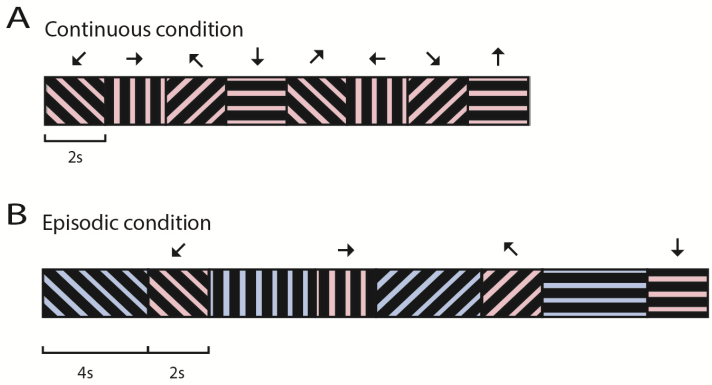

Figure 3.1. Schematic illustrating stimulus presentation dynamics.
A.) The "continuous" condition consists of grating stimuli of 2 second duration, drifting at 2 cycles/sec. The direction of drift increased in 225° intervals. B.) The episodic condition also consists of grating stimuli of 2 second duration, drifting at 2 cycles/sec, however, these stimuli are interspersed by 4 second stationary gratings of the same orientation as the following drifting grating. The same sequence of stimulus directions was used for both conditions. (Blue indicates stationary gratings, pink indicates drifting gratings).

shown sequentially as described above (Figure 3.1A). During the episodic condition, each drifting grating stimulus was additionally preceded by a stationary grating of the same orientation (4 seconds duration; Figure 3.1B). For both conditions, the stimulus set was repeated 6 times without interruption. During the continuous condition these 6 repetitions were preceded by an additional identical stimulus set which was not included in the analysis. This was done in an attempt to capture a steady state of adaptation. The sequence of stimulus orientations was kept constant over all repetitions.

Analysis of calcium signals

Two-photon imaging frames of 256×128 pixels were acquired at 7.6 Hz. After each recording, the focal plane and imaging position were checked and realigned with the initial image if necessary. Image sequences were aligned for tangential drift and analysed with custom programs written in ImageJ (NIH), MATLAB (Mathworks) and LabVIEW. Recordings with significant brain movements, vertical drift, or both were excluded from further analysis. Outlines of neurons recorded were semi-automatically defined using software written in MATLAB (Mathworks). All pixels within each ROI were averaged to give a single time course (ΔF/F), which was additionally highpass filtered at a cut off frequency of 0.02 Hz to remove slow fluctuations in the signal.

Spike trains were inferred from calcium signals using a fast non-negative deconvolution method that approximates the maximum a posteriori spike train for

each neuron, given the fluorescence observations (Vogelstein et al., 2010). Performance of the algorithm was tested by cell attached recordings performed simultaneously with calcium imaging (Hofer et al., 2011). Spike rates were inferred from spike probabilities according to the following equation: y=0.0028x+0.019. Inferred spike probabilities of 0.022 or less were typically not associated with actual spikes, and were therefore set to zero.

Data analysis

Analysis window

The neuronal responses to drifting stimuli were compared during the continuous and episodic presentation conditions. In order to avoid onset responses, the first 2 frames (corresponding to 264 ms) of each stimulus were discarded, and the response was taken as the mean calcium signal or inferred firing rate over the remaining 13 frames (1.72 second duration).

Selection criteria

For each neuron a one-way ANOVA was performed on the responses to the different stimulus orientations, averaged over all repetitions. Only neurons whose responses varied significantly across stimulus orientations ($p<0.05$) were considered to be responsive and were included in the analysis.

Response probability and activity sparseness

In order to calculate a neuron's response probability, its response to each stimulus was binarised, being classified as either active (if its firing rate exceeded zero) or inactive. The neuron's response probability for a given stimulus orientation was then defined as the mean binarised response across repetitions. Activity sparseness was defined as the proportion of neurons which were active during a given stimulus, averaged across all stimulus repetitions and orientations.

Trial-to-trial variability of individual neurons

The trial-to-trial variability of individual neurons was quantified as the coefficient of variation of the inferred spike rate during each stimulus repetition. If a neuron responded on 2 or more repetitions of a stimulus, its coefficient of variation was calculated as the standard deviation of the firing rate across repetitions, divided by the mean across repetitions. Neurons that failed to respond to the stimulus, or did so during only one repetition, were discarded when calculating this metric.

Trial-to-trial reliability of the population response

The Pearson correlation coefficient was computed between the population responses to each repetition of the stimulus set, for which each neuron's inferred firing rate during a given stimulus frame (13 analysis frames per stimulus orientation × 8 stimulus orientations × X neurons) was considered as an individual data point. Population reliability was defined as the average correlation coefficient across possible pairs of repetitions.

Stimulus selectivity of individual neurons

For individual neurons the stimulus selectivity was calculated based on the mean response to each stimulus orientation, averaged across all repetitions. From these average responses, the preferred stimulus was defined as the stimulus orientation and direction that gave the maximal response for that presentation condition (episodic/continuous).

The Orientation Selectivity Index (OSI) was calculated as:

$OSI = (R_{Pref} - R_{Orth}) / (R_{Pref} + R_{Orth})$

Where R_{Pref} is the inferred firing rate during the preferred stimulus and R_{Orth} is the average inferred firing rate during the orthogonal stimuli (those stimuli with a drift direction ±90° from the preferred stimulus).

The Direction Selectivity Index (DSI) was calculated as:

$DSI = (R_{Pref} - R_{Null}) / (R_{Pref} + R_{Null})$

Where R_{Null} is the inferred firing rate during the null stimulus (the stimulus with a drift direction 180° from the preferred stimulus).

Stimulus selectivity of population response

The population stimulus selectivity was calculated based upon the normalised firing rate responses of neurons within a given region. Neurons were grouped and aligned according to their orientation preferences to produce a "tuning curve" for each stimulus orientation (Busse et al., 2009). Each point on the curve represents the mean response of a subset of neurons with a given orientation preference. (Note that if there is an uneven distribution of orientation preferences within the population, the number of neurons contributing to each point in the tuning curve will vary). OSI and DSI were defined as detailed above, however in this case R_{Pref}, R_{Orth} and R_{Null} correspond to the average responses of different subsets of neurons:

R_{Pref}= average response of neurons whose preferred stimulus orientation is the same as the current stimulus.

R_{Orth}= average response of neurons whose preferred stimulus orientation is ± 90° from the current stimulus

R_{Null}= average response of neurons whose preferred stimulus orientation is 180° from the current stimulus

Correlations between neurons

The Pearson correlation coefficient was computed between the inferred firing rate responses of pairs of individual neurons. The inferred firing rate during each stimulus frame was considered as an individual data point, and responses across all orientations/repetitions were concatenated to give the full response of each neuron. The correlation between these full responses was then computed for all possible pairs of responsive neurons within a given imaging region. The total correlation for a given region was taken as the mean r value across all pairs of neurons for which there was a significant correlation ($p<0.05$) during at least one of the two stimulus conditions (episodic/continuous).

For a given stimulus, signal correlation was calculated as the correlation coefficient between the trial-averaged responses of each pair of responsive neurons. To calculate 'noise' correlation, the trial-averaged mean response was subtracted from the responses to each trail. Noise correlation was then calculated as the mean correlation coefficient between these mean-subtracted single-trial responses. Both signal and noise correlation measures were averaged over those cells for which the total correlation was significant during at least one of the two stimulus conditions (see above).

Decoding

Stimulus orientation/direction was decoded from population activity using the Euclidean distance metric, as described previously (Hofer et al., 2010; 2011). For each stimulus trial, the population response is represented as a point in multi-dimensional space (in which the responses of all neurons are given equal weighting). If distribution of the responses evoked by repetitions of the same stimulus is assumed to be Gaussian within that space, then the log likelihood that a response was evoked by a particular stimulus (assuming that all stimuli are equally

likely) is proportional to the square of its Euclidean distance from the average response for that stimulus.

For a given neuronal ensemble, decoding was performed as follows: 1) population response from a single trial of a single stimulus was removed from the full set of responses from all trials of all stimuli. 2) The removed trial was blindly assigned to the stimulus for which the trial-average-response was closest (in terms of Euclidean distance) to its own response, giving either a correct or incorrect judgement. 3) This process was repeated for all trials of all stimuli in order to calculate the decoder performance, defined as the percentage of correct judgements.

In order to compare how decoder performance varied across neuronal ensembles of increasing size, 500 ensembles of each size were randomly selected from the total population of responsive neurons across all imaging regions (n= 487), to give the mean and standard deviation of performance (Figure 3.8A). Note that as ensemble size approaches that of the total population, standard deviation will be limited, as the different ensembles will share an increasing proportion of neurons.

When comparing decoding performance across regions, values correspond to the mean performance of 200 randomly selected ensembles of 20 neurons taken from a given region (Figure 3.8B). In order to control for differences in performance levels between regions, equal representation was achieved in a two-step procedure by first randomly selecting 20 neurons from each region, and then randomly selecting a neuronal ensemble of a given size from this composite pool. This procedure was repeated 200 times for each ensemble size, to give a mean and standard deviation of decoding performance (Figure 3.8C).

Normalisation

To assess the response transformation between conditions, responses were first normalised across the population. For each neuron, responses across all conditions and stimulus orientations/directions were set between 0 and 100. For example, when comparing the responses during episodic and continuous presentation conditions the total number of conditions is 16 (8 stimulus directions × 2 conditions). For one of these conditions (n), the normalised response is calculated as:

$Rnorm_n = ((R_n - R_{min})/(R_{max}+R_{min}))\times 100$

Where Rmax and Rmin are the maximum and minimum across all 16 conditions.

Statistics

As described in Chapter 2, for all statistical comparisons normality was tested using a 2-sided Shapiro-Wilk test. Where the assumption of normality was violated, non-parametric analysis was used.

When comparing the responses of the same neurons across multiple conditions, where the number of conditions was greater than two, the effect of conditions was first assessed by a repeated measures ANOVA (or Friedman's non-parametric repeated measures ANOVA). If significant ($p<0.05$), this was followed by pairwise t-tests (or Wilcoxon signed-rank paired comparisons).

When comparing responses across multiple groups of neurons, the effect of group was first assessed by an ANOVA (or the Kruskal-Wallis non parametric ANOVA). If significant ($p<0.05$), this was followed by pairwise t-tests (or Wilcoxon rank-sum comparisons).

Where applicable, multiple comparisons were corrected for using the sequential Holm-Sidak correction (reviewed by Abdi, 2010). Unless otherwise specified error bars indicate mean ± standard error of the mean (S.E.M).

RESULTS

The aim of the study was to investigate how adaptation to dynamic grating stimuli influences population coding within V1. Two-photon calcium imaging was used to record the responses of neuronal populations in layer 2/3 of mouse V1, during continuous (adapted) and episodic (control) stimulus conditions.

During the continuous condition, grating stimuli (2 second duration) were shown successively drifting in different directions without interruption (Figure 3.1). This stimulation protocol was used to induce generalised adaptation across the V1 network. Responses evoked during the continuous condition were compared to those evoked during an episodic condition, consisting of an identical sequence of drifting gratings, interspersed with stationary gratings of 4-second duration (Figure 3.1; see methods). The stationary gratings, which themselves evoke minimal

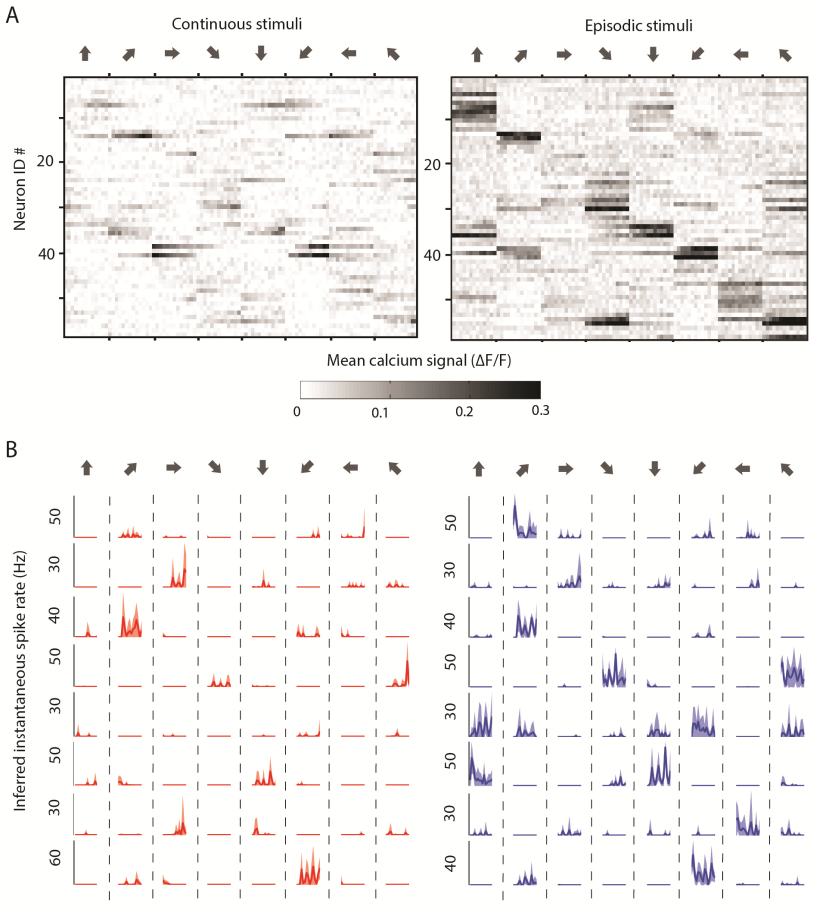

Figure 3.2. Example population responses
A.) Mean calcium signals of an example population of 59 neurons (pre-exclusion) during 6 repetitions of continuous (left panel) and episodic stimuli (right panel). Stimulus drift direction is indicated by arrows. B.) Inferred instantaneous firing rate of 8 example neurons during continuous (red) and episodic (blue) stimuli of 2 second duration. Stimulus drift directions are indicated by arrows. Thick line and shading represent mean ± standard deviation over 6 repetitions.

activity, were included to provide a recovery period between dynamic stimuli. There was no apparent response difference if the drifting grating periods were separated by a grey screen instead of a standing grating in the episodic condition (data not shown).

Recordings were made from 14 imaged regions (11 animals), each containing between 27 and 60 neurons. Of these neurons, analysis was restricted to those that were reliably responsive to the grating stimuli during at least one of the two presentation conditions (52 to 83% neurons per region, Supplementary Figure 3.1A). (Neurons were classified as responsive if their inferred firing rate varied significantly across stimuli of different orientations, ANOVA).

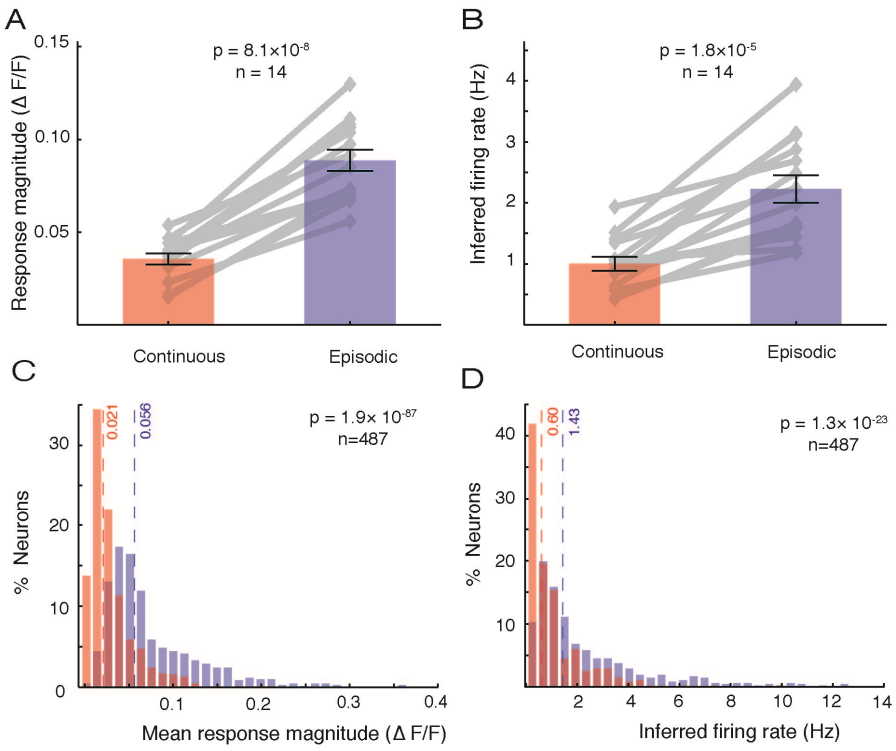

Figure 3.3 Response magnitude of individual neurons
A.) Mean amplitude of calcium signal (ΔF/F) during stimuli of preferred direction, averaged across all responsive neurons within each imaging region. (Error bars: mean ± S.E.M.) B.) As for A, for mean inferred firing rate. Inferred firing rate was derived from calcium signal using a spike extraction algorithm (Vogelstein et al., 2010). C.) Distributions of mean calcium signal amplitude of the entire population of responsive neurons across all imaging regions, during the preferred stimulus direction, within continuous (red) and episodic (blue) stimulus conditions. Dotted lines and corresponding values indicate population medians. Significance test: Kolmogorov-Smirnov. D.) As for C, for mean inferred firing rate.

Individual neuron response magnitude

Initially we assessed how adaptation influenced the response properties of individual neurons.

As seen in Chapter 2, adaptation to continuously drifting stimuli significantly reduced neuronal responsiveness (see Figure 3.2 for the responses of an example region). Across the imaging regions the mean calcium signal evoked by the neuron's preferred stimulus direction was 0.036 ΔF/F during the continuous condition, compared to 0.089 ΔF/F during the episodic condition (p= 8.1×10-8, Figure 3.3A). Consequentially, the inferred firing rate (obtained by a de-convolution spike extraction algorithm– Vogelstein et al., 2010) was also lower during the continuous condition (1.0 ± 0.12 Hz versus 2.2 ± 0.22 Hz; p= 1.8×10-5, Figure 3.3B). The difference in response strength was even more significant when

considered across the entire population of responsive neurons (n= 487, pooled across all imaging regions, Figure 3.3C&D). Thus adaptation to continuously drifting stimuli reduced the responses of individual neurons, both in terms of the calcium-based florescence signal and inferred firing rate, by more than 50% relative to the control condition.

Individual neuron trial-to-trial variability

In Chapter 2 we reported that 3.5 seconds of adaptation caused a significant reduction in trial-to-trial response reliability, although this effect was somewhat variable across the population (Figure 2.8E). We sought to corroborate this finding using two-photon calcium imaging in L2/3, by assessing response variability during the continuous and episodic conditions.

The probability with which a neuron responds to a given stimulus trial provides a straightforward measure of response consistency. If the neuron responds consistently, either on every repetition or none of the repetitions the response probability will be 1 or 0, respectively. As with overall response strength, adaptation appeared to reduce response probability; response probability for the neuron's preferred stimulus was significantly lower during the continuous than the episodic condition (0.64 ± 0.03 versus 0.88 ± 0.02, p= 1.7×10-5, Figure 3.4A). Again this effect was seen more clearly when considering the entire population of responsive neurons, for which the median response probability during the continuous condition was 0.66 (responding on 4 out of

6 repetitions) versus a median response probability of 1 (responding on every repetition) during the episodic condition (n= 487, p= 4.2×10-43, Figure 3.4B). As only the preferred stimulus orientation was considered for this analysis, there were no neurons with a response probability of 0. Hence the reduction in response probability cannot be explained by an increase in the proportion of neurons regularly failing to respond, but instead indicates a reduction in response consistency.

Correspondingly, trial-to-trial variability, quantified by the coefficient of variation of the inferred spike train, was greater during the continuous than the episodic condition (1.19 ± 0.04 versus 0.78 ± 0.05, p= 3.2×10-5, Figure 3.4C). This was also true across the entire population (median= 1.40 versus 1.12; p= 1.8×10-8, Figure. 3.4D).

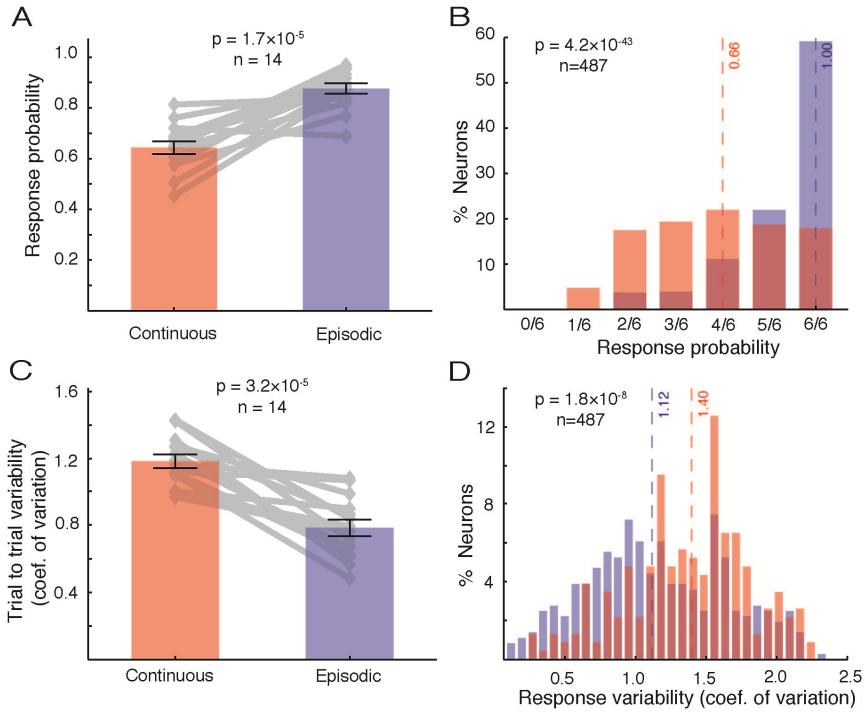

Figure 3.4. Trial-to-trial variability of individual neurons
A.) Response probability over 6 repetitions of the preferred stimulus, averaged across all responsive neurons within each imaging region. (Error bars: mean ± S.E.M.). B.) Distributions of the response probability of the entire population of responsive neurons during the preferred orientation of continuous (red) and episodic (blue) stimuli. Dotted lines and corresponding values indicate population medians. Significance test: Kolmogorov-Smirnov. C.) Trial-to-trial variability of inferred spike rate responses to the preferred stimulus, averaged across all responsive neurons within each imaging region. Trial-to-trial variability was calculated as the coefficient of variation of the inferred spike rate across all repetitions. D.) As for B, for trial-to-trail variability.

Together, these data indicate that adaptation to continuously presented stimuli reduces the consistency of V1 neurons' responses. As the consistency with which a neuron responds to a given stimulus is a key determinant of the information that it conveys (Grewe et al., 2007), such an effect may limit the information capacity of individual V1 neurons when they are adapted.

Individual neuron stimulus selectivity

We additionally compared how adaptation to continuously drifting stimuli influences the neurons' stimulus selectivity. By sequentially activating (and adapting) different neuronal subpopulations without bias for any stimulus direction, the continuous stimulus condition was expected to equally reduce intracortical activity across all stimuli. However, it was unclear how this generalised reduction in intracortical activity would interact with individual neurons' stimulus preferences.

The orientation and direction selectivity of individual neurons was quantified using their respective selectivity indices (see methods). When considered across regions, orientation selectivity (OSI) was not significantly different during the continuous and episodic conditions (continuous OSI: 0.80 ± 0.01; episodic OSI: 0.76 ± 0.03, p= 0.06, Figure 3.5C). Across the entire population of responsive neurons however, OSI was slightly greater during the continuous condition than the episodic condition (continuous median = 0.89, episodic median= 0.83, p= 1.0×10-4, Wilcoxon paired comparison, Figure 3.5D). Direction selectivity (DSI) on the other hand was significantly greater during the continuous condition, both across regions (continuous DSI: 0.66 ± 0.02; episodic DSI: 0.51 ± 0.02, p= 1.2×10-4, Figure 3.5E) and across all neurons in the population (continuous median = 0.73, episodic median= 0.50, p= 1.1×10-16, Figure 3.5F). Adaptation therefore appears to increase the neurons' preference for a particular stimulus direction whilst orientation preference remains relatively constant.

Taken together, adaptation during dynamic stimuli appears to have a strong influence on the response strength, reliability and direction selectivity of individual V1 neurons. We next asked how these differences in the response properties of single neurons affect sensory representations across the population as a whole.

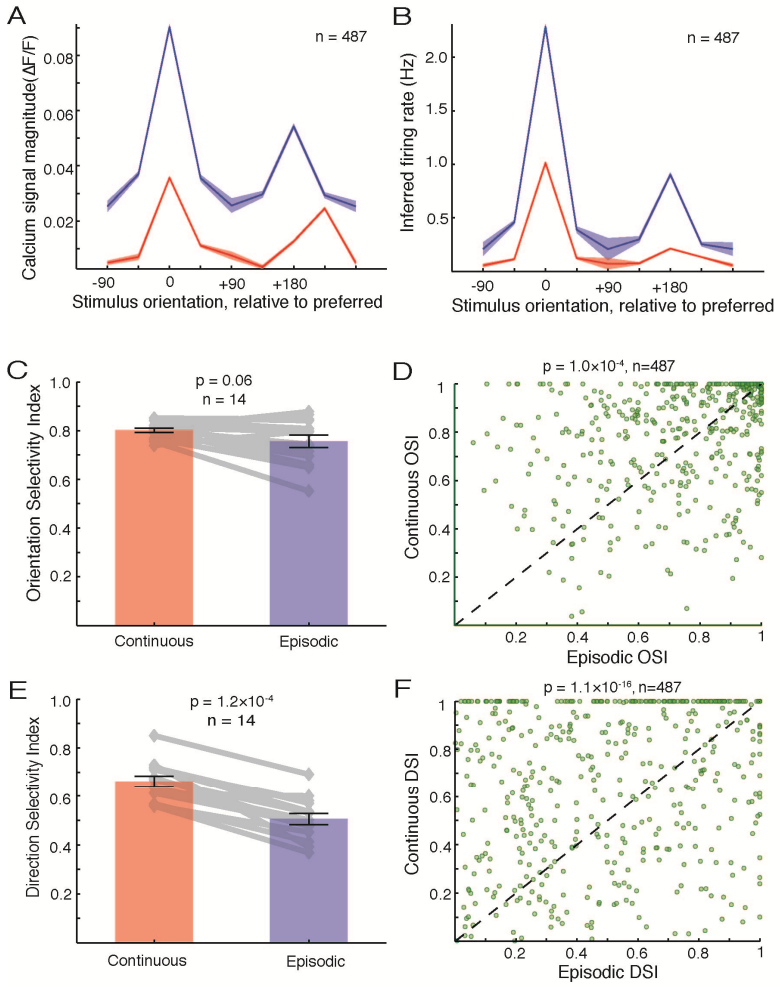

Figure 3.5. Stimulus selectivity of individual neurons
A.) Calcium signal amplitude across stimulus orientations for all responsive neurons, during continuous (red) and episodic (blue) stimuli. (Thick line and shading represent mean ± S.E.M). B.) As for A, for mean inferred firing rate. C.) Mean Orientation Selectivity Index (OSI), averaged across all responsive neurons within each imaging region. (Error bars: mean ± S.E.M.) D.) The OSI values of the entire population of responsive neurons during episodic and continuous stimulus conditions. Line of unity (where points would fall if a neuron exhibits no change in selectivity between conditions) is represented by the dashed line. Significance was computed using the Wilcoxon signed-rank test. E.) As in C, but for mean Direction Selectivity Index (DSI). F.) As in D, but for DSI values.

Population trial-to-trial reliability

At a population level, the trial-to-trial reliability of an imaged region was assessed by comparing the inferred spike trains of all responsive neurons across stimulus repetitions (see methods). The mean correlation coefficient between the different repetitions was significantly lower during the continuous condition (0.14 ± 0.02) than the episodic condition (0.23 ± 0.02, p= 3.5×10-4, Figure 3.6A). Thus, as expected from the reduced response reliability of individual neurons, adaptation also reduced the reproducibility of V1 population responses.

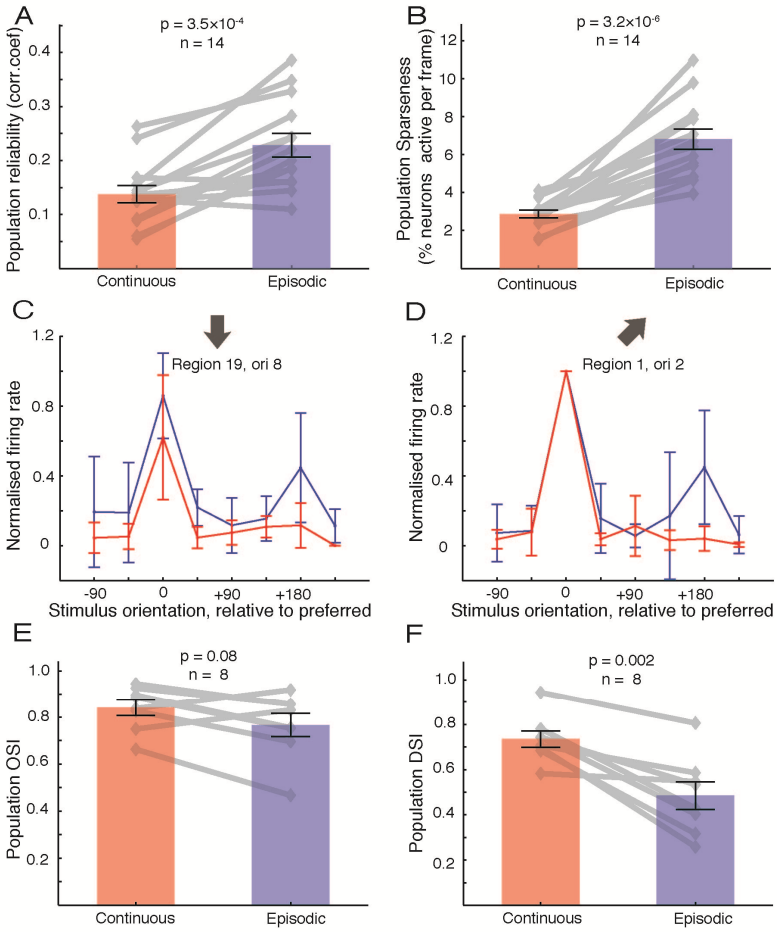

Figure 3.6 Trial-to-trial reliability and stimulus selectivity of population responses
A.) Population trial-to-trial reliability for each imaging region. Population reliability was defined as the mean correlation coefficient of the population response (spike trains of all responsive neurons within a region), between all stimulus orientations/repetitions (see text for details). B.) Population sparseness for each imaging region (percentage of all neurons within each imaging region that are active during a single stimulus presentation). Data are averaged across all stimulus orientations. C & D) Population tuning curves of two example regions during episodic (blue) and continuous (red) stimuli (see text for details). Stimulus drift direction as indicated by arrow (stimulus orientation is perpendicular to drift direction). E.) Population OSI across the 8 regions containing neurons covering the full range of orientation preferences F.) As for E, for Population DSI. (Error bars: mean ± S.E.M.).

Selectivity of population responses

Adaptation was associated with an increase in the direction (and to a lesser extent orientation) selectivity of individual neurons during the continuous condition. In order to assess the stimulus selectivity of the population responses, population tuning curves were obtained for each stimulus orientation during the two conditions (see example regions in Figure 3.6C&D). Neurons were binned by their orientation preference and their mean response to a given stimulus orientation was plotted as a function of the difference between this orientation and their own preferred orientation (see methods, (Busse et al., 2009). Such curves are equivalent to

vertical sections through the response map shown in Figure 3.2A, whilst the tuning curves of individual neurons (the average of which is shown in Figure 3.5B) are equivalent to horizontal sections. Tuning curves were obtained from those regions containing neurons with orientation preferences spanning the entire stimulus set (8/14 regions) and OSI and DSI of each curve was calculated as for individual neurons (see methods). The population OSI (averaged over all stimulus orientations) was not significantly different during the continuous and episodic conditions (continuous OSI: 0.84 ± 0.03; episodic OSI: 0.77 ± 0.05, p= 0.08, Figure 3.6E). However, in keeping with the findings for individual neurons, the population DSI was significantly greater during the continuous condition (continuous DSI: 0.74 ± 0.04; episodic DSI: 0.48 ± 0.06, p= 0.002, Figure 3.6F). Hence adaptation increases the direction selectivity of both single neurons and the population response.

Population sparseness (proportion of neurons active per stimulus)

Population sparseness describes the distribution of activity across a population; the smaller the fraction of neurons active per time window, the greater the sparseness of the representation. Sparse coding improves metabolic efficiency (Levy and Baxter, 1996; Lennie, 2003), and confers several computational advantages (as reviewed by (Olshausen and Field, 2004). A simple measure of population sparseness is 'activity sparseness'— the proportion of neurons that are active during a given stimulus. As for population selectivity (described above), activity sparseness corresponds to the activity of neurons within a vertical section of the response map in Figure 3.2A. However, whilst population selectivity considers the absolute firing rates and orientation preferences of the neurons, activity sparseness simply considers them as either active or inactive. In agreement with the effects on population selectivity, continuous stimulation was associated with an increase in activity sparseness (i.e. a decrease in the fraction of neurons active during the continuous condition: 2.9 ± 0.2%, versus 6.8 ± 0.5% during the episodic condition, p= 3.2×10-6, Figure 3.6B).

Correlations between neurons

Another measure related to population sparseness is the correlation between the responses of individual neurons. If two neurons share the same stimulus preference (or are both subject to the same stimulus-independent drive), they will be co-active at the same time (decreasing population sparseness) and their responses will be

more strongly correlated. The response of each neuron in such a pair provides roughly equivalent information about the stimuli, so little is gained by observing the responses to both (i.e. there is redundancy in their responses). Networks in which the average pairwise correlation is high, consequentially exhibit greater redundancy, and are therefore less metabolically efficient (providing less information per action potential) than those that are relatively decorrelated (Levy and Baxter, 1996; Laughlin et al., 1998; Attwell and Laughlin, 2001; Lennie, 2003).

Similar to the results in Chapter 2, adaptation appeared to reduce the correlation between neurons; across the imaging regions total pairwise correlations were smaller during the continuous condition (0.05 ± 0.003) than during the episodic condition (0.07 ± 0.007, p= 6.1×10-4, Figure 3.7B). Therefore, while more neurons are active during the episodic condition, there is also greater similarity, and hence redundancy, in their responses. As in Chapter 2, we decomposed total correlation into 'signal' and 'noise' components. Signal correlation was defined as the correlation between the neuron's mean responses, averaged across all repetitions in order to remove noise, while noise correlation was defined as the correlation between the mean-subtracted single-trial responses (see methods). As with the total pairwise correlation, signal correlations were smaller during the continuous condition than the episodic condition (continuous: 0.03 ± 0.004; episodic: 0.06 ± 0.014, p= 6.7×10-3, Figure 3.7C). Noise correlations were more similar during the two conditions, again being slightly smaller during the continuous condition (continuous: 0.010 ± 0.001; episodic: 0.013 ± 0.002, p= 0.01, Figure 3.7D). This suggests that the reduction in total pairwise correlations during the continuous condition is primarily a result of decorrelation of the stimulus dependent response, rather than a change in shared noise or stimulus independent drive.

Hence, the adaptation induced by continuously drifting gratings reduces the reliability, and increases the sparseness and decorrelation of V1 responses. Given the divergent implications of these effects for information coding, we next asked how adaptation influences the network's ability to differentiate between stimuli.

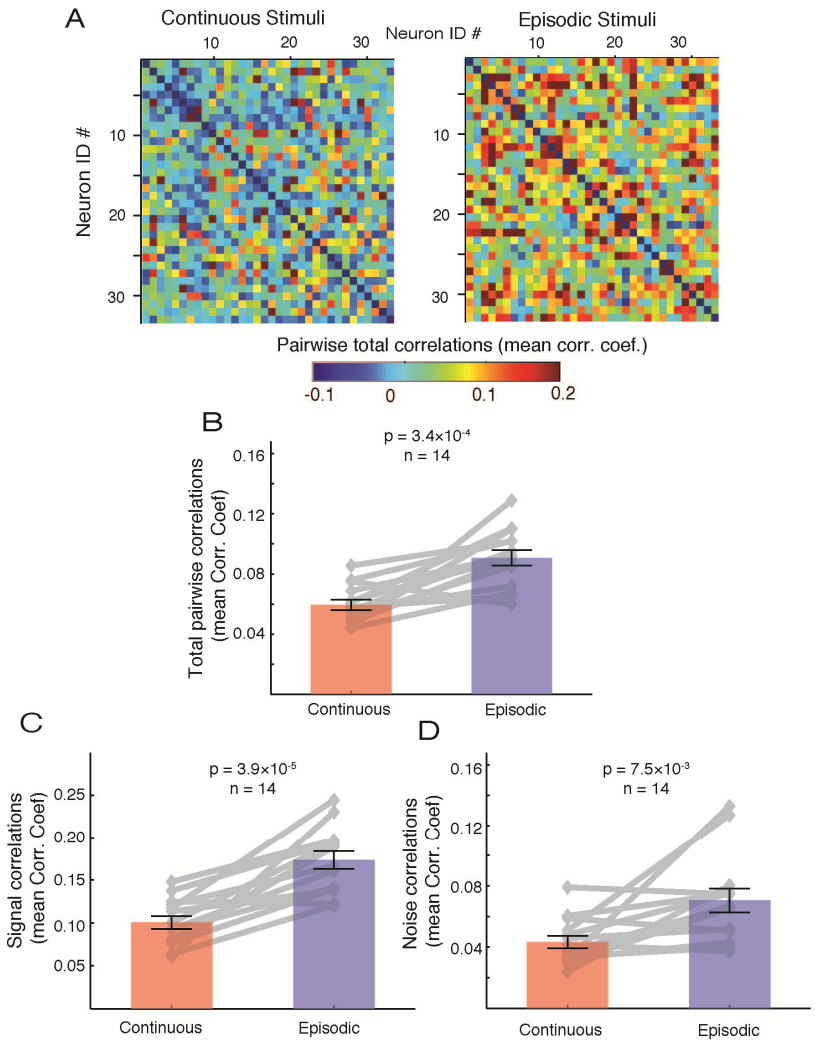

Figure 3.7. Pairwise correlations between neurons
A.) Correlation coefficients between all selected* pairs of neurons within an example imaging region, averaged across all repetitions of continuous (left panel) and episodic stimuli (right panel). B.) The mean total correlation coefficient across all selected* pairs of neurons within each imaging region. (Error bars: mean ± S.E.M.) C.) The mean signal correlation coefficient (see text) across all selected* pairs of neurons within each imaging region. D.) The mean noise correlation coefficient (see text) across all selected* pairs of neurons within each imaging region. * Analysis was restricted to pairs of responsive neurons for which there was a significant correlation between responses during at least one stimulus condition. (Error bars: mean ± S.E.M.)

Decoding performance

The network's ability to differentiate stimulus orientation or direction was assessed using a decoding algorithm based on the Euclidean distance metric of the multi-dimensional population response (see methods). This distance metric was used to determine the putative identity of an unknown stimulus, by comparing the population response it evoked with those evoked by other known stimuli. The algorithm's performance was compared during both continuous and episodic conditions, and by

incorporating the responses of an increasing number of responsive neurons, which were randomly selected across all imaging regions (see below).

For both episodically and continuously drifting stimuli, discrimination performance increased with neuronal ensemble size (Figure 3.8A). However, for smaller ensemble sizes (<300 neurons), this relationship was considerably shallower for continuous stimuli, with smaller increases in performance for each additional neuron included (maximum performance improvement rate: 0.8% per neuron during continuous condition versus 1.7% per neuron during episodic condition). This difference in gradient is likely related to the relatively low reliability of individual neurons during the continuous condition; each neuron provides comparatively less information than during the episodic condition. As ensemble size increases beyond ~100 neurons the relationship begins to plateau for episodic stimuli, with each additional neuron providing a smaller increase in performance. On the other hand for continuously presented stimuli performance does not plateau until the ensemble size reaches ~ 300 neurons. This disparity is likely to reflect the greater redundancy between neurons during the episodic condition; the similarity of their responses reduces the additional information that can be gained by observing more neurons. Note however that we only tested discrimination between 8 stimulus directions, which is a relatively trivial task for the network.

Ultimately, high discriminatory performance (>95% correct) can be achieved during both conditions, however a relatively larger number of neurons is required to reach this performance level during the continuous condition (~350 neurons during the continuous condition versus ~150 neurons during the episodic condition). Note these theoretical neuronal ensembles were comprised of only responsive neurons (see selection criteria detailed in methods), which were randomly selected across all imaging regions. Assuming that on average 70% of neurons within a region are responsive, the performance levels in Figure 3.8A reflect those of a neuronal population of approximately 1.4 times the stated ensemble size. This implies that a neuronal population of approximately 500 neurons should be sufficient to accurately decode either stimulus condition. Given the cortical magnification factor of mouse V1 (Schuett et al., 2002) and the reported neuronal density/thickness of layer 2/3 (Schüz and Palm, 1989), the number of neurons in this region that could potentially respond to current stimuli is likely to be nearly 2 orders of magnitude greater than this.

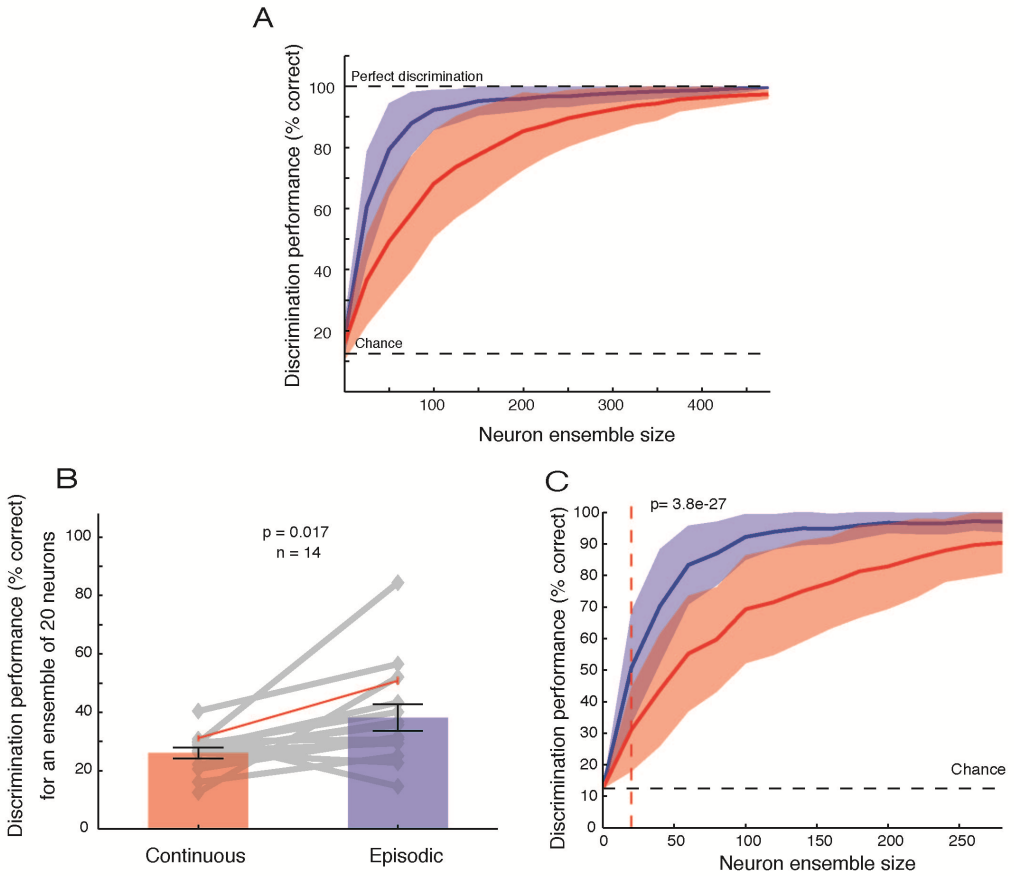

Figure 3.8. Population stimulus discrimination
A.) Stimulus decoder performance for neuronal ensembles of increasing size, during continuous (red) and episodic (blue) conditions (see text for details). Lines and shading indicate mean ± standard deviation across 500 randomly selected ensembles of each size. B.) Comparison of average decoder performance for a neuronal ensembles of 20 neurons during continuous (red) and episodic (blue) stimulus conditions. Grey lines show data from the 14 regions. Red line indicates average decoding performance of an ensemble of 20 neurons randomly selected from a combined pool of responsive neurons, containing an equal representation of 20 neurons from each region. (Error bars: mean ± S.E.M.) C.) As for A, when drawing neuronal ensembles from a combined pool of neurons containing an equal representation of 20 neurons from each region. Lines and shading indicate mean ± standard deviation across 200 randomly selected ensembles of each size. Red vertical line indicates the performance levels for an ensemble of 20 neurons (as also shown by red line in B). *P* value corresponds to a Wilcoxon rank sum test of the equality of median performance levels across stimulus conditions for an ensemble of 20 neurons.

Therefore the decorrelation and reduced reliability associated with adaptation appear to alter the coding strategies implemented within V1. Whilst accurate discrimination can be achieved during both conditions, the relatively dispersed representation during the continuous condition will require observation of a larger neuronal population in order to reach a similar level of performance to that seen during the episodic condition. However in practice, given that the spatial extent of the stimuli is fixed for both conditions, the neuronal population that represents them is assumed to remain constant.

For the preceding analysis, theoretical neuronal ensembles were created by randomly selecting responsive neurons from any region. In Figure 3.8B, we additionally compared the decoding performance across the individual regions. As each region contained a different number of responsive neurons, we were limited to an ensemble size of 20 neurons (the lowest total number of responsive neurons in a given region). For each region the average decoding performance of an ensemble of 20 neurons was compared during continuous and episodic conditions (see Methods). While a range of performance levels was observed across individual regions (likely due to differences in anaesthesia levels and preparation condition), there was also a significant effect of stimulus condition, with higher decoding performance during the episodic condition ($p= 0.017$, Figure 3.8B).

Given that different regions contained different numbers of responsive neurons, their relative contribution to the random neuronal ensembles in Figure 3.8A also varied. Therefore we repeated this analysis, by including only 20 neurons per region in order to ensure equal representation (see Methods). This restriction limited the maximum ensemble size to 280 neurons (20 neurons × 14 regions), however, the general trend remained, with a steeper increase and earlier plateau of decoding performance during the episodic condition than the continuous condition (Figure 3.8C). As seen for the individual regions, for a ensemble of 20 neurons randomly selected across the regions, decoding performance was significantly greater during the episodic condition than the continuous condition ($p= 3.8 \times 10\text{-}27$).

Gain modulation

The findings of Chapter 2 indicate that, for high contrast stimuli, adaptation primarily caused a reduction in response gain (an effect that appeared to be cortically mediated). In order to assess the nature of response modulation elicited by the current protocol, we compared the relative firing rates during the continuous and episodic conditions, across all stimulus directions.

If adaptation reduced the responses to all stimuli by an equal amount, this would cause a subtractive shift in the neuron's tuning curve, and a decrease in the intercept of the linear relationship between conditions (Figure 3.9C&D). Alternatively, if adaptation divided the responses by a constant amount, this would shrink the neuron's tuning curve, and reduce the gradient of the linear relationship between conditions without affecting its intercept (Figure 3.9A&B). If, as in Chapter

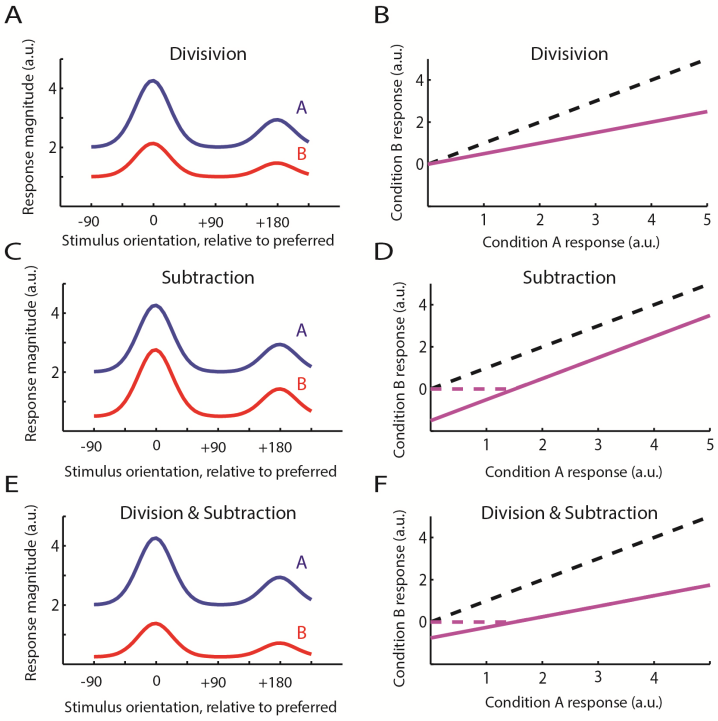

Figure 3.9 Schematic of different modes of linear gain transformations
A & B.) A divisive scaling of tuning curve results in a reduction of the slope of the relationship between the condition A and condition B, without a change in intercept. C & D.) A subtractive shift in the tuning curve results in a decrease in the intercept of the relationship between the condition A and condition B, without a change in the slope. E & F.) A combination of divisive scaling and a subtractive shift will result in reduction of both the intercept of the relationship between the condition A and condition B, and its slope. However, as illustrated by the dotted lines in D and F, firing rate rectification may cause subtractive shifts to appear divisive when initial firing rates are low.

2, adaptation primarily affects response gain, we would expect to see evidence of a divisive scaling of responses between the episodic condition and continuous conditions.

Of the 487 neurons that met the selection criteria (see above), 401 neurons (82%) gave their maximal responses during the episodic condition. The following analysis was restricted to these neurons. For each neuron, the normalised inferred firing rates during the episodic and continuous conditions were plotted against each other (see Figure 3.10D for the responses of 2 example neurons).

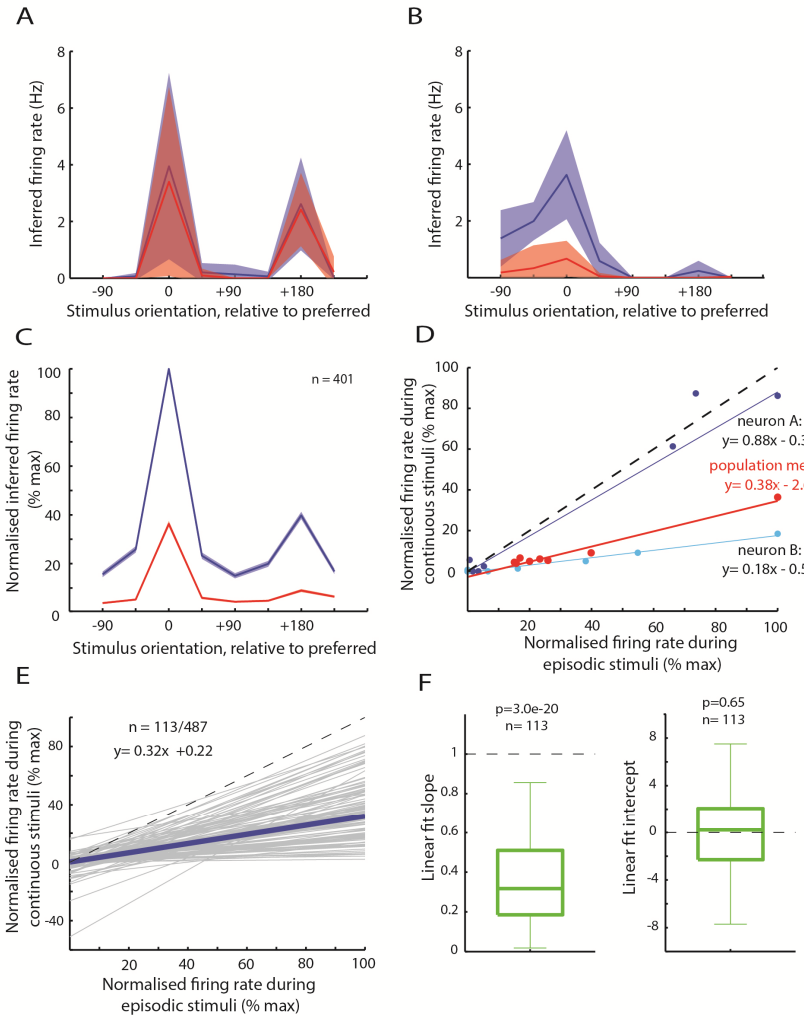

Figure 3.10. Linear gain transformation
A & B) Normalised inferred firing rate across stimulus orientations for 2 example neurons, during continuous (red) and episodic (blue) stimuli. (Thick line and shading represent mean ± S.D. over repetitions). C) Normalised inferred firing rate across stimulus orientations for entire population of responsive neurons (n= 487, Thick line and shading represent mean ± S.E.M.). D) Normalised firing rate responses to episodic (x-axis) and continuous stimuli (y-axis). Dashed line indicates line of unity, (where points would fall if a neuron exhibits no change in firing rate between conditions). Dark/light blue points and fit lines correspond to responses of neurons shown in A and B respectively. Red points and fit line correspond to population mean values, as shown in C. E.) Fit lines for all neurons that displayed a significant linear relationship between their non-zero responses to episodic and continuous stimuli. Blue line indicates median slope and intercept across these neurons. F.) Distribution of slopes and intercepts of fit lines shown in E.

As illustrated in Figure 3.9, firing rates inferred from calcium signals cannot fall below zero, and any subtractive shift in the responses during the two conditions could be masked by this flooring effect. Therefore only non-zero responses were considered for the current analysis. 113 out of 401 neurons displayed a significant linear correlation between their non-zero responses to the two conditions (Figure 3.10E). The median intercept (0.79) across these neurons was not significantly different from 0 (p= 0.65, Figure 3.10F), however the median slope (0.32) was

significantly less than 1 ($p = 3.0 \times 10^{-20}$, Figure 3.10F). As illustrated in Figure 3.9, this indicates that responses are divisively scaled between conditions. Therefore, in keeping with Chapter 2, adaptation appears to reduce V1 response gain.

While only a subset of neurons was included in the current analysis, the generality of divisive scaling is indicated by the responses across the population of neurons. For all 401 neurons that gave their maximal responses during the episodic condition, the firing rate during the preferred stimulus orientation was compared between episodic and continuous conditions. When responses during the continuous condition were plotted as a function of those during the episodic condition, the parameters of the linear relationship across neurons showed a markedly similar scaling to that seen in individual neurons, with a roughly three-fold reduction in firing rate (Supplementary Figure 3.1E).

The notion of divisive scaling initially appears to be at odds with the increased direction selectivity observed during the continuous condition; if responses to all stimuli are proportionally scaled this should have no impact on orientation/ direction selectivity indices. However, as illustrated in Figure 3.11A, this discrepancy can be explained by response rectification. Response rectification when combined with low trial-to-trial variability creates a 'response floor' below which even non-zero values become insignificant (when the average firing rate is greater than zero but response probability is low). If the responses during Condition A are sufficiently elevated above zero (and response probability is sufficiently high), divisive scaling will lead to a proportional reduction across all stimuli during Condition B, with no change in selectivity. However if divisive scaling reduces responses to the floor level, this will cause selectivity to increase.

In the current data, adaptation was associated with an increase in direction selectivity but not orientation selectivity (when compared across imaging regions). This can potentially be explained by the difference in the response probability for orthogonal and null stimuli during the episodic condition, and hence their relative proximity to the floor (see Figure 3.11B). Even during the episodic condition, many neurons failed to respond to orthogonal stimuli. As their responses are already 'floored', and cannot be reduced further during the continuous condition, their OSI remains constant at a value of 1. However, the majority of neurons do respond to the null stimulus during the episodic condition. During the continuous condition,

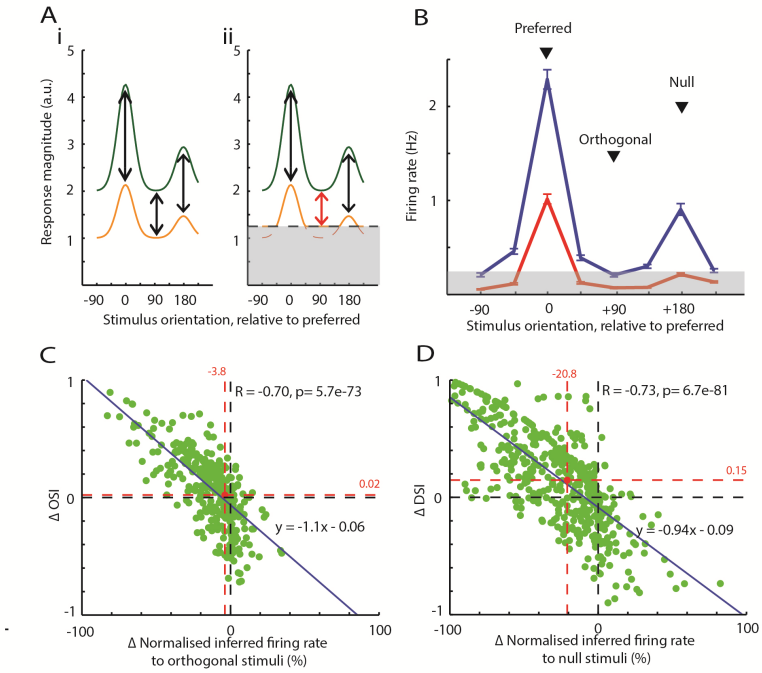

Figure 3.11. Schematic showing influence of the 'response floor'
A.) The effect of a response "floor" on stimulus selectivity. i) In the absence of a response floor (or if responses are sufficiently elevated above it), divisive scaling will not affect stimulus selectivity, as responses to all stimulus orientation are reduced by the same proportion. ii) If divisive scaling causes some responses to reach floor levels (as shown here for orthogonal stimuli) this will limit the reduction observed for this orientation relative to that seen at the preferred orientation, leading to an increase in selectivity (in this case OSI). B.) Mean firing rate across stimulus orientations for all responsive neurons, during continuous (red) and episodic (blue) stimuli (error bars: ± S.E.M). If responses <0.25 Hz are considered to be "floored" (as indicated by gray background), responses to orthogonal stimuli are already floored during the episodic condition, leaving little room for further reduction (i.e. change in OSI) during the continuous condition. Responses to null stimuli however are above floor during the episodic condition but are reduced to floor levels during the continuous condition, increasing DSI. C.) The change in OSI during the continuous condition relative to the episodic condition, as a function of the change in the normalised inferred firing rate to orthogonal stimuli. Red dotted lines indicate population medians. D.) The change in DSI during the continuous condition relative to the episodic condition, as a function of the change in the normalised inferred firing rate to null stimuli.

these responses are reduced, in many cases to floor level, leading to an increase in DSI.

Indeed the relative increase in orientation/direction selectivity during the continuous condition is significantly correlated with the decrease in firing rate to the orthogonal/null stimuli (Figure 3.11C&D). As the average reduction in firing rate is greater for null than orthogonal stimuli (20.8% versus 3.8%, Figure 3.11C&D) there is a greater increase in direction selectivity than orientation selectivity (0.15 versus 0.02).

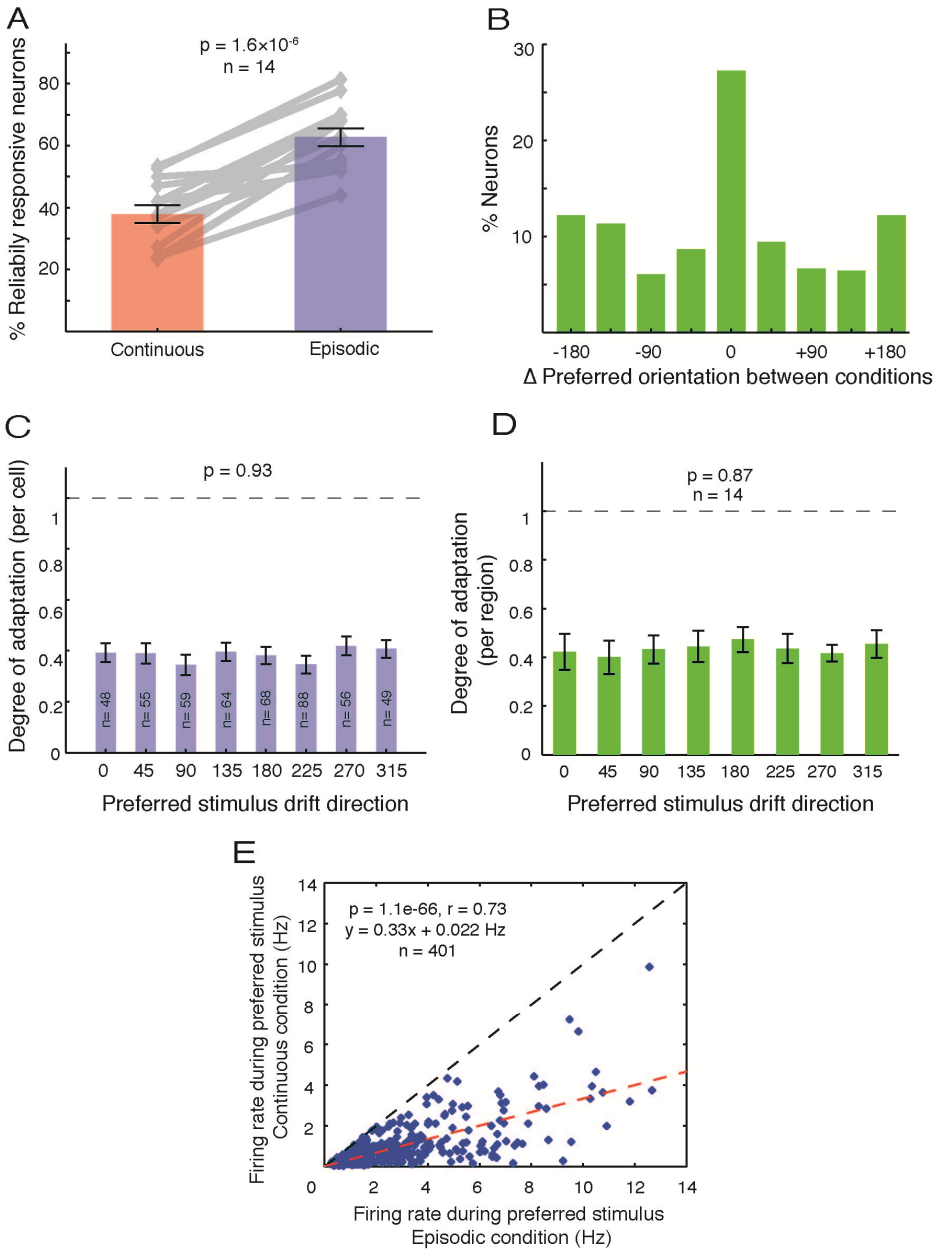

Supplementary Figure 3.1.
A.) Percentage of all neurons within each imaging region that were significantly responsive, i.e. their inferred spike rate significantly varied across stimuli of different orientations, during at least one of the stimulus conditions. (Error bars: mean ± S.E.M.) Neurons that were significantly responsive during at least one of the two conditions were included in analysis. B.) Difference in neurons' preferred direction during continuous condition relative to episodic condition, for all responsive neurons (n= 487). C.) Normalised firing rate during continuous condition (relative to episodic), for all responsive neurons, grouped by their preferred stimulus direction. D.) Normalised firing rate during continuous condition (relative to episodic) for each stimulus direction (averaged over all neurons and stimulus repetitions), for the 14 imaging regions. (Error bars: mean ± S.E.M.). E.) Firing rates of the 401 neurons that gave their maximal response during the episodic condition, during the preferred stimulus orientation in both the episodic and continuous conditions. As seen for firing rate functions of individual neurons, during the continuous condition responses were reduced to approximately one third of those during the episodic condition. The black line indicates the line of unity, where points would fall if the responses were equal during the two conditions. The red line indicates linear fit as obtained by the least squares method.

DISCUSSION

The aim of this study was to investigate how adaptation to dynamic stimuli influences population coding in mouse V1. Continuously drifting stimuli induced widespread, non-orientation specific adaptation, which had a marked impact on the response properties of both individual neurons and the population as a whole.

Main findings:

1. At a single neuron level, adaptation was associated with a significant reduction in responsiveness, increased trial-to-trial variability, and an increase in direction selectivity.

2. At a population level, adaptation caused decorrelation and increased sparseness across the network, reduced reliability and increased direction selectivity of the population responses.

3. Adaptation hence leads to a dispersed representation, in which the average neuron is relatively less informative, but accurate stimulus discrimination can still be achieved by incorporating the responses of a larger population.

4. In keeping with Chapter 2, the adaptation-induced reduction in responsiveness is well described by divisive scaling (i.e. a decrease in response gain), while nonlinearities introduced by the reduced response probability can account for the increased direction selectivity during the continuous (adapted) condition.

These findings are all in keeping with the effects seen following short-term (3.5s) adaptation to a single grating stimulus, as described in Chapter 2. The relatively greater strength of adaptation observed in the current study is likely to reflect the considerably longer duration of adapting stimuli (continuous stimuli were shown for a total of 112 seconds). Furthermore, by using gratings of multiple orientations, the current stimuli are expected to cause adaptation in a larger proportion of the network (as discussed in Chapters 1 and 2).

Possible benefits of network adaptation

The amount of information that can be encoded by a network of neurons is dependent on its 'representational capacity' or the number of recognizably different

patterns of spikes that can be generated. This will in turn determine the number of different situations that the network can represent. For a theoretical network of binary neurons, representation capacity is dependent on both the population size and the proportion of active neurons. If, in a population of 'n' neurons, only 1 neuron is active at a given time, the maximum number of codewords that can be represented is n. Conversely, if 50% of neurons are active the number of possible codewords is 2^n. Therefore the same representational capacity can be achieved by a large population of which only a few neurons are active, and a small population in which a larger proportion of neurons are active. Which coding strategy is implemented is likely determined by relative energy costs of maintaining quiescent neurons verses firing action potentials. Experimental data (Sibson et al., 1998; Rothman et al., 1999) and bottom up calculations (Attwell and Laughlin, 2001) agree that signalling costs account for approximately 80% of the brain's energy expenditure, while the cost of maintaining inactive neurons represents less than 15%. This suggests that 'sparse' representations, in which relatively few neurons are active, are the most energetically efficient (Levy and Baxter, 1996; Laughlin, 2001).

In the current data, the spatial extent of neuronal activity is assumed to be equal for both continuous and episodic stimulus conditions, and hence the energy costs of maintaining the neuronal population should remain constant. However, as the number of spikes is approximately 3 times lower during the continuous condition, this will be associated with significantly lower energy expenditure for similar decoding performance (assuming a constant population size of >500 neurons- see Figure 3.8A). Reduced redundancy (pairwise correlations between neurons) also increases the information per spike, and hence metabolic efficiency during the continuous condition. Therefore the most obvious benefit of adaptation to continuously drifting stimuli is in terms of energy expenditure.

Sparse and decorrelated coding strategies also confer potential benefits for information processing and memory storage (Olshausen and Field, 2004). However such advantages may be mitigated in the current dataset by the decrease in response reliability. This low reliability means that a greater number of neurons are required to attain the same level of performance (Figure 3.8A), however this is enabled by the high degree of over-representation in the visual cortex (Olshausen and Field, 1997).

Locus

In Chapter 2 we found that, for high contrast stimuli, the effects of adaptation were largely counteracted when cortical activity was suppressed. This suggests that this adaptation is predominately cortically mediated (either within V1 or via feedback from higher visual areas). Given the similarity of the current results, we predict that these effects may also be cortical in origin.

Layer 2/3 neurons receive only a small fraction of their synaptic inputs directly from the thalamus, with the majority coming from other cortical neurons. If adaptation reduces cortical response gain whilst leaving subcortical activity relatively unaffected (at least for high contrast stimuli), subcortical inputs should become relatively more prominent/effective during the adapted condition. The fact that stimulus preferences and selectivity were largely similar in the episodic and continuous conditions is therefore in keeping with reports of similar subthreshold orientation tuning with/without cortical inactivation (Ferster et al., 1996; Chung and Ferster, 1998; Lien and Scanziani, 2012).

Mechanisms

As discussed in the Chapter 2, cortical mechanisms of adaptation are likely to involve both intrinsic effects within the recorded neuron (such as increased membrane conductance (Sanchez-Vives et al., 2000a) and the amplification of these effects via network interactions (the simultaneous adaptation of the neuron's presynaptic partners (Kohn, 2007)). Our results are consistent with a significant involvement of network interactions in adaptation within mouse V1. Although neurons were only exposed to their preferred stimulus once every 16s during the continuous condition, they still exhibited a marked reduction in responsiveness. This suggests that a large proportion of this response reduction is a consequence of reduced activity in the surrounding network, and the resultant reduction in intracortical inputs.

Methodological limitations

The reduced responsiveness during the continuous condition is associated with a reduction in the signal to noise ratio of the florescence signal, and reduced probability of event detection by the spike extraction algorithm. The probability of event detection is only approximately 50% for single spikes, but >90% for events

involving two or more spikes (Hofer et al., 2011). This could potentially lead to an overestimation of the difference in firing rates between stimulus conditions, and will additionally influence measures of reliability and pairwise correlations. Furthermore, the reduced response probability will have the effect of raising the 'response floor' as described in Figure 3.11. This is likely to enhance apparent stimulus selectivity during the continuous condition. Unfortunately these caveats are unavoidable with the current method, in which firing rates are inferred from calcium based florescence signals. Therefore, in order to confirm these results, in the following chapter (Chapter 4) we performed direct electrophysiological recordings from individual neurons. Using whole-cell patch clamp recordings of the subthreshold membrane potential, we were also able to assess how adaptation influences the synaptic inputs that a neuron receives.

CHAPTER 4: ADAPTATION OF SPIKING AND SUBTHRESHOLD RESPONSES OF SINGLE NEURONS

INTRODUCTION

In Chapter 3, adaptation during continuously drifting gratings caused a non-specific reduction in the response gain of V1 neurons. The associated decorrelation and increase in population sparseness led to a more distributed stimulus representation across the population, providing potential metabolic and computational benefits.

In this chapter, we aimed to explore the underlying mechanisms of these adaptation-induced effects. Whole-cell patch clamp recordings were performed in order to compare the subthreshold inputs that a neuron receives during continuously and episodically drifting gratings. We found that adaptation during the presentation of continuously drifting gratings caused a subtractive reduction in the membrane potential depolarisation evoked by stimuli of different orientations/directions, combined with a marked increase in subthreshold trial-to-trial variability. Together these effects can explain the divisive gain change observed in the firing rate responses. Interestingly, similar changes in membrane depolarisation and trial-to-trial variability were also observed during stimuli mimicking natural viewing, suggesting that mechanisms and effects of adaptation described here may generalise across stimuli of differing statistics.

METHODS

Animals and surgical procedures

Experiments were performed in 16 C57Bl/6 mice (male and female) between postnatal day 29–40. All experimental procedures were carried out in accordance with institutional animal welfare guidelines and licensed by the UK Home Office.

Anaesthesia and surgery were carried out as detailed in detail in Chapter 2. Briefly, animals were anesthetized with a mix of fentanyl, metatomidine, and midazolam. The skull was exposed and a metal head plate was attached with dental cement. A craniotomy was made over the contralateral V1, based on stereotaxic coordinates. The dura was removed and the cortex was kept moist with cortex buffer solution

(125 mM NaCl, 5 mM KCl, 10 mM glucose, 10 mM HEPES, 2 mM $MgSO_4$, and 2 mM $CaCl_2$ [pH 7.4]).

***In vivo* electrophysiological recordings**

A silver reference electrode was fixed under the skin of the neck and fixed in place using 2% agarose in cortex buffer. Patch pipettes were made using thick-walled filamentous borosilicate glass capillaries (G150F-3, Harvard apparatus, 1.5 mm outer diameter, 0.86 mm inner diameter) using a horizontal puller (Sutter, P1000) adjusted to produce a tip size of approximately 1 µm and resistance of 5-7 MΩ when filled with intracellular solution containing (in mM): K-Gluconate 120, NaCL 4, HEPES 40, Mg-ATP 2, NaCl-GTP 0.3 (pH 7.4, 295 mOsm).

Pipettes and head stage were mounted on a remote controlled motorised micromanipulator ('Junior', Luigs & Neuman) and orientated at an elevation of approximately 45˚ from horizontal. The signal was amplified using a Multiclamp 700B amplifier (Molecular Devices), processed by a 50/60Hz noise eliminator (Humbug, Digitimer) and digitized at 20kHZ by an 18-bit ADC/DAC board (National Instruments) and low pass filtered at 6kHz. Data acquisition was controlled by a computer running either Igor Pro (Wavemetrics)/Neuromatic (Jason Rothman, UCL) or a custom Matlab program. Data were digitally stored for off-line analysis.

Recordings were made using the blind whole-cell patch technique (Margrie et al., 2002). The pipette was quickly lowered to the desired cortical depth (~150µm below pial surface) under approximately 500mBar of pressure to prevent tip blockage or contamination. Once the target depth was reached, pressure was reduced to 30mBar and the pipette was advanced in steps of 2.5µm. Neurons were searched for in voltage clamp mode, monitoring the current response to a square voltage step of 10-20mV (20Hz) on an oscilloscope as a measure of pipette resistance. When the pipette encountered a neuronal membrane this caused its resistance to increase, which could be observed as a decrease in current step size on the oscilloscope. Once a neuron was encountered pressure was quickly released and the holding voltage was set to -70mV to allow formation of a GΩ seal. Mild suction was applied if required. Once a seal was formed (typically >2GΩ) whole-cell configuration was achieved by applying slow ramping suction. If this was unsuccessful, short suction pulses or the amplifier's 'zap' function were also attempted. Once the whole-cell configuration was achieved the amplifier was

switched to current clamp mode (0pA holding current) and recordings were made at a frequency of 10kHz.

Visual stimuli

Visual stimuli were presented "full field", on a 43 × 23cm LCD monitor with a refresh rate of 60 Hz. The monitor was located 16 cm from the eye, covering approximately 106° of the visual field along the azimuth. At the beginning of each experiment, a rough retinotopic map was acquired for each neuron. Patches of moving black and white gratings were presented in 28 different locations on a grey background, in a pseudorandom order (stimulus duration= 600 ms; interstimulus interval= 400 ms). The monitor position was adjusted to centre the receptive field on the middle of the screen.

Test stimuli consisted of square-wave gratings of 4 orientations drifting in 8 evenly spaced directions spanning 0-360°. Stimulus orientation was perpendicular to drift direction (see Figure 4.1). Stimuli were presented in a fixed sequence, with the direction of drift increasing in 135° increments. Spatial and temporal frequencies of all stimuli were 0.04 cycles/degree and 3 cycles/sec respectively, contrast was set at 50% and stimulus duration was 1666 ms.

'Continuous' stimuli consisted of gratings drifting in different orientations (1.7 second duration), shown consecutively without interruption (Figure 4.1B). Three different 'episodic' conditions were also included, in which drifting gratings (also 1.7 second duration) were interspersed with stationary gratings (of 0.4, 1.7 or 4 second duration; Figure 4.1C). Stationary gratings during the episodic conditions were of the same orientation and spatial frequency as the subsequent drifting grating.

Each recording session comprised 30 seconds of baseline (grey screen), followed by 5 repetitions of the entire stimulus sequence, and another 30 seconds of baseline (Figure 4.1A). Due to the presence/absence of the stationary screens and their varying durations, the duration of a single stimulus sequence repetition varied between conditions; continuous condition: 13.3 seconds; episodic (400ms stationary screens): 16.5 seconds; episodic (1666 ms stationary screens: 26.7 seconds; episodic (4000ms stationary screens): 45.3 seconds.

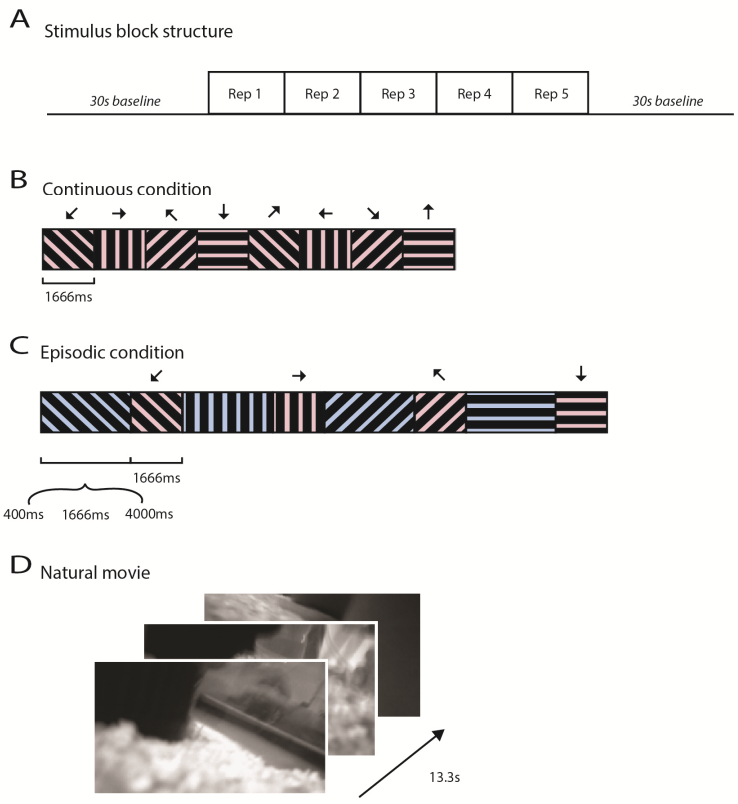

Figure 4.1. Stimulus Schematic
A.) Structure of single stimulus block, consisting of 5 repetitions of a given condition (continuous/episodically drifting gratings or a natural movie). Note that the duration of a single stimulus repetition varied across conditions (see text), leading to a difference in total stimulation time. B.) A single repetition of the continuous condition. Grating orientation as shown, drift direction as indicated by arrows. C.) Part of a repetition of the episodic condition. Blue shading indicates stationary gratings, while pink indicates drifting gratings (drift direction indicated by arrows). The duration of stationary screen differed between conditions as shown, whilst the duration of the drifting gratings remained constant at 1666ms (as for the continuous condition). D.) Example frames from the natural movie. The movie was 13.3 s in duration (corresponding to a single repetition of the continuous grating condition) and was repeated 5 times, as shown in A.

A subset of neurons (n= 13) were also recorded during natural movie stimulation (Figure 4.1D). Each movie was of 13.3 seconds duration (corresponding to one repetition of the full stimulus set during the continuous grating condition). The movie was repeated 5 times, and was preceded and followed by 30 seconds of baseline recording. This enabled a direct comparison of the relative change in responses over repetitions of continuous gratings and natural movie stimuli.

Data analysis

All analysis was carried out in Matlab (Mathworks).

Analysis window and selection criteria

Responses to the drifting stimuli were compared across the different stimulus conditions. For each condition, analysis was restricted to an "analysis window", commencing 250ms after the onset of each drifting stimulus and lasting for 1333ms (i.e. 4 periods of the 3Hz square wave grating). The onset of the analysis window was delayed relative to the start of the stimulus in order to avoid the neuron's initial onset response.

As described above, each recording session was composed of 5 repetitions of the stimulus sequence spanning all orientations/directions. For the comparison between conditions (see Results Part 1 & 2), measurements were calculated from the final 3 repetitions of the stimulus sequence, for all available recording blocks (resulting in a total of 3 x n trials, where n is the number of recording blocks). When comparing the magnitude of response across subsequent repetitions (Results Part 3), the responses to each of the 5 repetitions were considered separately for all available recording blocks (resulting in n trials per repetition, where n is the number of recording blocks). For reliability/variability measurements, multiple responses to the same stimulus repetition were required, restricting measurements to those neurons for which multiple recording blocks were obtained.

Recordings were selected on the basis of stability. Recordings for which the pre and post stimulus baseline value differed by more than 5 mV were excluded. Neurons were excluded if they fired less than 2 spikes on average to the preferred stimulus orientation/direction during at least one stimulus condition. This resulted in a total of 25 neurons for which recording blocks were available for all stimulus conditions (the responses of which are discussed in Results Part 1 and 2). A further 13 neurons which met the above criteria were recorded only during the continuous condition. These neurons were combined with the original 25 to give a population of 38 neurons whose responses were compared across repetitions of the grating stimuli. The same 13 neurons were also recorded during natural movies (see above), enabling a comparison of adaptation across repetitions of continuous gratings and more naturalistic stimuli.

Spike removal

Spike thresholds were localised to the maximum second differential within the 5ms period preceding the action potential peak and spike timing was recorded at 1ms

precision. For each spike, the subthreshold trace was capped at the threshold value (from the point of threshold until the point at which the membrane potential passed back below this value). If spikes occurred within 10ms of each other the trace was capped until the membrane potential passed below threshold following the last spike. Following spike removal, traces were smoothed with a 7ms sliding window and down sampled at 1kHz.

Membrane potential depolarisation

The baseline membrane potential of each recording block was defined as follows. The pre and post stimulus baseline conditions were divided into 1 sec sections and the minimum membrane potential observed during each section was averaged to give the baseline of that recording session.

The membrane potential depolarisation was calculated as the mean membrane potential (relative to baseline) during the analysis window, averaged over all trials of a given stimulus orientation. For subthreshold/spiking analysis the neuron's preferred stimulus was defined as the orientation/direction that elicited the greatest mean depolarisation/mean spike rate respectively. Unless otherwise specified, results presented refer to responses to the preferred stimuli.

Membrane potential modulations

The amplitude of the stimulus-locked membrane potential modulations was obtained for each stimulus orientation/direction by Fourier transformation of trial-averaged subthreshold response. Modulation amplitude was quantified as the magnitude of the amplitude spectrum at the stimulus temporal frequency (F1). The F1/F0 ratio was taken as the ratio of the modulation amplitude to the mean membrane potential depolarisation (F0, relative to baseline).

Reliability/variability measures

Spike train reliability was quantified as the mean correlation coefficient between the spike trains (50ms time bins) across all trials of a given stimulus orientation/direction. Spike count variability was quantified as the spike count Fano factor (the variance in spike count over all trials of a given stimulus divided by the mean). To measure subthreshold variability, the coefficient of variation of the subthreshold membrane potential response (standard deviation divided by the

mean) across all trials was calculated for each time point and averaged over the analysis window.

Membrane potential dynamics

The mean rate of change of the membrane potential was calculated for each trial as the mean of the absolute values of the first differential (ie including both the rate of hyperpolarisation and depolarisation; Cardin et al., 2007). For each stimulus orientation/direction the response was averaged across all trials.

Stimulus selectivity

Firing rate selectivity was based on the mean firing rate across all stimulus orientations, while subthreshold selectivity was based on the mean depolarisation (averaged over all trials). The Orientation and Direction Selectivity Indices (OSI/DSI) were calculated as described in Chapters 2 and 3.

Vm distributions

Membrane potential distributions during the total stimulation period were obtained from the subthreshold recordings for each neuron (at 1 ms precision) as follows:

1. For each repetition of a given stimulus condition, a histogram was obtained giving the number of time points for which the membrane potentials fell within 0.5 mV bins from -5 mv to +45 mV (relative to baseline).

2. These values were summed over all repetitions/blocks of that stimulus.

3. The normalised distributions of all neurons were averaged to give the population distribution.

Membrane potential distributions during the drifting grating stimuli were obtaining in a similar manner:

1. For each trial of a given stimulus direction/orientation, a histogram was obtained giving the number of time points for which the membrane potentials fell within 0.5mV bins (as described above). The first 333ms of these trials were excluded, removing any influence of response latency.

2. These values were averaged across all repetitions/stimulus directions/orientations and presentation blocks to give the average drift distribution per cell.

3. The normalised distributions per cell were averaged across the population

Normalisation

For both firing rate and mean depolarisation measures, responses across all conditions and stimulus orientations/directions were normalised for each cell. For example, when comparing the responses during episodic and continuous presentation conditions the total number of conditions is 16 (8 stimulus directions × 2 conditions). For one of these conditions (n), the normalised response is calculated as:

$Rnorm_n = ((R_n - R_{min})/(R_{max}-R_{min}))\times 100$

where Rmax and Rmin are the maximum and minimum across all 16 conditions.

Statistics

As described in Chapter 2, for all statistical comparisons normality was tested using a 2-sided Shapiro-Wilk test. Where the assumption of normality was violated, non-parametric analysis was used.

When comparing the responses of the same neurons across multiple conditions, where the number of conditions was greater than two, the effect of conditions was first assessed by a repeated measures ANOVA (or Friedman's non-parametric repeated measures ANOVA). If significant ($p<0.05$), this was followed by pairwise t-tests (or Wilcoxon signed-rank paired comparisons).

When comparing responses across multiple groups of neurons, the effect of group was first assessed by an ANOVA (or the Kruskal-Wallis non parametric ANOVA). If significant ($p<0.05$), this was followed by pairwise t-tests (or Wilcoxon rank-sum comparisons).

Where applicable multiple comparisons were corrected for using the sequential Holm-Sidak correction (reviewed by Abdi, 2010). Unless otherwise specified error bars indicate mean ± standard error of the mean (S.E.M).

RESULTS

Whole-cell recordings were obtained from neurons in layers 2/3 of mouse V1 using the blind patch-clamp technique. As in Chapter 3, responses were compared during sequences of continuously and episodically drifting gratings (see Figure 4.2). During the episodic condition, drifting gratings were interspersed with stationary gratings that provided recovery time between dynamic stimuli. We additionally investigated the dependence of adaptation on stationary grating duration by including two intermediate episodic conditions, giving a total of 4 conditions: continuous (no stationary gratings, Figure 4.2A) and episodic conditions in which drifting gratings were interspersed by stationary gratings of 0.4, 1.7 or 4 seconds duration (Figure 4.3B,C&D respectively). Subthreshold responses (following spike removal, see methods) and firing rates were analysed separately (see Figure 4.3 for the isolated subthreshold and spiking responses of an example neuron). The magnitude, reliability and stimulus selectivity of spiking and subthreshold responses were compared across conditions.

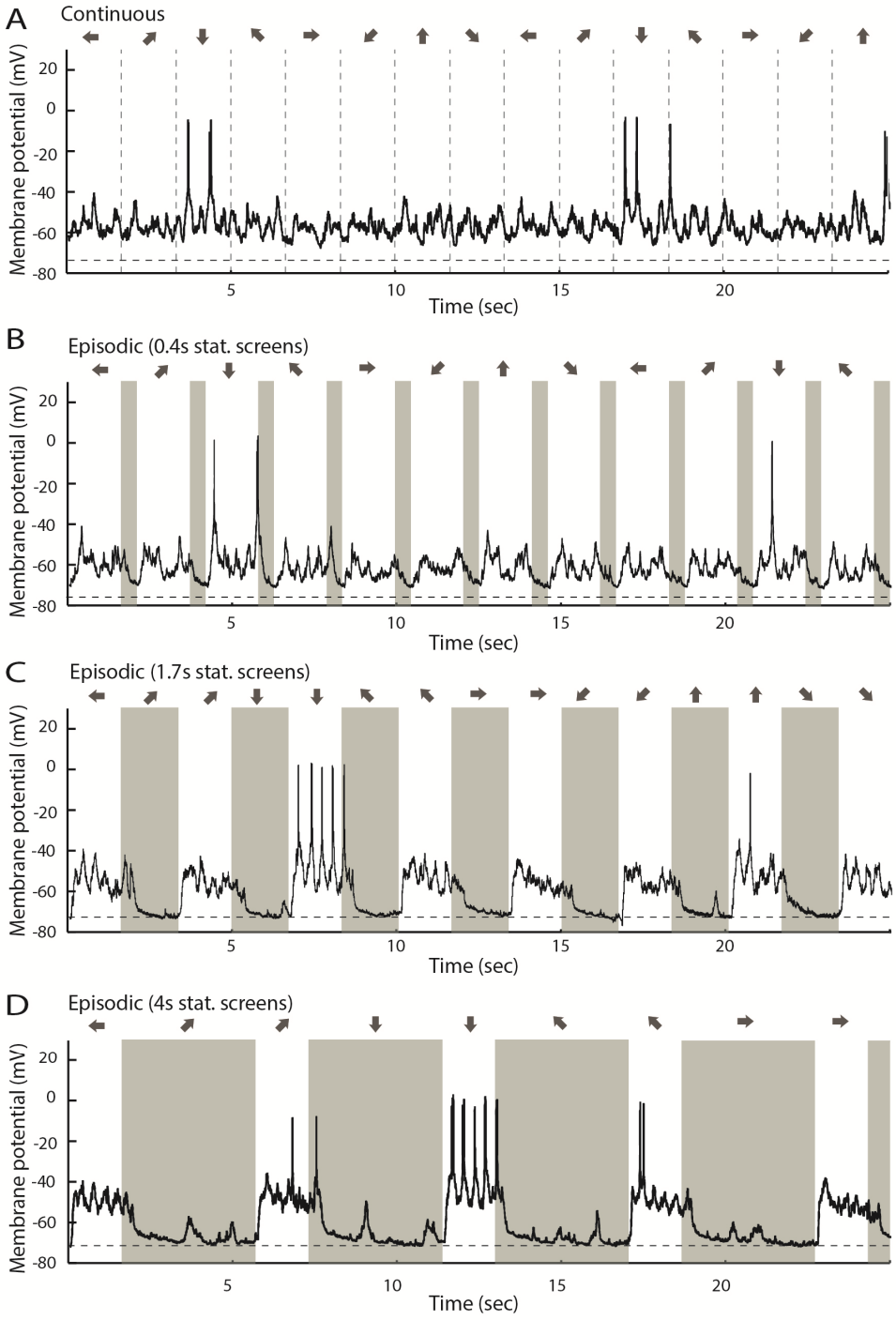

Figure 4.2. Example whole cell recordings.
Membrane potential recordings of an example neuron during different stimulus conditions: A) continuous condition (without stationary screens); B) An episodic condition containing 0.4 sec stationary screens (indicated by grey blocks); C.) an episodic condition containing 1.7 sec stationary screens; D.) An episodic condition containing 4 sec stationary screens. Stimulus orientation/drift direction indicated by arrows.

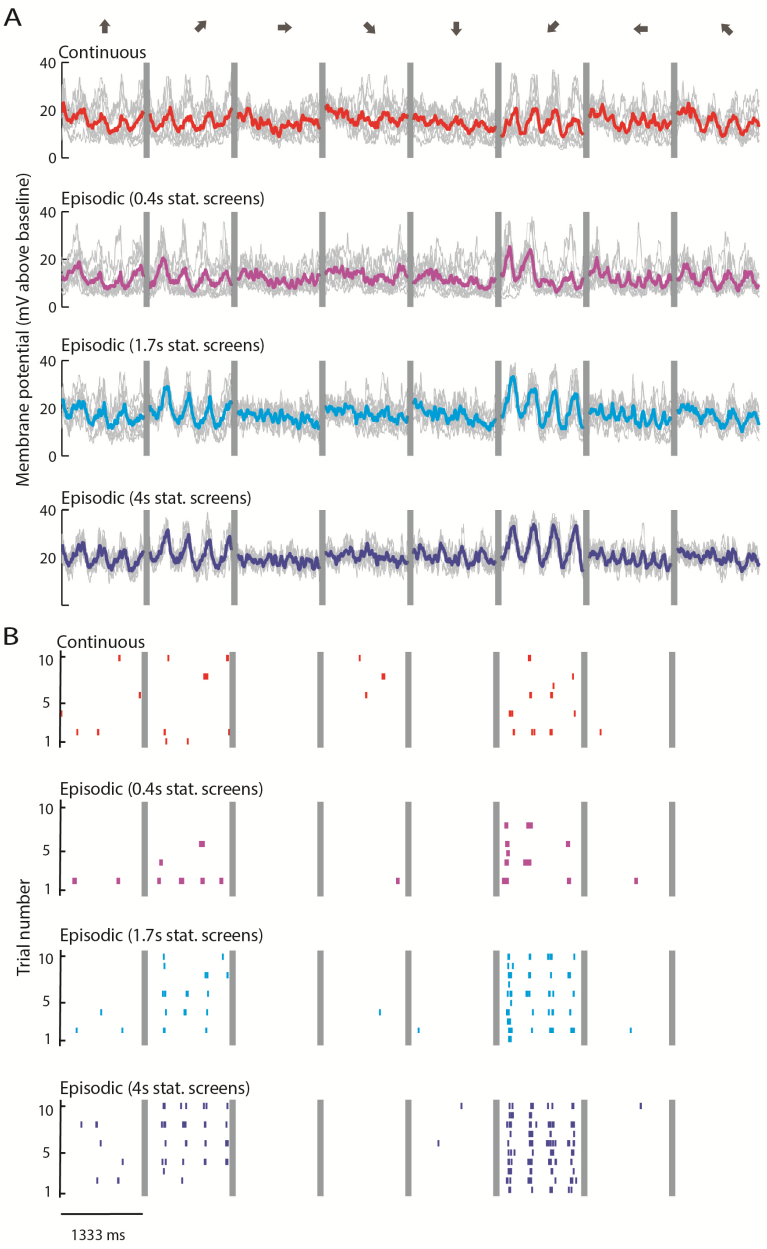

Figure 4.3. Subthreshold and spiking responses of an example neuron
Subthreshold membrane potential recordings of an example neuron across 10 repetitions of continuous and episodic stimuli. Stimulus orientation/drift direction indicated by arrows. B.) The corresponding spiking responses of the neuron shown in A. Stimulus duration and orientation as in A.

Response magnitude

A comparison of firing rate responses during continuously or episodically presented gratings confirmed the calcium imaging results in Chapter 3; adaptation during the continuous condition was associated with a significant reduction in responsiveness. Firing rates were found to increase with the duration of the stationary gratings included in the episodic conditions (p= 1.6×10-10, Fig. 4.4A). The average firing

rate during the preferred stimulus direction was 2.0 ± 0.38Hz during the continuous condition, compared to 5.6 ± 0.82Hz during the longest (4s stationary gratings) episodic condition. This is in close agreement with the 2-fold reduction in responsiveness observed in calcium signals (Figure 3.3B), despite the use of lower contrast stimuli during the current study (50% versus 100%).

We next analysed stimulus driven membrane potential depolarisation (subthreshold) during these conditions. The mean depolarisation similarly showed clear stimulus dependency, being lowest during the continuous condition and increasing with stationary grating duration during the episodic conditions (p= 2.7×10-17, Figure 4.4B).

Whilst significant, the stimulus-locked modulations of the subthreshold response (F1), showed relatively little variance across conditions (p= 0.017, Figure 4.4C), in keeping with previous reports on contrast adaptation in cat V1 (Carandini and Ferster, 1997; Sanchez-Vives et al., 2000a). There was no significant difference in F1/F0 ratios across conditions (Figure 4.4D.

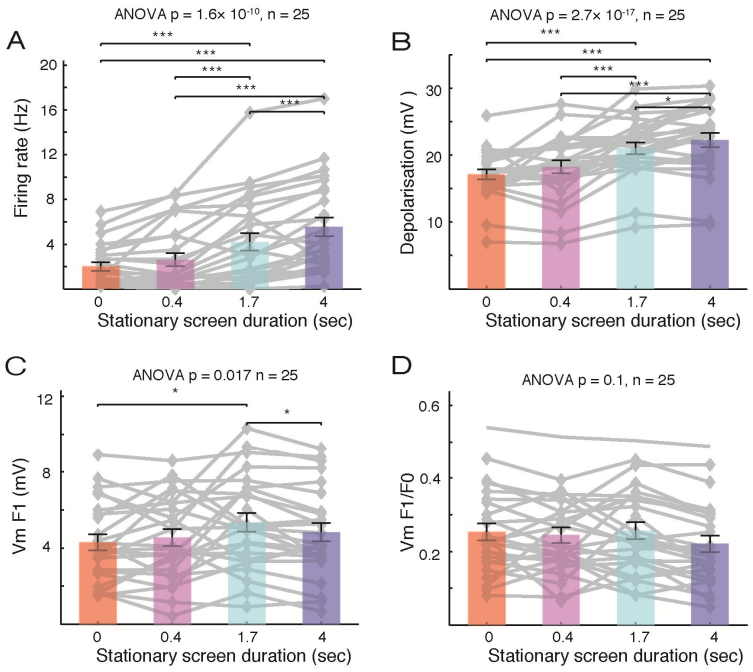

Figure 4.4 Response magnitude
Firing rate of all neurons to their preferred stimulus, during the continuous condition (red) and episodic conditions with varying stationary screen durations. B.) Mean membrane potential depolarisation (F0) across conditions. C.) Amplitude of membrane potential modulations (F1) across conditions. D.) Membrane potential F1/F0 ratio. (Error bars: mean ± S.E.M.)

Membrane potential distributions

As shown above, the membrane depolarisation and firing rate evoked by the drifting gratings varied systematically with stationary screen duration. In order to further assess the impact of stationary screens on membrane potential during drifting gratings, we compared the distributions of membrane potentials recorded during the entire stimulation period (including periods of stationary gratings, when present), averaged over all neurons, for each stimulus condition (see methods).

During the continuous condition (consisting only of drifting screens), there was a unimodal distribution of membrane potential values, peaking at 13.5 mV above baseline (Figure 4.5A). With the inclusion of stationary screens, the distributions become more bimodal, with the shortest episodic conditions (containing 400ms stationary screens) showing peaks at 7 and 10.5 mV (Figure 4.5B). With longer stationary screens there is an increased segregation of membrane potential values relating to the drifting and static stimuli (Figure 4.5C&D).

A similar pattern can also be observed in the example recordings in Figure 4.2. As the duration of the stationary screens increases, the membrane potential during these static periods returns closer to baseline, followed by a stronger depolarisation during the drifting stimuli increase. Therefore it appears that the 'lower the lows' during the stationary gratings, the 'higher the highs' during the drifting gratings. This is in keeping with the notion that the stationary screens provide a recovery period from the adaptation to the dynamic stimuli. A straightforward explanation for this effect is that the driving force for excitatory inputs will be greater when the initial membrane potential is lower but with shorter stationary screens there is insufficient time for the membrane potential to return to baseline conditions. Additionally, the membrane potential repolarisation could coincide with time-dependent recovery from short-term synaptic depression (see Discussion).

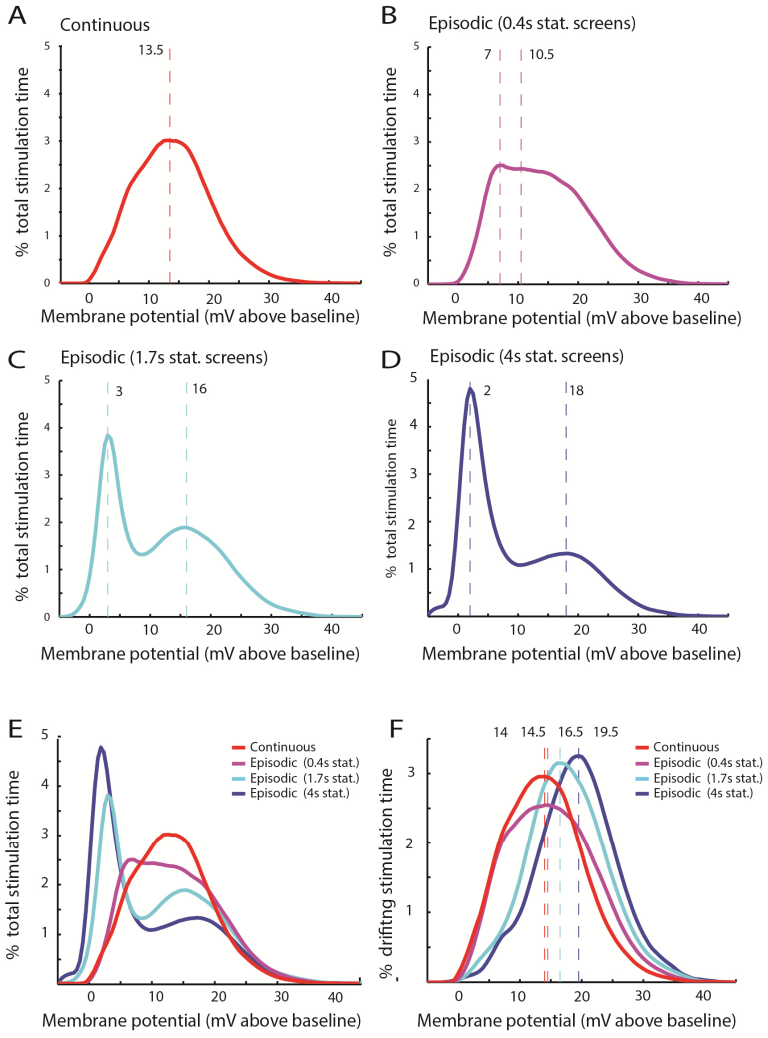

Figure 4.5. Membrane potential distributions
Distributions of the membrane potential of all neurons over the total stimulation period (all orientations, including stationary screens if present), during continuous and episodic conditions. Dashed lines/values indicate peaks of bimodal/unimodal distributions. E.) Overlay of data shown in A-D. F.) Distributions of membrane potentials during drifting stimuli only (after removing stationary screens). Dashed lines correspond to distribution peaks.

Regardless of the underlying mechanism, these data reveal that the membrane potential is higher, and hence closer to spike threshold (assuming threshold is unaltered by adaptation; Carandini and Ferster, 2000) for a greater proportion of the drifting stimulation time during the longest episodic condition (Figure 4.5F). This is in keeping with the greatest firing rates observed during this condition.

Trial-to-trial reliability

We next compared trial-to-trial reliability across stimulus conditions. Spike train reliability (quantified as the mean correlation coefficient across repetitions of the preferred stimulus) was significantly lower during the continuous condition than

during any of the 3 episodic conditions ($p=1.8\times10\text{-}3$, Figure 4.6A). This result is in agreement with the adaptation-induced decrease in spiking/calcium signal reliability observed during the previous two chapters. However, there was no significant difference in spike count Fano factor (variance/mean, based on the number of spikes per 1.5 second trial; Figure 4.6B).

Interestingly, both the results of this chapter and those from the extracellular recordings in Chapter 2 show a decrease in spike train trial-to-trial correlation (reliability) without a change in spike count variability. This discrepancy could suggest that the reduced reliability is primarily due to a lack of temporal precision rather than a change in spike number. However, this seems unlikely, given the reduced response probability observed here and in Chapter 3. Therefore it may be that the Fano factor measure in its current form lacks sufficient temporal resolution to fully capture these effects.

Subthreshold variability (coefficient of variation of the subthreshold response quantified as the standard deviation/mean) showed a strong dependence on stationary screen duration, being consistently greater during the continuous and shorter episodic condition than the longer episodic conditions ($p=6.0\times10\text{-}8$, Figure 4.6C). Therefore, adaptation to continuously presented stimuli increases subthreshold variability. This is a key finding; not only is subthreshold variability likely to contribute to the decrease in spiking reliability, but it will also influence spike probability (Anderson et al., 2000; Finn et al., 2007; Schreiber et al., 2008) and may be critical in explaining the changes in response gain (see Discussion).

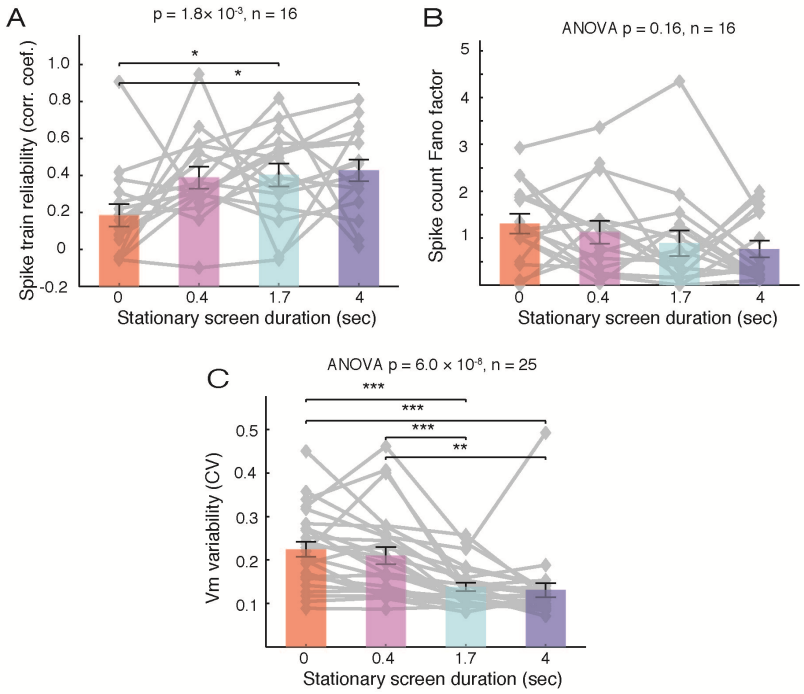

Figure 4.6. Trial-to-trial reliability
Trial-to-trial reliability of spike trains (quantified by mean correlation coefficient between repetitions of the preferred stimulus) during the continuous and episodic conditions with stationary screens of varying duration. B.) As in A, but for spike count variability (Fano factor). C.) As in A, but for membrane potential variability (coefficient of variation across repetitions). Error bars: mean ± S.E.M.

Membrane potential dynamics

In addition to comparing the magnitude and reliability of subthreshold responses during different conditions, we also investigated membrane potential dynamics by quantifying the average rate of change during depolarization/hyperpolarization (absolute dV/dT; see Methods). This measure is influenced by both the membrane time constant and the synchrony of the inputs that the neuron is receiving (Azouz and Gray, 2003; Cardin et al., 2007). Membrane potential dynamics also showed significant stimulus dependency, being slowest during the continuous condition and increasing with stationary screen duration (p= 1.1×10-5, Figure 4.7). While the current data do not allow an assessment of the membrane time constant, adaptation has been found to increase membrane conductance in cat V1 neurons (Sanchez-Vives et al., 2000a; 2000b). Higher conductance (and lower capacitance) will reduce the membrane time constant and should give faster dynamics. Hence, the fact that the opposite pattern is observed here (adaptation is associated with slower membrane dynamics), suggests that there is a significant decrease in input

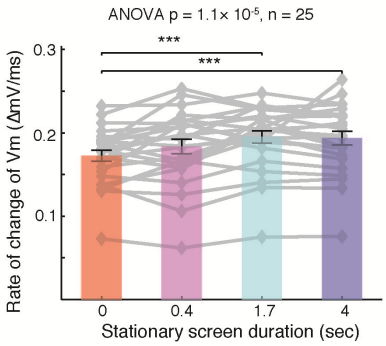

Figure 4.7. Membrane potential dynamics
Absolute mean rate of change (absolute dmV/ms) of membrane potential during the preferred stimulus, in the continuous condition and episodic conditions with stationary screens of varying duration. Error bars: mean ± S.E.M.

synchrony. This is in keeping with the decorrelation between V1 neurons reported in Chapters 2 and 3.

Stimulus selectivity

In Chapter 3, adaptation to continuously drifting stimuli was associated with an increase in direction selectivity, and to a lesser extent orientation selectivity. In the current data we did not observe a consistent change in either the orientation or direction selectivity of spiking responses across the four stimulus conditions (Figure 4.8C&E). However, when comparing firing rate selectivity between only the continuous and the longest episodic conditions (equivalent to the continuous-episodic comparison made in Chapter 3), both OSI and DSI were found to be significantly greater during the continuous condition (OSI: p= 0.049; DSI: p= 0.018).

At the subthreshold level, the orientation selectivity (OSI) of the mean membrane depolarisation (F0 component, OSI Vm) was greatest during the continuous condition and decreased with increasing stationary screen duration (p= 6.0×10-5, Figure 4.8D).

Subthreshold directional selectivity showed a similar trend, again being greatest during the continuous condition (p= 1.2×10-3, Figure 4.8F).

Interestingly, the difference in depolarisation OSI between continuous and episodic conditions was negatively correlated with a neuron's subthreshold linearity (F1/F0 ratio) during the episodic condition (p= 9.6 ×10-3, r= -0.51, data not shown). This implies that adaptation preferentially increases the subthreshold orientation selectivity of more 'complex' cells (i.e. cells with lower F1/F0 ratios). However there

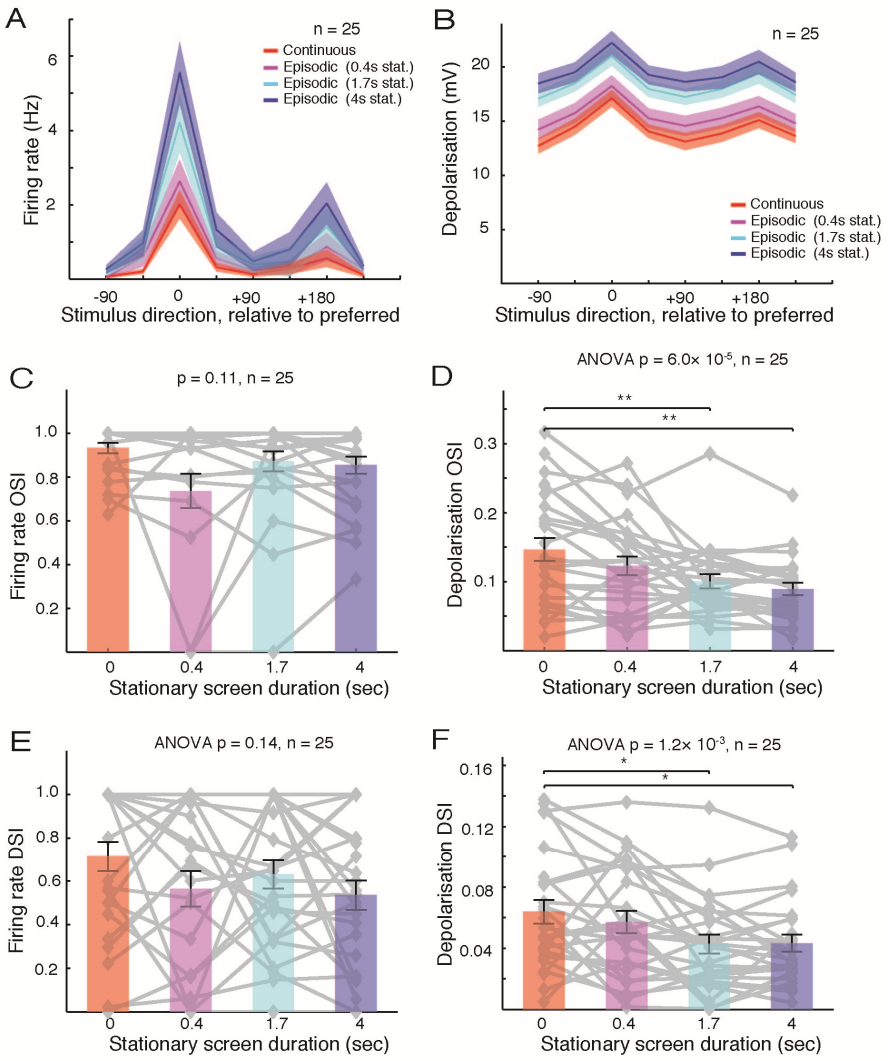

Figure 4.8. Stimulus selectivity
Firing rate as a function of stimulus orientation/direction, during the continuous and episodic conditions. B.) Mean membrane depolarisation as a function of stimulus orientation. C.) Orientation Selectivity Index (OSI) of firing rate responses. D.) OSI of membrane potential responses (mean depolarisation). E.) Direction Selectivity Index (DSI) of firing rate response. F.) DSI of membrane potential responses (mean depolarisation). (Error bars: mean ± S.E.M.)

was no significant relationship between subthreshold F1/F0 and the change in subthreshold DSI or firing rate OSI/DSI.

Stationary screen duration appeared to have a more consistent influence on the stimulus selectivity of subthreshold responses than spiking responses. This difference may reflect the nature of gain modulation experienced by these response measures; while the population tuning curve for the spiking responses (Figure 4.8A) appears to show divisive scaling across conditions (which should not alter the OSI and DSI measures), the population tuning curve for the mean depolarisation (Figure

4.8B) appears to undergo a subtractive shift (which would affect OSI and DSI). Next, we therefore quantitatively assessed the gain modulation of both subthreshold and spiking responses.

Response gain modulation

The nature of gain modulation was explored, as in Chapter 3, by comparing the response for a given stimulus direction during the continuous and the two intermediate episodic conditions, relative to the response evoked during the longest episodic condition (Figure 4.9B-D). As described in Chapter 3, the presence of a subtractive shift can be masked by firing rate rectification (Figure 3.9), and therefore only non-zero values were included in this analysis. Due to low firing rates observed within the current dataset, the criteria of linear fit significance was relaxed; the fits shown correspond to all neurons which exhibited non-zero responses during at least 3 stimulus directions across both conditions. In close agreement with Chapter 3, adaptation appeared to result in a divisive scaling of firing rate, whereby the responses during the continuous condition were reduced to approximately a third of those during the episodic condition (Figure 4.9B). Responses during the two intermediate episodic conditions were also divisively scaled with respect to those during the longest episodic condition (Figure 4.9C&D). This divisive scaling is captured by the fit gradients; for those neurons for which fits could be obtained across all stimulus conditions (n= 7), the fit gradients appeared to increase systematically with stationary screen duration ($p= 0.021$, Figure 4.9E), being significantly lower than zero during the continuous condition. The fit intercepts however did not differ significantly from 1 for any condition, providing no evidence of a subtractive reduction in response (Figure 4.9F).

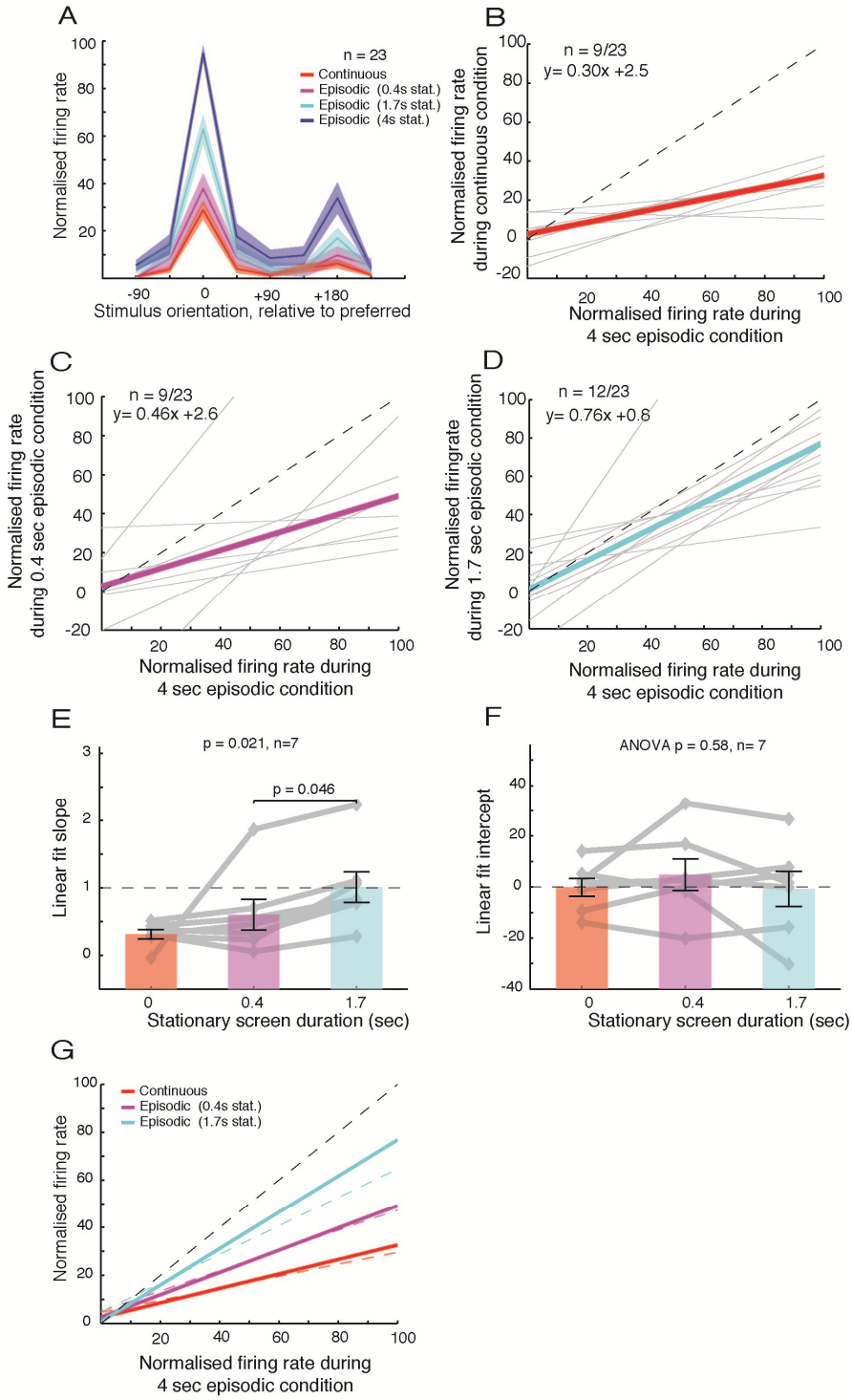

Figure 4.9. Gain modulation of spiking responses
Normalised firing rate as a function of stimulus orientation for 23 neurons that gave their maximum firing rate responses during one of the episodic conditions. B.) The linear fit between the normalised firing rate during the continuous and longest episodic condition (containing 4s stationary screens), for all neurons with at least 3 non-zero responses. C.) As in B, but for the shortest episodic condition (containing 400ms stationary screens). D.) As in B, but for the mid length episodic condition (containing 1.7 sec stationary screens). E.) The slopes of the linear fits shown in B-D. F.) The linear fits intercepts shown in B-D. Error bars: mean ± SEM. G.) Merged of data from B-D. Solid lines represent median fit parameters across stimulus conditions, while dotted lines are the corresponding linear fits from the population tuning curves shown in A.

The same analysis was also applied to subthreshold responses. Note that, as firing rate rectification does not affect subthreshold data, it was not necessary to exclude any cells. Hence, as in Chapter 3, only neurons with a significant linear correlation between conditions were included for the current analysis. In contrast to the divisive scaling observed in the firing rate responses, the mean membrane potential depolarisation appeared to undergo a subtractive shift across conditions (Figure 4.10A). This was also evident when comparing the linear fits across conditions (Figure 4.10B-C); whilst there was no change in fit gradients (Figure 4.10E), the intercepts were significantly reduced by adaptation, showing a clear dependence on stationary grating duration ($p= 1.4\times10\text{-}5$, Figure 4.10F). Therefore, the divisive scaling of the firing rate responses during adaptation is accompanied by a subtractive reduction of the underlying membrane potential depolarisation.

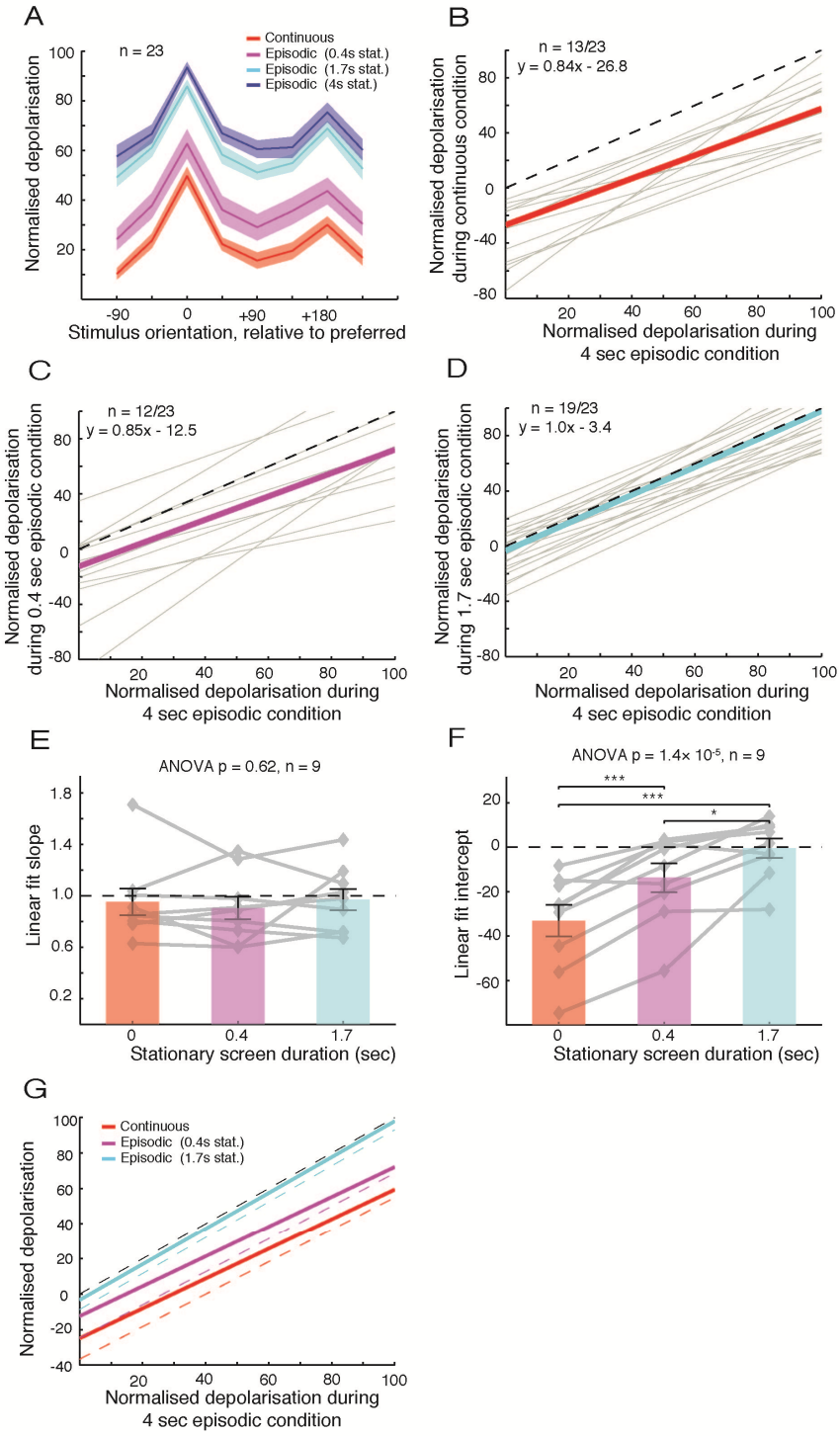

Figure 4.10. Gain modulation of subthreshold responses
Analysis of gain changes of mean membrane potential depolarisation (F0). Analysis is restricted to those neurons which exhibited a significant linear correlation between the respective conditions. Description of analysis and panel sequence as in Fig. 4.9.

As discussed above, these analysis of firing rate gain modulation was confined to a subset of neurons which exhibited non-zero responses during at least 3 stimulus directions across both conditions. In order to explore the generality of these conclusions, as in Chapter 3, we additionally assessed the gain modulation across the population of neurons. For each neuron, we compared the firing rate and membrane depolarisation in response its preferred stimulus orientation during the different stimulus conditions (Supplementary Figure 4.1). As seen within individual neurons, firing rate responses during the continuous condition and intermediate episodic conditions appeared to be divisively scaled with respect to those during the longest episodic condition (Supplementary Figure 4.1A-C). However, while the subthreshold depolarisation of individual neurons had appeared to undergo a subtractive shift between conditions, across the population of neurons subthreshold responses appeared to be subject to divisive scaling (Supplementary Figure 4.1D-F). Those neurons that exhibited the greatest depolarisation during the longest episodic condition underwent the greatest reduction in depolarisation during the continuous and intermediate episodic conditions.

Given this finding, we also re-examined how the subthreshold gain modulation varied between individual neurons. For those neurons which exhibited a linear relationship between subthreshold responses during the continuous/long episodic conditions, there was a significant negative correlation between the gradient of this relationship and the magnitude of depolarisation during the episodic condition ($r = -0.74$ $p = 3.5e\text{-}03$, Supplementary Figure 4.2). As a negative gradient indicates a divisive scaling of responses, this result implies that, in addition to showing the largest decreases in depolarisation between conditions, those neurons which exhibited the greatest depolarisation during the long episodic condition also underwent a divisive scaling of subthreshold responses during the continuous condition (see Discussion).

Prolonged adaptation during multiple stimulus repetitions

As the preceding analysis aimed to assess spiking and subthreshold response properties during a steady state of adaptation, responses during the initial two repetitions of each stimulus block were discarded. Here we explored how adaptation evolved over multiple presentations of the continuous stimulus condition. For this, we compared responses to the preferred stimulus direction, across the 5 sequential repetitions of the continuous condition. For neurons for which multiple

stimulus blocks were presented, it was also possible to assess how trial-to-trial reliability differed across repetitions. In addition to the population of 25 neurons that contributed to the data discussed above, a further 13 neurons were also recorded during the continuous condition (and natural movie stimuli, see below), and were included in the following analysis (total n= 38).

Firing rate changed significantly over repetitions of the continuous condition, decreasing after the first repetition and then remaining relatively stable ($p= 5.5\times10^{-7}$, Figure 4.11A&B). There was no significant change in the orientation or direction selectivity of spiking responses across repetitions (Figure 4.11C&D). Nor was there was any consistent change in the reliability of spiking responses across repetitions, either in terms of spike train reliability (Figure 4.11E) or spike count Fano factor (Figure 4.11F). This may indicate that the effect of adaptation on these measures emerges early during the first repetition of the continuous condition. However, these measures are somewhat limited by the low number of neurons with sufficiently high spiking activity, for which multiple stimulus blocks were recorded.

At the subthreshold level, the mean membrane depolarisation decreased successively across repetitions ($p= 3.1\times10\text{-}16$, Figure 4.12A&B). There was even a significant reduction in depolarisation between the final 2 repetitions, indicating that adaptation had not yet plateaued after a total of 112 seconds of stimulation. In keeping with previous reports (Carandini and Ferster, 1997; Sanchez-Vives et al., 2000a), the stimulus modulated (F1) component of the membrane potential response did not vary significantly during the course of adaptation (Figure 4.12C). Consequently the F1/F0 ratio increased over repetitions ($p= 7.2\times10\text{-}6$, Figure 4.12D).

The orientation selectivity of the mean membrane depolarisation was found to increase over repetitions ($p= 2.2\times10\text{-}6$, Figure 4.12E). Interestingly, a subpopulation of neurons appeared to be driving this effect, and the neurons that showed the greatest increase in Vm OSI across repetitions were found to all exhibit relatively low linearity (F1/F0 ratio) in their subthreshold responses. This supports the finding that the overall difference in orientation selectivity between the continuous and longest episodic conditions was significantly correlated with Vm F1/F0 ratios, and suggests that adaptation preferentially increases the subthreshold orientation tuning

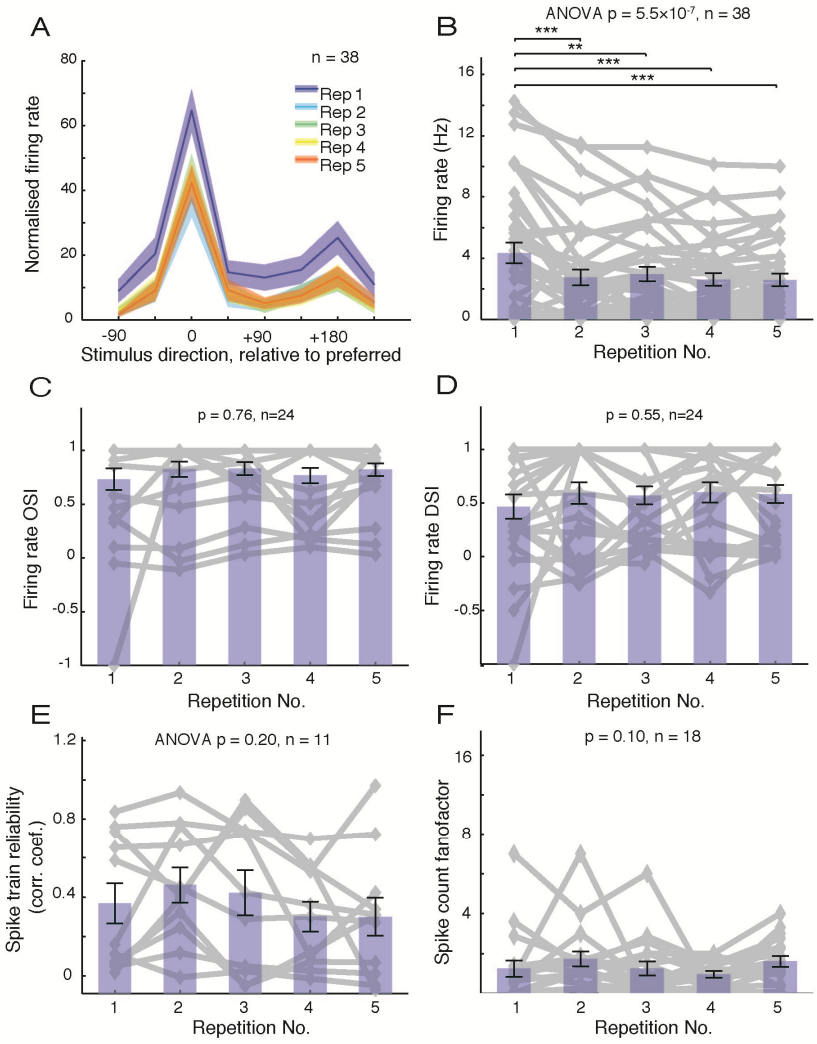

Figure 4.11. Spiking response properties over stimulus repetitions
A.) Population average of normalised firing rate as a function of stimulus direction, across subsequent repetitions of the continuous condition. (Lines and shading indicate mean ± SEM.) B.) Mean firing rate (during preferred stimulus direction), across subsequent repetitions. C.) Orientation selectivity (OSI) of firing rate responses across repetitions. D.) Direction selectivity (DSI) of firing rate responses across repetitions. E.) Spike train reliability (mean correlation coefficient between multiple stimulus blocks) F.) Spike count variability (Fano factor between multiple stimulus blocks). (Error bars: mean ± SEM).

of complex cells. However, there was no consistent change in the direction selectivity of subthreshold inputs across stimulus repetitions (Figure 4.12F).

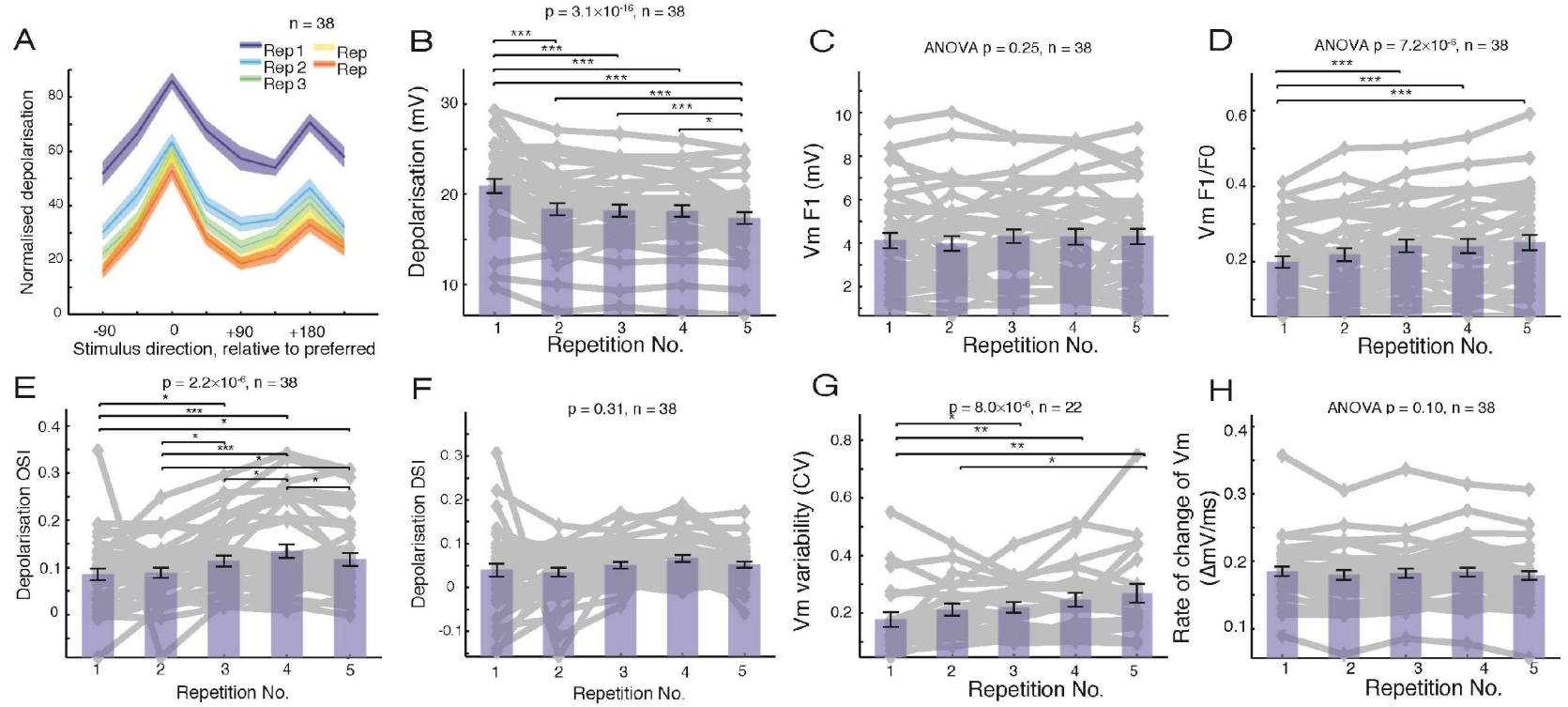

Figure 4.12. Subthreshold response properties over stimulus repetitions.
A.) Normalised depolarisation of the population as a function of stimulus direction, across subsequent repetitions of the continuous condition. B.) Membrane depolarisation (F0) during the preferred stimulus direction across subsequent repetitions. C.) Amplitude of stimulus-locked membrane potential modulations (F1). D.) Membrane potential F1/F0 ratio. E.) Orientation selectivity (OSI) of membrane depolarisation. F.) Direction selectivity (DSI) of membrane depolarisation. G.) Membrane potential variability (coefficient of variation between multiple stimulus blocks). H.) Rate of change of membrane potential. (Error bars: mean ± SEM.)

Subthreshold variability increased significantly after the first stimulus repetition ($p = 8.0 \times 10^{-6}$, Figure 4.12G). The concurrent decrease in membrane depolarisation and increase in subthreshold variability, is likely to be a key determinant of suprathreshold firing rate and gain modulation (see Discussion). There was, however, no consistent evolution of membrane potential dynamics (absolute dV/dT) across stimulus repetitions (Figure 4.12H).

Adaptation during naturalistic stimuli

Finally, we assessed how the adaptation described here during grating stimuli relates to that seen during more naturalistic stimuli (Yao et al., 2007). A total of 13 neurons were recorded during multiple repetitions of both continuously drifting gratings and a movie that mimicked natural viewing in mice (see Methods; Figure 4.13). We compared the overall magnitude and reliability of spiking and subthreshold responses during each stimulus condition, and determined how these response properties evolved across multiple repetitions of the same stimulus sequence.

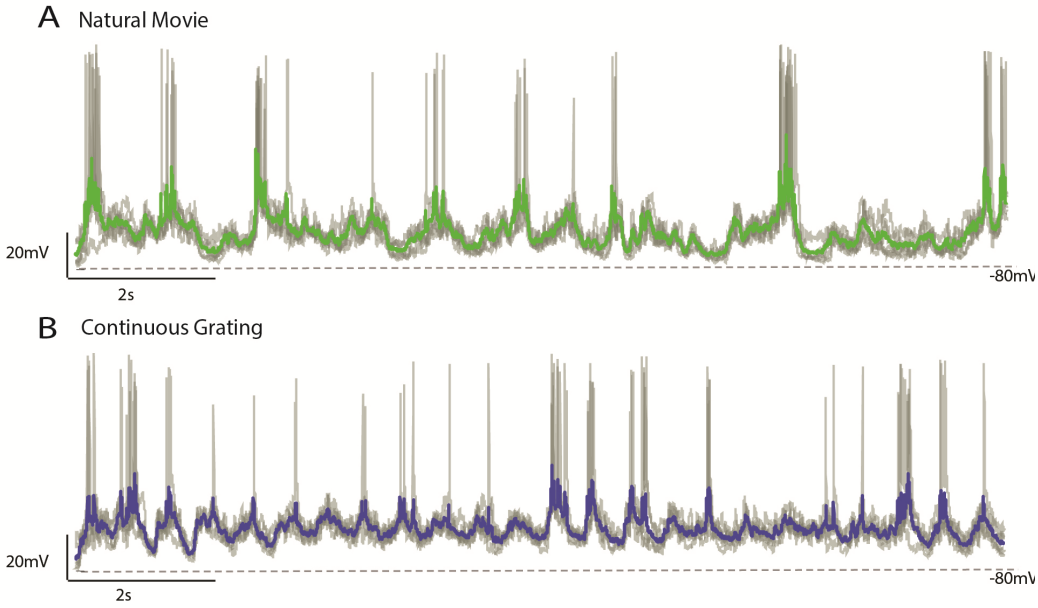

Figure 4.13. Example whole cell recordings during natural movie and continuous grating stimuli.
Current clamp recordings from an example neuron (pre spike removal), during 6 repetitions of the natural movie (A), and continuous grating stimuli (B). Coloured lines indicate mean across repetitions. Baseline membrane potential (-80mV) is indicated by dashed lines.

There was no significant difference in mean firing rate (averaged over all repetitions) elicited by continuous gratings and natural movie stimuli (Figure 4.14A). For these neurons there was also no significant change in firing rate over repetitions of the continuous grating (Figure 4.14B), however firing rate decreased over subsequent repetitions of the natural movie (Figure 4.14C). Likewise, there was no difference in overall spike count variability (Fano factor, measured across stimulus blocks), between conditions (Figure 4.14D) or across repetitions of either stimulus (Figure 4.14E&F).

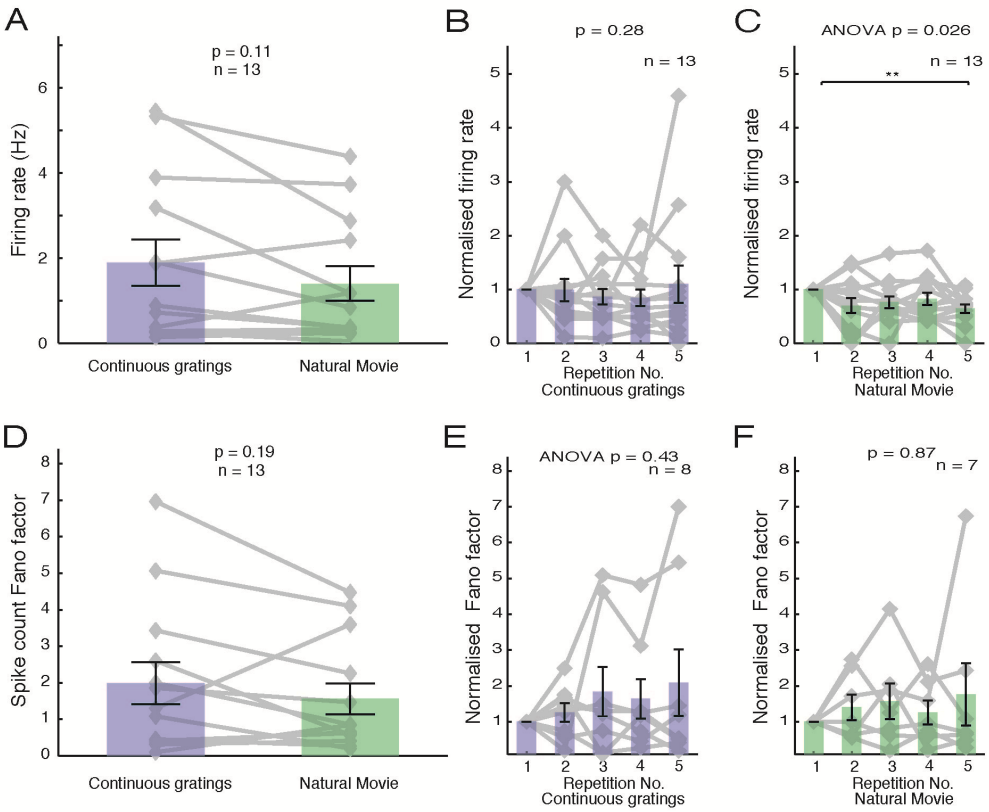

Figure 4.14. Adaptation of spiking responses during continuous gratings and natural movie stimuli.
A.) Firing rate during continuous grating and natural movie stimuli (averaged over all repetitions). B.) Firing rate across subsequent repetitions of continuous gratings. C.) As for B, for natural movie stimuli. D.) Overall spike count variability (Fano factor between stimulus blocks) during continuous grating and natural movie stimuli (averaged over all repetitions). E.) Spike count variability across subsequent repetitions of continuous gratings. F.) As for E, for natural movie stimuli. (Error bars: mean ± SEM).

At a subthreshold level, the mean membrane depolarisation was significantly higher during the continuous grating condition than the natural movie (18.0± 0.88Hz versus

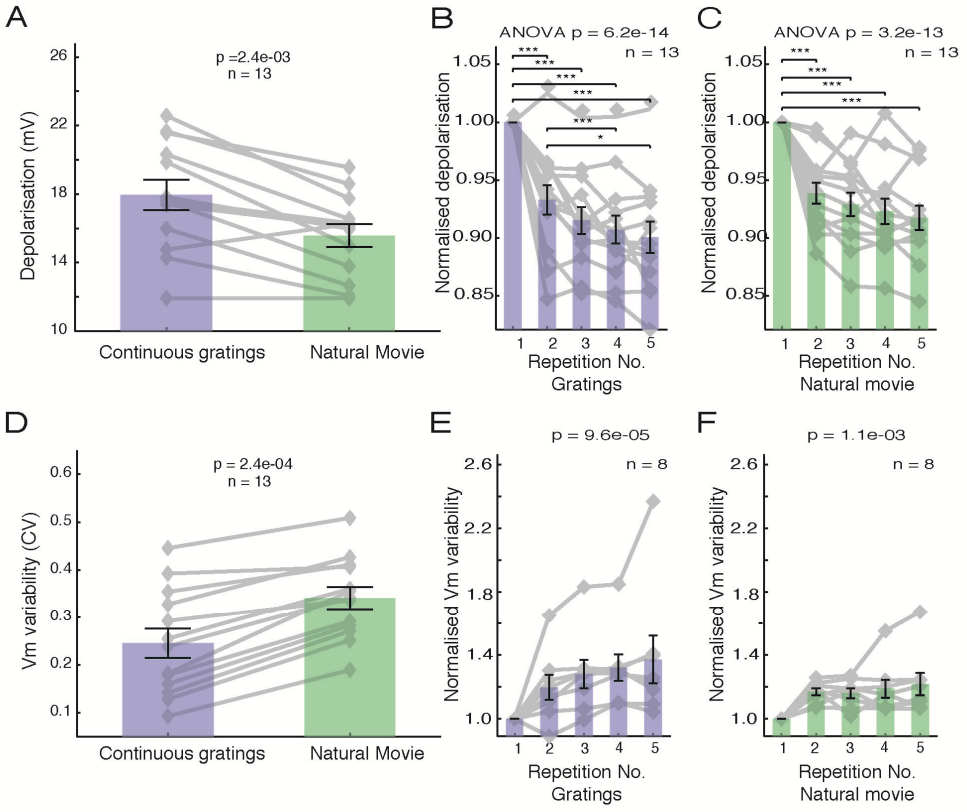

Figure 4.15. Adaptation of subthreshold responses during continuous gratings and natural movie stimuli.
A.) Mean membrane potential depolarisation during continuous grating and natural movie stimuli (averaged over all repetitions). B.) Mean depolarisation across subsequent repetitions of continuous gratings. C.) As for B, for natural movie stimuli. D.) Overall subthreshold variability (CV between stimulus blocks), during continuous grating and natural movie stimuli (averaged over all repetitions). E.) Subthreshold variability across subsequent repetitions of continuous gratings. F.) As for E, for natural movie stimuli. (Error bars: mean ± SEM)

15.6± 0.67Hz, p= 2.4×10-3, Figure 4.15A). During both conditions, the mean depolarisation decreased over subsequent stimulus repetitions (continuous grating p= 6.2×10-14, Figure 4.15B; natural movie p=3.2×10-13, Figure 4.15C). The extent of the reduction was also similar in both cases; for the continuous grating condition the mean depolarisation during the 5th repetition was 90 ± 1.3% of that during the 1st repetition. Similarly, for the natural movies, the mean depolarisation during the 5th repetition was 92 ± 1.1% of that observed during the 1st repetition.

Conversely, subthreshold variability (across trials) was greater during the natural movie than the continuous grating (0.34 ± 0.02 versus 0.25 ± 0.03, p= 2.4×10^{-4}, Figure 4.15D). Subthreshold variability increased over repetitions of both continuous gratings (p= 9.6×10^{-5}, Figure 4.15E) and natural movies (p=1.1×10^{-3}, Figure 4.15F). However, while during the natural movies there was a step increase in variability

after the first repetition and little subsequent change, the increase appeared to occur more gradually during the continuous gratings.

Therefore, at least at a subthreshold level, adaptation during both stimuli appear to involve similar mechanisms, with a steady decrease in mean depolarisation, accompanied by an increase in subthreshold variability. The combination of these effects is likely to cause a divisive scaling of spiking responses (Chance et al., 2002; Mitchell and Silver, 2003; Ayaz and Chance, 2008), as observed during the grating stimuli.

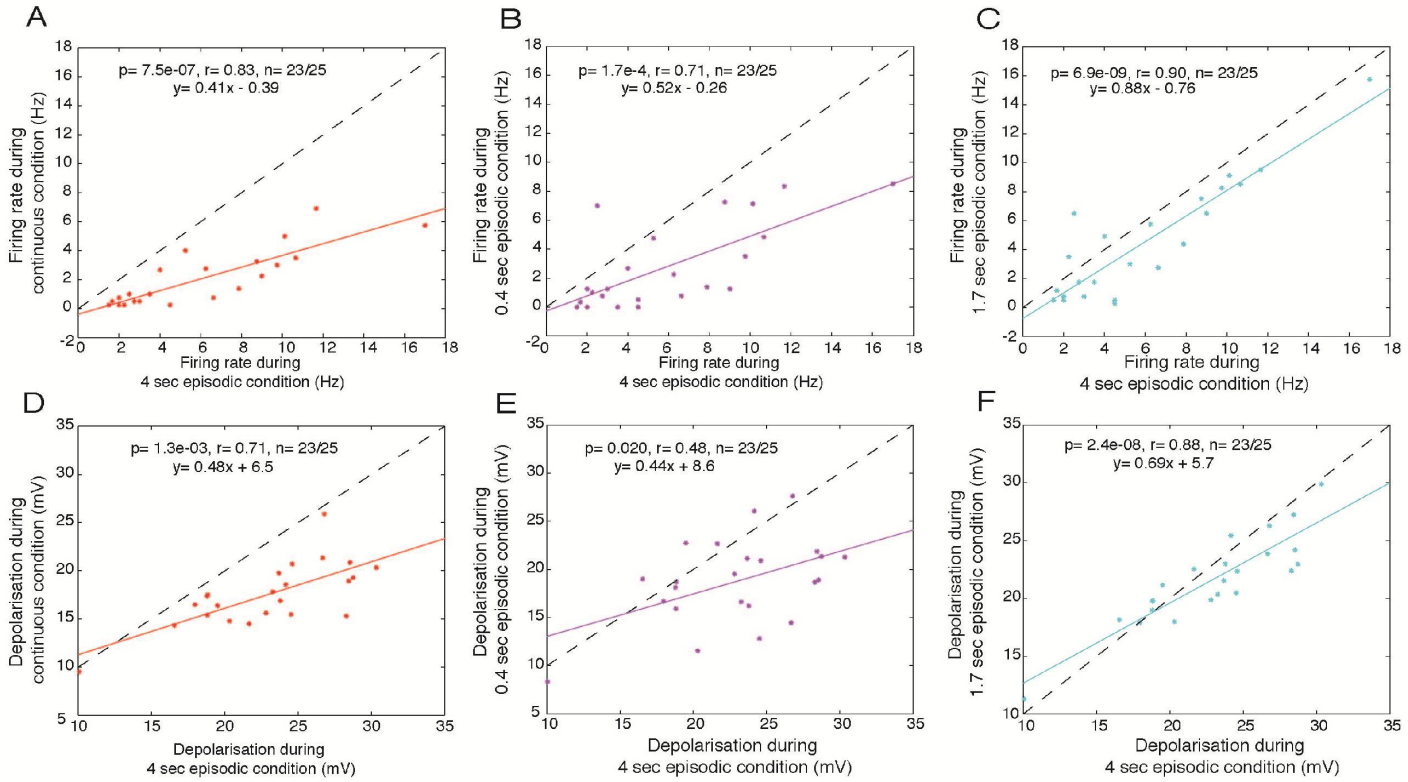

Supplementary Figure 4.1 Population gain modulation of firing rate and membrane potential responses.
A.) Firing rate of individual neurons in response to their preferred stimulus orientation during the continuous condition, plotted as a function of the response during the 4-sec episodic condition. B & C), as for A, for neurons' firing rate responses during the 0.4 sec and 1.5 sec episodic conditions. D.) Membrane depolarisation (relative to baseline) of individual neurons in response to their preferred stimulus orientation during the continuous condition, plotted as a function of the response during the 4-sec episodic condition. E & F), as for D, for neurons' membrane depolarisation during the 0.4 sec and 1.5 sec episodic conditions.

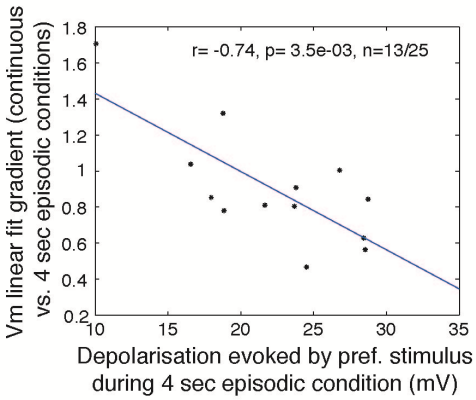

Supplementary Figure 4.2
The gradient of the linear relationship between membrane depolarisation between the continuous and 4 sec episodic conditions, expressed as a function of the membrane depolarisation evoked by the preferred stimulus orientation during the 4 sec episodic condition. Each point corresponds to a single neuron (restricted to those 13 neurons which exhibited a significant linear relationship between the depolarisation evoked during continuous and 4 sec episodic conditions).

DISCUSSION

The aim of this Chapter was to gain further insight into the circuit mechanisms of adaptation by recording both spiking and subthreshold responses in the same cells with patch clamp recordings. The results largely confirm the findings based on suprathreshold data of Chapters 2 & 3.

Main findings:

1. As seen in Chapter 3, adaptation led to a divisive scaling of firing rate responses across stimulus orientations/directions, indicating a reduction in response gain. In contrast, at a subthreshold level, adaptation induced a subtractive reduction in membrane depolarisation, which was similar across all stimuli.

2. As also seen in Chapter 3, adaptation was associated with a decrease in spike train reliability. Consistent with this finding, subthreshold variability was also significantly greater during the continuous (adapted) condition.

3. The majority of spiking and subthreshold response parameters varied systematically with the duration of the stationary screens included in the episodic conditions, supporting the notion that these stimuli provide a 'recovery period' from adaptation.

4. Firing rate and mean membrane depolarisation decreased over subsequent repetitions of the continuous stimuli, whilst subthreshold variability and the orientation specificity of membrane depolarisation increased.

5. A similar progressive decline in membrane depolarisation, and increase in subthreshold variability, was observed across subsequent repetitions of continuous gratings and natural movie stimuli, suggesting similar underlying mechanisms of adaptation in both cases.

Firing rate and subthreshold response gain

The current data indicate that adaptation induces a divisive scaling of firing rate responses. This is in keeping with the reduction in response gain following brief adaptation in Chapter 2 and, furthermore, the scaling factor of approximately 1/3 is in close agreement with that seen in Chapter 3.

Previous studies have shown that adaptation is associated with a hyperpolarisation of V1 neurons, and increase in their membrane conductance (Carandini and Ferster, 1997; Sanchez-Vives et al., 2000a), however it was not clear how these effects might interact with neurons' tuning preferences. Unspecific hyperpolarisation would be expected to equally affect responses to all stimulus directions, producing a subtractive shift in depolarisation tuning curves. However, due to Ohm's Law (V=IR), an increase in membrane conductance should result in a divisive scaling of the membrane potential (Carandini and Heeger, 1994; Borg-Graham et al., 1998), and may introduce nonlinearities through its effects on dendritic integration (Rudolph and Destexhe, 2003; for review see Destexhe et al., 2003). Our data show that adaptation to continuously drifting gratings is primarily associated with a subtractive reduction in membrane depolarisation across all stimulus directions, suggesting that hyperpolarisation may be the dominant influence in this process. However, as a large proportion of the neurons did not display a significant linear correlation across conditions, concurrent changes in membrane conductance may also be introducing nonlinearities.

Conductance changes are also implicated when comparing membrane potential responses across the population of neurons. For each neuron, the membrane depolarisation evoked by its preferred stimulus orientation was compared during the

continuous and the longest episodic stimulus conditions (Supplementary Figure 4.1D-F). These population responses appear to show evidence of divisive scaling, as those neurons which exhibit the greatest depolarisation during the episodic condition are subject to the greatest response reduction during the continuous and intermediate episodic conditions. Intriguingly, these same neurons were also the most likely to display a divisive scaling of subthreshold responses across stimulus orientations. For those neurons which displayed a linear relationship between their membrane depolarisation during the continuous and long episodic conditions, the gradient of this relationship was inversely correlated to the depolarisation exhibited during the episodic condition (Supplementary Figure 4.2).

One possible explanation for these findings is inter-neuronal differences in tonic membrane conductance. Neurons with a lower membrane conductance (and hence greater membrane resistance) during the episodic condition will exhibit a larger depolarisation in response to equivalent input currents. If adaptation causes these neurons to undergo an increase in membrane conductance (as suggested by Sanchez-Vives et al., 2000a;2000b) their responses will be reduced via divisive scaling. However, for those neurons in which membrane conductance is already relatively high during the episodic condition, further gain control may be mediated by alternative mechanisms (e.g. a reduction in synaptic drive), leading to a predominantly subtractive reduction in membrane depolarisation. This hypothesis is consistent with other studies which have found significant conductance increases in only a small proportion of neurons in vivo (Sanchez-Vives et al., 2000a).

Is hyperpolarisation (or reduction of depolarisation) sufficient to explain the divisive scaling of firing rate responses? Computational models suggest that subtractive/additive transformations of input current can indeed give rise to multiplicative scaling of a neuron's firing rate tuning curves (when accounting for nonlinearities between stimulus direction and input current, and between input current and firing rate; Murphy and Miller, 2003). A key requirement for such models is the presence of noisy synaptic conductances, which give rise to an expansive power-law relationship between the average membrane potential and firing rate (see Introduction, Figure 1.6H). Similarly, a significant increase in synaptic variability will steepen the power-law, and could be sufficient to induce a change in firing rate gain on its own (Anderson et al., 2000; Mitchell and Silver, 2003; Ayaz

and Chance, 2008). Our data show that both hyperpolarisation and increased variability are likely to contribute to the firing rate adaptation of V1 neurons.

If hyperpolarisation (or reduced depolarisation) were the dominant result of adaptation, this should cause a small but significant decrease in firing rate tuning width, while with the involvement of subthreshold variability, tuning would be predicted to remain relatively constant (Ayaz and Chance, 2008). With coarse sampling across stimulus directions (45 degree increments) and low firing rates it is not possible to differentiate between these possibilities in the current study. However, further clarification could be gained in future studies by measuring contrast-response functions during the different stimulus conditions. Pure hyperpolarisation should lead to a decrease in contrast gain (increase in C50), whilst the divisive scaling associated with subthreshold noise would reduce response gain (reduction in Rmax). With the combined involvement of both factors, one would expect to see changes in both contrast and response gain.

These measurements could also be used to test the hypothesis outlined above, whereby a neuron's tonic membrane conductance determines its susceptibility to adaptation-induced increases in conductance. If this is the case, one would expect those neurons with a low tonic membrane conductance to undergo larger changes in contrast gain.

Origins of hyperpolarisation

As described above, at a subthreshold level, the primary influence of adaptation in the majority of neurons appears to be subtractive reduction in depolarisation, rather than a change in membrane conductance. This suggests that any hyperpolarisation caused by an increase in membrane conductance is significantly amplified by network interactions (i.e. alterations in the synaptic inputs a neuron receives).

In Chapter 2, inhibitory (PV) neurons appeared to initially undergo less adaptation than pyramidal neurons. This cell-type differences could shift the E/I balance towards inhibition, and could contribute to observed membrane hyperpolarisation. Ideally, the source of hyperpolarisation (increased inhibition/reduced excitation) could be investigated in future experiments by comparing the relative changes in excitatory and inhibitory conductances during continuous and episodic stimulus conditions. Theoretically this could be done using the voltage clamp technique,

however, as discussed in Chapter 2, the accuracy of this method is limited by the filtering properties of dendrites (Williams and Mitchell, 2008). Visually targeted recordings could also be made from genetically labelled inhibitory cell types, in order to identify which interneuron populations are most influential to the adaptation of principal neurons.

Origins of subthreshold variability

In addition to increasing responsiveness to low intensity inputs, subthreshold variability will also translate into firing rate variability (as observed in the reduced spike train reliability). Indeed, subthreshold variability may provide something of a trade-off between response probability and spike timing precision (Schreiber et al., 2008). Such effects are likely to be further amplified by network interactions; subthreshold variability will be influenced by the spiking variability of the neuron's presynaptic partners. But where does this variability originate? Subthreshold variability has also been shown to contribute to contrast invariance of orientation tuning (Anderson et al., 2000; Finn et al., 2007) (see Introduction). This contrast-dependent variability is unaffected by cortical inactivation and can already be observed in LGN neurons (Sadagopan and Ferster, 2012), with suggestions it may be retinal in origin (Berry et al., 1997). Hence the adaptation-induced variability observed in the current data could, at least partially, also be inherited from the early visual system. In order to ascertain the source of subthreshold variability, membrane potential recordings could be made during the continuous condition whilst inactivating cortical activity by inactivating cortical principal neurons with Archaerhodopsin.

The dependence of adaptation of stationary screen duration

The majority of response properties measured not only differed between the continuous and longest episodic conditions but additionally exhibited a systematic dependence on stationary screen duration. This supports the notion that the stationary screens provide recovery from adaptation, reducing its effects. However, the current data do not allow an accurate estimation of the recovery timecourse. As there are significant differences in the responses between the two longest episodic conditions, it is possible that with even longer stationary screens, the responses would be greater still. Therefore the current results may be underestimating the effects of adaptation.

A simple explanation for the influence of the stationary grating duration on response magnitude is that, when the membrane potential has sufficient time to return towards baseline, this will increase the driving force across the membrane for excitatory inputs during the subsequent stimulus. In this case the drifting stimuli should be similarly affected when interspersed with any relatively weak stimulus.

The time dependent recovery between stimuli may also be indicative of recovery from short-term synaptic depression. There are several possible mechanisms of synaptic depression, however, the most widespread is the use-dependent depletion of the readily releasable vesicle pool (RRP), from which most models assume a mono-exponential rate of recovery. If the stationary screens in our stimuli do not provide sufficient time for the RRP to be replenished, this would leave fewer vesicles available for release during the subsequent drifting grating, leading to reduced responses. Significant synaptic depression has been reported in rat V1 slices (Varela et al., 1997), and modelling studies suggest synaptic depression can account for many of the response properties of V1 neurons observed in vivo (Chance et al., 1998). However, it is not clear what degree of synaptic depression is likely to occur during the higher levels of spontaneous activity observed in vivo (Reig et al., 2006). Furthermore, while synaptic depression is specific to previously active synapses, during the current stimulation procedure the orientations of subsequent gratings were separated by 135 degree increments. Therefore, in order to contribute to the current findings, synaptic depression would need to occur in presynaptic neurons with relatively low orientation selectivity.

Alternatively, rather than considering the stationary gratings as recovery periods from adaptation to drifting stimuli, one could argue that the visual system is adapting to the stationary gratings themselves (Saul and Cynader, 1989; Gutnisky and Dragoi, 2008). In this case, the influence of the intermittent stimuli is likely to depend, not only on its duration and the membrane depolarisation it evokes, but also on the variance of its spatial and temporal statistics over time and the similarity between these statistics and those of the test stimuli. It would therefore be interesting to compare how stimuli are represented when embedded amongst other stimuli of differing statistics and which evoke differing degrees of cortical activity.

Adaptation during naturalistic stimuli

Naturalistic stimuli have unique spatial and temporal characteristics, which are very different from the artificial stimuli (e.g. gratings or bars) typically used to probe the visual system of mammals (Simoncelli and Olshausen, 2001). Interestingly, the adaptation during continuously presented drifting gratings and natural movies was similar (both being associated with a decrease in membrane depolarisation and an increase in subthreshold variability), suggesting this may be a common mechanism of adaptation across dynamic stimuli with differing statistics. It would therefore be interesting to assess whether adaptation can be 'transferred' between stimuli (assuming each evokes responses of a similar strength). For example this could be tested by comparing the response to a natural movie when preceded by either 4 repetitions of the continuous grating stimulus or 4 repetitions of the movie. This could also be repeated with stimuli of more/less similar spatiotemporal statistics to those seen in the natural movie.

Future directions

As discussed above, there are several experiments which should be performed in order to further establish the mechanisms, source and consequences of the adaptation observed in our data. These include recording from genetically identified cell types; inactivating the cortex to compare the variability of cortical/subcortical inputs; obtaining contrast response functions to better describe changes in firing rate gain; and interleaving different stimuli to establish the stimulus-specificity of adaptation. Furthermore, in an alternative approach, cortical adaptation could be studied in the absence of sensory input, via light activation of ChR2 expressing principal neurons. Unlike current-injection studies on adaptation, in which only the recorded neuron is affected (Sanchez-Vives et al., 2000a), such widespread activity would also evoke network interactions. Pairing diffuse light stimulation with electrode array recordings would enable one to measure input-output functions at a population level.

CHAPTER 5: GENERAL DISCUSSION

The aim of this thesis was to explore visual adaptation in mouse V1. While numerous studies have investigated contrast adaptation in carnivorans and primates, it has thus far remained relatively unexplored in mice. Due to the availability of genetic tools, the mouse is fast becoming the experimental model of choice, and while many of the response properties of mouse V1 neurons are reportedly comparable to those in other species, it is unclear how the underlying computations are influenced by the lack of the large scale functional organisation (orientation/ocular dominance columns) in this species.

I used a combination of complementary techniques to investigate the effects of adaptation on mouse V1 neurons across multiple levels, including both the input/output of individual neurons and combined population response. Using extracellular tetrode recordings it was possible to directly record the spiking activity of multiple neurons with high temporal precision. With calcium imaging we could simultaneously record the activity of local populations of neurons. Intracellular recordings provided additional insight into the biophysical mechanisms underlying the change in firing rate gain. Furthermore, by utilising the genetic tools available in the mouse it was possible to both delineate the adaptation of PV interneurons and reversibly silence cortical activity in order to assess the relative roles of cortical and subcortical mechanisms of adaptation.

Chapter summaries

Chapter 2

In Chapter 2 we assessed the orientation specificity of adaptation in putative pyramidal neurons. While in the cat V1, adaptation is strongest for test stimuli that have the same orientation as the adapting stimulus, in our data the degree of adaptation was equally strong for test stimuli whose orientation was orthogonal to that of the adapting stimulus. This supports and expands upon a previous study in which the orientation of the test stimulus was held constant while the adapting stimulus was varied (Stroud et al., 2012), and is consistent with response normalisation across the local network (or inherited adaptation of broadly tuned presynaptic neurons).

A key determinant of the degree of adaptation that a neuron experienced appeared to be the firing rate evoked during the adapting stimulus. This is consistent with the fatigue hypothesis, whereby the responsiveness of the recorded neuron is determined by its own activity history and that of its presynaptic inputs (Georgeson and Harris, 1984). However, the relationship between preceding firing rate and subsequent adaptation appeared to vary between individual neurons. Adaptation was also associated with a decrease in neurons' trial to trial reliability and decorrelation of the responses of simultaneously recorded pairs of neurons.

Using optogenetics we were also able to identify PV expressing interneurons and compare their response properties to those of putative pyramidal neurons. The novel finding that PV neurons initially undergo less adaptation than putative pyramidal neurons (hence disrupting the balance of excitation and inhibition) may represent an additional mechanism by which adaptation reduces cortical responsiveness. The same technique was also used to reversibly silence the activity of cortical principal neurons, in order to assess the relative influence of cortical/sub-cortical mechanisms of adaptation. While there are potential caveats to this approach (see Chapter 2 Discussion), these data suggest that adaptation induced changes in contrast and response gain may be mediated independently (see below).

Chapter 3

In Chapter 3 we investigated how the adaptation of individual neurons affected population coding during continuously and episodically drifting grating sequences. This is important because the perceptual effects of adaptation are poorly predicted by the responses of single neurons, making it necessary to consider the combined population response. Consistent with the adaption data from Chapter 2, the magnitude and reliability of responses during the continuous condition were reduced relative to those during the episodic condition. Likewise, the responses of simultaneously recorded pairs of neurons became relatively more decorrelated during the continuous condition. These effects led to an increase in population sparseness (overall, few action potentials), and thus improved metabolic efficiency. However, any potential benefits for information processing may be offset by the reduction in trial-to-trial reliability.

Chapter 4

In Chapter 4 we further explored the mechanisms underlying adaptational effects by performing whole cell recordings in V1 neurons. By comparing effects across stimulus orientations, we were able to assess the influence of adaptation on firing rate/subthreshold stimulus selectivity and gain modulation. Overall these recordings revealed a largely subtractive reduction in membrane depolarisation between episodic and continuous conditions, while firing rate responses were subject to divisive scaling.

However, in the presence of subthreshold variability, a subtractive reduction in membrane potential will translate into a divisive scaling of firing rates (Murphy and Miller, 2003). Interestingly, subthreshold variability was also found to increase during the continuous condition. Indeed, this may be sufficient to cause a scaling of firing rate responses, by increasing the steepness of the power law relationship between mean membrane potential and firing rate (see Chapter 1; Anderson et al., 2000; Mitchell and Silver, 2003; Ayaz and Chance, 2008).

While the predominant effect was a subtractive reduction in membrane depolarisation, some neurons exhibited divisive scaling (consistent with an increase in membrane conductance). This could suggest that the conductance changes a neuron experiences is subject to individual variation, and may be related to its tonic membrane conductance (see Chapter 4 Discussion). An interesting question therefore is whether individual variability in conductance changes is related to the individual variation in the firing rate dependency of adaptation observed in Chapter 2.

Finally, we also compared the adaptation observed during the continuously drifting gratings to that during naturalistic movie stimuli. Despite their dissimilar spatio-temporal statistics, both stimuli evoked similar changes in firing rate and subthreshold responses. This suggests that natural vision may evoke a similar state of adaptation to that seen during continuous gratings.

Locus of adaptation

Numerous studies have described contrast adaptation in V1 neurons, yet the relative contribution of different mechanisms is still not clear. Several lines of

evidence suggest that adaptation is cortically mediated, but some effects may also be inherited from the retina or LGN. To explore this question in mouse V1, we assessed the relative influence of cortical and subcortical mechanisms on contrast adaptation, by suppressing cortical activity during the adapting stimulus (via the optical activation of ChR2 expressed in PV interneurons). This optogenetic manipulation was aimed at disrupting activity-dependent adaptation within the cortex, while leaving any subcortical mechanisms of adaptation largely unaffected. During control conditions (in the absence of cortical silencing), adaptation led to a decrease in both contrast and response gain (evident as a rightward and downward shift in the contrast response function, respectively). Cortical silencing largely counteracted the effect of adaptation on response gain, however, it had little impact on contrast gain. These findings suggest that the effects of adaptation on contrast and response gain are separable. While adaptation of response gain appears to be cortically mediated, the adaptation of contrast gain could be mediated by a different cortical mechanism, over a different time course, or even at an earlier stage of the visual processing hierarchy (retina or LGN).

The notion that response gain is mediated cortically, and independently of contrast gain, is consistent with results from several studies: (1) Intracortical iontophoresis of acetylcholine leads to an increase in response gain, without affecting contrast gain (Soma et al., 2013), although there is some variability across cortical layers (Disney et al., 2012); (2) Manipulation of PV neuron activity (Atallah et al., 2012)/ cortical iontophoresis of $GABA_A$ antagonists in V1 (Katzner et al., 2011) affect response gain but not contrast gain. Conversely, there is evidence to suggest that contrast gain may be mediated subcortically. Although adaptation can be transferred between the eyes, contrast gain control is predominantly monocular in cat V1 (Truchard et al., 2000), suggesting it may be mediated prior to binocular convergence in the cortex.

These findings suggest that subcortical mechanisms may be important for the adaptation-induced change in contrast gain. To examine this possibility, one could perform whole-cell recordings in cortical neurons while suppressing cortical activity (with Archaerhodopsin expressed in principal neurons), and compare the contrast gain of the isolated subcortical inputs to that seen during control conditions (in the absence of cortical suppression).

Mechanisms of adaptation

Excitation-inhibition (E/I) balance

As discussed in Chapter 1, the role of cortical inhibition in contrast adaptation has been largely discounted due to multiple studies that found adaptation was unaffected by the administration of the $GABA_A$ antagonist bicuculline (DeBruyn and Bonds, 1986; Vidyasagar, 1990; Nelson, 1991; McLean and Palmer, 1996). However, as bicuculline has substantial side effects (Debarbieux et al., 1998), these results are difficult to interpret. Furthermore, by blocking normal inhibition, such pharmacological interventions are associated with abnormally high levels of excitation, which may lead to unknown compensatory effects in the cortical network.

In Chapter 2, putative PV interneurons were found to undergo less early adaptation (within 2 seconds) than putative pyramidal neurons. These cell type specific differences could contribute to the later stages of adaptation observed in pyramidal neurons. Differential adaptation of inhibitory and excitatory neurons will shift the E-I balance towards inhibition, contributing to the observed decrease in principal cell responsiveness. Dense reciprocal connections between excitatory and inhibitory neurons will cause interneuron activity to decline in concert with principal cell activity, consistent with the observation that latter stages of adaptation followed a similar trajectory in both cell types. In support of this hypothesis, manipulations that increase PV neuron activity have be found to decrease response gain (Atallah et al., 2012; Wilson et al., 2012), as also seen in our data. Correspondingly, cortical iontophoresis of gabazine (a selective GABAA antagonist), has been found to reduce response gain (Katzner et al., 2011). Furthermore, a similar disruption of E-I balance has also been suggested to underlie surround suppression in cat V1 (Ozeki et al., 2009).

This differential adaptation of excitation and inhibition could result from either cell-type specific synaptic depression, or differences in intrinsic cell properties (Cardin et al., 2007). The latter option is supported by the finding that fast-spiking neurons also undergo less firing rate adaptation than regular spiking neurons during current pulse injection (Nowak et al., 2003).

To confirm and extend our findings, targeted patch-clamp recordings could be made from different subtypes of inhibitory cells (e.g. those expressing PV, somatostatin,

or VIP) in transgenic mice in which these neurons are fluorescently labelled, allowing a comparison of adaptation in visually, electrophysiologically, and genetically-defined cell types. This would reveal whether any cell-type specific differences in adaptation arise from the intrinsic properties of these neurons or the synaptic inputs that they receive. While pharmacological interventions may be associated with compensatory effects, the role of inhibition in visual adaptation could be further investigated by comparing animals in which inhibitory function is impaired (Hua et al., 2009), or while the inhibitory network is still maturing after eye-opening.

Cell intrinsic adaptation and network effects

High contrast visual stimulation has been shown to induce cell-intrinsic adaptation in active neurons (Sanchez-Vives et al., 2000). Due to the rich interconnectivity in cortical networks, such effects will also be propagated to the postsynaptic targets of adapted neurons (Kohn, 2007). Indeed, our data emphasise the role of network interactions in contrast adaptation: (1) adaptation following short duration stimuli is not orientation specific; (2) adaptation during a stimulus sequence comprised of multiple orientations leads to a strong reduction in responsiveness across all stimuli (these findings are both consistent with a normalisation of responses between neurons with different orientation preferences); (3) at a subthreshold level, the predominant effect of adaptation appears to be a subtractive reduction in membrane depolarisation without clear evidence of a change in membrane conductance of the recorded neuron (i.e. the dominant effect of adaptation appears to be a change in synaptic inputs that the neuron receives). Therefore, network interactions appear to play a prominent role in cortical adaptation. However, it remains unclear how these network effects contribute to the stimulus-specific adaptation observed in cat V1, where the responses to over-represented stimuli are selectively reduced (Benucci et al., 2013). One possibility is that the repeated presentation of a stimulus will invoke relatively greater intrinsic adaptation in those neurons selective for that stimulus.

Subthreshold variability

A key finding in this thesis is the adaptation-induced increase in subthreshold variability. By increasing the likelihood that a weaker average membrane depolarization will reach spike threshold, subthreshold noise may significantly increase the sensitivity of a cell to weak inputs, contributing to the observed change in firing rate gain. Contrast-dependent subthreshold variability is thought to underlie

the contrast invariance of orientation tuning in cat V1 (Anderson et al., 2000; Finn et al., 2007), and studies have suggested this variability is present in the LGN, and may even be retinal in origin (Berry et al., 1997; Sadagopan and Ferster, 2012). This therefore raises the intriguing possibility that the adaptation-induced increase in subthreshold variability could also be inherited from the early visual system. This hypothesis could be tested by carrying out whole-cell recordings during cortical silencing (via optical inactivation of cortical principal neurons expressing Archaerhodopsin). These experiments could be supplemented by directly measuring adaptation in populations of mouse LGN neurons, to determine the consequences of visual adaptation on their covariance and trial-to-trial variability.

Consequences of adaptation

Population coding

Data from two-photon calcium imaging (Chapter 3) indicate that the adaptation-induced reduction in neuronal responsiveness is associated with both an increase in population sparseness (fewer neurons are active per time bin) and decorrelation of neuronal firing. By reducing the number of energetically expensive action potentials (Laughlin et al., 1998; Attwell and Laughlin, 2001; Lennie, 2003), such sparse coding increases metabolic efficiency. Therefore, one of the main benefits of visual adaptation is a reduction in energy expenditure.

Sparse coding may also confer additional advantages for information transmission and explicit stimulus representations (Olshausen and Field, 2004). Specifically, sparsification and decorrelation of neuronal responses will reduce the redundancy with which V1 populations represent sensory input. However, these benefits are likely to be limited by the adaptation-induced decrease in response reliability, which limits information capacity (Grewe et al., 2007). In the adapted state, subthreshold variability maintains sensitivity to weak inputs by increasing spike probability, but this also reduces response reliability, generating a more probabilistic code. As a result, a larger population of neurons is required to reach the same level of discriminatory performance when using simple models to ‘decode’ sensory stimuli (Figure 3.8A). The increased number of neurons required to discriminate sensory stimuli, however, is likely accommodated by the ‘over-complete representation’ within V1, whereby the number of neurons used to represent the image is much

greater than the dimensionality of the input (i.e. number of pixels; Olshausen and Field, 1997).

Similar adaptation during natural and artificial stimuli

Natural stimuli have unique spatial and temporal properties, which differ greatly from artificial stimuli such as gratings (Simoncelli and Olshausen, 2001). Natural stimuli are believed to be encoded sparsely in cortical populations (Olshausen and Field, 1996; Vinje and Gallant, 2000; Hromádka et al., 2008). In Chapter 4 we found that naturalistic stimuli, which mimic the mouse's natural visual environment, evoked similar adaptation (at a subthreshold level) to that seen during continuously presented grating stimuli. This suggests that the mechanisms of adaptation may be similar across stimuli with differing spatiotemporal statistics. Previous studies in cat and monkey V1 have reported reliable and precise spiking responses during natural stimuli (Vinje and Gallant, 2000; Haider et al., 2010). While this level of temporal precision was not evident in our data from mouse V1, these differences may reflect differences in cortical organisation between species; species with functional columns may receive more numerous and coincident input from their neighbours which share the same receptive properties, and thus might fire more reliably to stimulus features than neurons in rodent V1, where neighbours prefer diverse stimulus features (Ohki et al., 2005).

Conclusions

The data in this thesis demonstrate that adaptation in mouse V1 has significant effects on stimulus representation, at both a single neuron and population level. Therefore, identical grating stimuli presented either continuously or intermittently drifting induce different fundamentally different activity regimes within V1, each of which is able to achieve high decoding performance, albeit via different coding strategies.

Which of these stimulation regimes is more relevant for understanding coding under natural viewing conditions, in which stimuli are constantly viewed, but include relatively abrupt changes in local and global contrast (Simoncelli and Olshausen, 2001)? In our data, subthreshold responses to natural movie stimuli were subject to similar adaptation to that seen during continuously drifting gratings, suggesting that during natural viewing, the mouse visual system may also be in an 'adapted' state.

However, historically, the majority of studies of visual function have utilised episodic stimulation protocols, in which test stimuli are interleaved with grey/blank screens. In future I would recommend an increased use of longer duration/continuously presented stimuli (such as those used in Chapter 3 and 4), in order to gain a better understanding of visual processing during adapted conditions, which may provide a closer approximation to natural vision.

Nonetheless, it remains to be seen to what extent contrast adaptation is observed in awake, behaving animals. In future studies, calcium imaging in head-fixed animals could be combined with a virtual reality environment, in order to simultaneously compare the effects of adaptation on population coding and perceptual performance.

As discussed above, the current results support the notion that adaptation is at least partially mediated at processing stages prior to V1. However, the contribution of each level of the visual system hierarchy remain to be elucidated, and may even be stimulus dependent (Baccus, 2004). Without a better understanding of the location and mechanisms of adaptation, its usefulness as a tool for investigating other cortical functions will be limited.

These results also emphasize the nonlinear properties (such as adaptation) of subcortical visual processing, which are often disregarded when modeling cortical function. However, several computational functions traditionally ascribed to V1 may also be evident, at least in part, at earlier stages of the visual system (Camp et al., 2009; Preibe et al.,2006; Scholl et al.,2013; Desbordes et al, 2008). Therefore, in order to determine cortical computations that underlie V1 response properties, it is essential to fully characterise the nature of the inputs this region receives.

REFERENCES

Abdi H (2010) Holm's sequential Bonferroni procedure. In: Encyclopedia of research design, N Salkind (Ed). Sage Publications.

Akasaki T, Sato H, Yoshimura Y, Ozeki H, Shimegi S (2002) Suppressive effects of receptive field surround on neuronal activity in the cat primary visual cortex. Neurosci Res 43:207–220.

Albrecht DG (1995) Visual cortex neurons in monkey and cat: effect of contrast on the spatial and temporal phase transfer functions. Visual Neurosci 12:1191–1210.

Albrecht DG, Farrar SB, Hamilton DB (1984) Spatial contrast adaptation characteristics of neurones recorded in the cat's visual cortex. J Physiol (Lond) 347:713–739.

Anderson JS, Lampl I, Gillespie DC, Ferster D (2000) The contribution of noise to contrast invariance of orientation tuning in cat visual cortex. Science 290:1968–1972.

Atallah BV, Bruns W, Carandini M, Scanziani M (2012) Parvalbumin-expressing interneurons linearly transform cortical responses to visual stimuli. Neuron 73:159–170.

Attwell D, Laughlin SB (2001) An energy budget for signaling in the grey matter of the brain. J Cereb Blood Flow Metab 21:1133–1145.

Ayaz A, Chance FS (2008) Gain modulation of neuronal responses by subtractive and divisive mechanisms of inhibition. J Neurophysiol 101:958–968.

Ayaz A, Saleem AB, Schölvinck ML, Carandini M (2013) Locomotion controls spatial integration in mouse visual cortex. Curr Biol 23:890–894.

Azouz R, Gray CM (2003) Adaptive coincidence detection and dynamic gain control in visual cortical neurons in vivo. Neuron 37:513–523.

Baccus SA, Meister M (2004) Retina versus cortex: contrast adaptation in parallel visual pathways. Neuron 42:5–7.

Bardy C, Huang J, Wang C, FitzGibbon T, Dreher B (2006) ‘Simplification’of responses of complex cells in cat striate cortex: suppressive surrounds and ‘feedback’inactivation. J Physiol (Lond) 574:731.

Barlow H, Foldiak P (1989) Adaptation and decorrelation in the cortex. Addison-Wesley Longman Publishing Co., Inc.

Barlow HB (1990) A theory about the functional role and synaptic mechanism of visual after-effects. In: Vision: coding and efficiency, C B Blakemore (Ed). Cambridge University Press.

Barlow HB, Hill RM (1963) Selective sensitivity to direction of movement in ganglion cells of the rabbit retina. Science 139:412–414.

Benucci A, Saleem AB, Carandini M (2013) Adaptation maintains population homeostasis in primary visual cortex. Nat Neurosci 16:724–729.

Berry MJ, Warland DK, Meister M (1997) The structure and precision of retinal spike trains. Proc Natl Acad Sci USA 94:5411–5416.

Bishop PO, Kozak W, Levick WR, Vakkur GJ (1962) The determination of the projection of the visual field on to the lateral geniculate nucleus in the cat. J Physiol (Lond) 163:503–539.

Blakemore C, Campbell FW (1969) On the existence of neurones in the human visual system selectively sensitive to the orientation and size of retinal images. J Physiol (Lond) 203:237–260.

Blakemore C, Muncey JP, Ridley RM (1973) Stimulus specificity in the human visual system. Vision Res 13:1915–1931.

Bonds AB (1991) Temporal dynamics of contrast gain in single cells of the cat striate cortex. Visual Neurosci 6:239–255.

Borg-Graham LJ, Monier C, Frégnac Y (1998) Visual input evokes transient and strong shunting inhibition in visual cortical neurons. Nature 393:369–373.

Boudreau C, Ferster D (2005) Short-term depression in thalamocortical synapses of cat primary visual cortex. J Neurosci 25:7179–7190.

Boyden ES, Zhang F, Bamberg E, Nagel G, Deisseroth K (2005) Millisecond-timescale, genetically targeted optical control of neural activity. Nat Neurosci 8:1263–1268.

Boynton GM, Finney EM (2003) Orientation-specific adaptation in human visual cortex. J Neurosci 23:8781–8787.

Brainard DH (1997) The Psychophysics Toolbox. Spatial Vision 10:433–436.

Burkhalter A (1989) Intrinsic connections of rat primary visual cortex: laminar organization of axonal projections. J Comp Neurol 279:171–186.

Busse L, Wade AR, Carandini M (2009) Representation of concurrent stimuli by population activity in visual cortex. Neuron 64:931–942.

Calderone JB, Jacobs GH (1995) Regional variations in the relative sensitivity to UV light in the mouse retina. Visual Neurosci 12:463–468.

Camp AJ, Tailby C, Solomon SG (2009) Adaptable mechanisms that regulate the contrast response of neurons in the primate lateral geniculate nucleus. J Neurosci 29:5009–5021.

Carandini M, Ferster D (1997) A tonic hyperpolarization underlying contrast adaptation in cat visual cortex. Science 276:949–952.

Carandini M, Ferster D (2000) Membrane potential and firing rate in cat primary visual cortex. J Neurosci 20:470–484.

Carandini M, Heeger DJ (1994) Summation and division by neurons in primate visual cortex. Science 264:1333–1335.

Carandini M, Heeger DJ (2012) Normalization as a canonical neural computation. Nature Rev Neurosci 13:51–62.

Cardin JA (2012) Dissecting local circuits in vivo: Integrated optogenetic and electrophysiology approaches for exploring inhibitory regulation of cortical activity. J Physiol Paris 106:104–111.

Cardin JA, Palmer LA, Contreras D (2007) Stimulus feature selectivity in excitatory and inhibitory neurons in primary visual cortex. J Neurosci 27:10333–10344.

Chance FS, Abbott LF, Reyes AD (2002) Gain modulation from background synaptic input. Neuron 35:773–782.

Chance FS, Nelson SB, Abbott LF (1998) Synaptic depression and the temporal response characteristics of V1 cells. J Neurosci 18:4785–4799.

Chapman B, Bonhoeffer T (1998) Overrepresentation of horizontal and vertical orientation preferences in developing ferret area 17. Proc Natl Acad Sci USA 95:2609–2614.

Chelaru MI, Dragoi V (2007) Asymmetric synaptic depression in cortical networks. Cerebral Cortex 18:771–788.

Cheng H, Chino YM, Smith EL, Hamamoto J, Yoshida K (1995) Transfer characteristics of lateral geniculate nucleus X neurons in the cat: effects of spatial frequency and contrast. J Neurophysiol 74:2548–2557.

Choi JH, Jung HK, Kim T (2006) A new action potential detector using the MTEO and its effects on spike sorting systems at low signal-to-noise ratios. IEEE Trans Biomed Eng 53:738–746.

Chow BY, Han X, Dobry AS, Qian X, Chuong AS, Li M, Henninger MA, Belfort GM, Lin Y, Monahan PE, Boyden ES (2010) High-performance genetically targetable optical neural silencing by light-driven proton pumps. Nature 463:98–102.

Chung S, Ferster D (1998) Strength and orientation tuning of the thalamic input to simple cells revealed by electrically evoked cortical suppression. Neuron 20:1177–1189.

Chung S, Li X, Nelson SB (2002) Short-term depression at thalamocortical synapses contributes to rapid adaptation of cortical sensory responses in vivo. Neuron 34:437–446.

Clifford CWG (2002) Perceptual adaptation: motion parallels orientation. Trends Cogn Sci 6:136–143.

Contreras D, Palmer L (2003) Response to contrast of electrophysiologically defined cell classes in primary visual cortex. J Neurosci 23:6936–6945.

Crowder NA (2005) Relationship between contrast adaptation and orientation tuning in V1 and V2 of cat visual cortex. J Neurophysiol 95:271–283.

Dan Y, Atick JJ, Reid RC (1996) Efficient coding of natural scenes in the lateral geniculate nucleus: experimental test of a computational theory. J Neurosci 16:3351–3362.

De Valois RL, Yund EW, Hepler N (1982) The orientation and direction selectivity of cells in macaque visual cortex. Vision Res 22:531–544.

Dean AF, Tolhurst DJ (1986) Factors influencing the temporal phase of response to bar and grating stimuli for simple cells in the cat striate cortex. Exp Brain Res 62:143–151.

Debarbieux F, Brunton J, Charpak S (1998) Effect of bicuculline on thalamic activity: a direct blockade of IAHP in reticularis neurons. J Neurophysiol 79:2911–2918.

DeBruyn EJ, Bonds AB (1986) Contrast adaptation in cat visual cortex is not mediated by GABA. Brain Res 383:339–342.

Desbordes G, Jin J, Weng C, Lesica NA, Stanley GB, Alonso J-M (2008) Timing Precision in Population Coding of Natural Scenes in the Early Visual System. PLoS Biology 6:e324.

Destexhe A, Rudolph M, Paré D (2003) The high-conductance state of neocortical neurons in vivo. Nature Rev Neurosci 4:739–751.

Disney AA, Aoki C, Hawken MJ (2012) Cholinergic suppression of visual responses in primate V1 is mediated by GABAergic inhibition. J Neurophysiol 108:1907–1923.

Dragoi V, Rivadulla C, Sur M (2001) Foci of orientation plasticity in visual cortex. Nature 411:80–86.

Dragoi V, Sharma J, Miller EK, Sur M (2002) Dynamics of neuronal sensitivity in visual cortex and local feature discrimination. Nat Neurosci 5:883–891.

Dragoi V, Sharma J, Sur M (2000) Adaptation-induced plasticity of orientation tuning in adult visual cortex. Neuron 28:287–298.

Felsen G, Touryan J, Han F, Dan Y (2005) Cortical sensitivity to visual features in natural scenes. PLoS Biology 3:e342.

Fenno L, Yizhar O, Deisseroth K (2011) The development and application of optogenetics. Annu Rev Neurosci 34:389–412.

Ferster D, Chung S, Wheat H (1996) Orientation selectivity of thalamic input to simple cells of cat visual cortex. Nature 380:249–252.

Field GD, Chichilnisky EJ (2007) Information processing in the primate retina: circuitry and coding. Annu Rev Neurosci 30:1–30.

Finn IM, Priebe NJ, Ferster D (2007) The emergence of contrast-invariant orientation tuning in simple cells of cat visual cortex. Neuron 54:137–152.

Finn IM, Priebe NJ, Ferster D (2007) The emergence of contrast-invariant orientation tuning in simple cells of cat visual cortex. Neuron 54:137–152.

Freeman T, Durand S, Kiper D, Carandini M (2002) Suppression without inhibition in visual cortex. Neuron 35:759–771.

Frisby JP, Stone JV (2010) Seeing, Second Edition: The Computational Approach to Biological Vision. The MIT Press.

Georgeson MA, Harris MG (1984) Spatial selectivity of contrast adaptation: Models and data. Vision Res 24:729–741.

Gonchar Y, Wang Q, Burkhalter A (2007) Multiple distinct subtypes of GABAergic neurons in mouse visual cortex identified by triple immunostaining. Front Neuroanat 1:3.

Gradinaru V, Zhang F, Ramakrishnan C, Mattis J, Prakash R, Diester I, Goshen I, Thompson KR, Deisseroth K (2010) Molecular and cellular approaches for diversifying and extending optogenetics. Cell 141:154–165.

Graham N (2001) Visual Pattern Analyzers. Oxford University Press.

Gray CM, Maldonado PE, Wilson M, McNaughton B (1995) Tetrodes markedly improve the reliability and yield of multiple single-unit isolation from multi-unit recordings in cat striate cortex. J Neurosci Methods 63:43–54.

Grewe J, Weckstrom M, Egelhaaf M, Warzecha A-K (2007) Information and discriminability as measures of reliability of sensory coding. PLoS ONE 2:e1328.

Grubb MS, Thompson ID (2003) Quantitative characterization of visual response properties in the mouse dorsal lateral geniculate nucleus. J Neurophysiol 90:3594–3607.

Guillery RW, Sherman SM (2002) Thalamic relay functions and their role in corticocortical communication: generalizations from the visual system. Neuron 33:163–175.

Gutnisky DA, Dragoi V (2008) Adaptive coding of visual information in neural populations. Nature 452:220–224.

Haider B, Krause MR, Duque A, Yu Y, Touryan J, Mazer JA, McCormick DA (2010) Synaptic and network mechanisms of sparse and reliable visual cortical activity during nonclassical receptive field stimulation. Neuron 65:107–121.

Hammond P, Pomfrett C, Ahmed B (1989) Neural motion after-effects in the cat's striate cortex: orientation selectivity. Vision Res 29:1671–1683.

Harris KD, Henze DA, Csicsvari J, Hirase H, Buzsaki G (2000) Accuracy of tetrode spike separation as determined by simultaneous intracellular and extracellular measurements. J Neurophysiol 84:401–414.

Heeger DJ (1992) Normalization of cell responses in cat striate cortex. Visual Neurosci 9:181–197.

Heiss JE, Katz Y, Ganmor E, Lampl I (2008) Shift in the balance between excitation and inhibition during sensory adaptation of S1 neurons. J Neurosci 28:13320–13330.

Hofer SB, Ko H, Pichler B, Vogelstein J, Ros H, Zeng H, Lein E, Lesica NA, Mrsic-Flogel TD (2011) Differential connectivity and response dynamics of excitatory and inhibitory neurons in visual cortex. Nat Neurosci 14:1045–1052.

Hofer SB, Mrsic-Flogel TD, Horvath D, Grothe B, Lesica NA (2010) Optimization of population decoding with distance metrics. Neural Netw 23:728–732.

Hromádka T, DeWeese MR, Zador AM (2008) Sparse representation of sounds in the unanesthetized auditory cortex. PLoS Biology 6:e16.

Hua T, Li G, Tang C, Wang Z, Chang S (2009) Enhanced adaptation of visual cortical cells to visual stimulation in aged cats. Neuroscience Letters 451:25–28.

Hubel DH, Wiesel TN (1962) Receptive fields, binocular interaction and functional architecture in the cat's visual cortex. J Physiol (Lond) 160:106–154.

Hubel DH, Wiesel TN (1969) Anatomical demonstration of columns in the monkey striate cortex. Nature 221:747–750.

Huberman AD, Niell CM (2011) What can mice tell us about how vision works? Trends Neurosci 34:464–473.

Huberman AD, Wei W, Elstrott J, Stafford BK, Feller MB, Barres BA (2009) Genetic identification of an On-Off direction-selective retinal ganglion cell subtype reveals a layer-specific subcortical map of posterior motion. Neuron 62:327–334.

Ibbotson MR (2005) Contrast and temporal frequency-related adaptation in the pretectal nucleus of the optic tract. J Neurophysiol 94:136–146.

Jeon CJ, Strettoi E, Masland RH (1998) The major cell populations of the mouse retina. J Neurosci 18:8936–8946.

Jeyabalaratnam J, Bharmauria V, Bachatene L, Cattan S, Angers A, Molotchnikoff S (2013) Adaptation shifts preferred orientation of tuning curve in the mouse visual cortex. PLoS ONE 8:e64294.

Kaplan E, Shapley R (1984) The origin of the S (slow) potential in the mammalian lateral geniculate nucleus. Exp Brain Res 55:111–116.

Kaplan E, Shapley RM (1982) X and Y cells in the lateral geniculate nucleus of macaque monkeys. J Physiol (Lond) 330:125–143.

Katzner S, Busse L, Carandini M (2011) GABAA inhibition controls response gain in visual cortex. J Neurosci 31:5931–5941.

Kawaguchi Y, Kubota Y (1993) Correlation of physiological subgroupings of nonpyramidal cells with parvalbumin- and calbindinD28k-immunoreactive neurons in layer V of rat frontal cortex. J Neurophysiol 70:387–396.

Kerlin AM, Andermann ML, Berezovskii VK, Reid RC (2010) Broadly tuned response properties of diverse inhibitory neuron subtypes in mouse visual cortex. Neuron 67:858–871.

Ko H, Hofer SB, Pichler B, Buchanan KA, Sjöström PJ, Mrsic-Flogel TD (2011) Functional specificity of local synaptic connections in neocortical networks. Nature 473:87–91.

Kohn A (2007) Visual adaptation: physiology, mechanisms, and functional benefits. J Neurophysiol 97:3155–3164.

Kohn A, Movshon JA (2003) Neuronal adaptation to visual motion in area MT of the macaque. Neuron 39:681–691.

la Rocha de J, Doiron B, Shea-Brown E, Josić K, Reyes A (2007) Correlation between neural spike trains increases with firing rate. Nature 448:802–806.

Laughlin SB (2001) Energy as a constraint on the coding and processing of sensory information. Curr Opin Neurobiol 11:475–480.

Laughlin SB, de Ruyter Van Steveninck RR, Anderson JC (1998) The metabolic cost of neural information. Nat Neurosci 1:36–41.

Lennie P (2003) The cost of cortical computation. Curr Biol 13:493–497.

Levy M, Fournier J, Frégnac Y (2013) The role of delayed suppression in slow and fast contrast adaptation in V1 simple cells. J Neurosci 33:6388–6400.

Levy WB, Baxter RA (1996) Energy efficient neural codes. Neural Comput 8:531–543.

Li B, Peterson MR, Freeman RD (2003) Oblique effect: a neural basis in the visual cortex. J Neurophysiol 90:204–217.

Lien AD, Scanziani M (2012) Processing of visual stimuli by recurrent circuits in layer 4 of mouse visual cortex. Society for Neuroscience Abstract:569.04–BB5.

Lima SQ, Hromádka T, Znamenskiy P, Zador AM (2009) PINP: A new method of tagging neuronal populations for identification during in vivo electrophysiological recording. PLoS ONE 4:e6099.

Ma W-P, Liu B-H, Li Y-T, Huang ZJ, Zhang LI, Tao HW (2010) Visual representations by cortical somatostatin inhibitory neurons-selective but with weak and delayed responses. J Neurosci 30:14371–14379.

Maffei L, Fiorentini A, Bisti S (1973) Neural correlate of perceptual adaptation to gratings. Science 182:1036–1038.

Mangini NJ, Pearlman AL (1980) Laminar distribution of receptive field properties in the primary visual cortex of the mouse. J Comp Neurol 193:203–222.

Manookin MB, Demb JB (2006) Presynaptic mechanism for slow contrast adaptation in mammalian retinal ganglion cells. Neuron 50:453–464.

Margrie T, Brecht M, Sakmann B (2002) In vivo, low-resistance, whole-cell recordings from neurons in the anaesthetized and awake mammalian brain. Pflugers Arch 444:491–498.

Mariño J, Schummers J, Lyon DC, Schwabe L, Beck O, Wiesing P, Obermayer K, Sur M (2005) Invariant computations in local cortical networks with balanced excitation and inhibition. Nat Neurosci 8:194–201.

Markram H, Toledo-Rodriguez M, Wang Y, Gupta A, Silberberg G, Wu C (2004) Interneurons of the neocortical inhibitory system. Nature Rev Neurosci 5:793–807.

McLean J, Palmer LA (1996) Contrast adaptation and excitatory amino acid receptors in cat striate cortex. Visual Neurosci 13:1069.

McNaughton BL, O'Keefe J, Barnes CA (1983) The stereotrode: a new technique for simultaneous isolation of several single units in the central nervous system from multiple unit records. J Neurosci Methods 8:391–397.

Meister M, Berry MJ (1999) The neural code of the retina. Neuron 22:435–450.

Métin C, Godement P, Imbert M (1988) The primary visual cortex in the mouse: receptive field properties and functional organization. Exp Brain Res 69:594–612.

Mitchell SJ, Silver RA (2003) Shunting inhibition modulates neuronal gain during synaptic excitation. Neuron 38:433–445.

Movshon JA, Lennie P (1979) Pattern-selective adaptation in visual cortical neurones. Nature 278:850–852.

Mrsic-Flogel TD, Hofer SB, Ohki K, Reid RC, Bonhoeffer T, Hübener M (2007) Homeostatic regulation of eye-specific responses in visual cortex during ocular dominance plasticity. Neuron 54:961–972.

Muller JR, Metha AB, Krauskopf J, Lennie P (1999) Rapid adaptation in visual cortex to the structure of images. Science 285:1405–1408.

Müller JR, Metha AB, Krauskopf J, Lennie P (2003) Local signals from beyond the receptive fields of striate cortical neurons. J Neurophysiol 90:822–831.

Murphy BK, Miller KD (2003) Multiplicative gain changes are induced by excitation or inhibition alone. J Neurosci 23:10040–10051.

Murphy BK, Miller KD (2009) Balanced amplification: a new mechanism of selective amplification of neural activity patterns. Neuron 61:635–648.

Nagel G, Szellas T, Huhn W, Kateriya S, Adeishvili N, Berthold P, Ollig D, Hegemann P, Bamberg E (2003) Channelrhodopsin-2, a directly light-gated cation-selective membrane channel. Proc Natl Acad Sci USA 100:13940–13945.

Nelson SB (1991) Temporal interactions in the cat visual system. III. Pharmacological studies of cortical suppression suggest a presynaptic mechanism. J Neurosci 11:369–380.

Niell CM, Stryker MP (2008) Highly selective receptive fields in mouse visual cortex. J Neurosci 28:7520–7536.

Niell CM, Stryker MP (2010) Modulation of visual responses by behavioral state in mouse visual cortex. Neuron 65:472–479.

Nimmerjahn A, Kirchhoff F, Kerr JND, Helmchen F (2004) Sulforhodamine 101 as a specific marker of astroglia in the neocortex in vivo. Nature Methods 1:31–37.

Nowak LG (2005) Role of synaptic and intrinsic membrane properties in short-term receptive field dynamics in cat area 17. J Neurosci 25:1866–1880.

Nowak LG, Azouz R, Sanchez-Vives MV, Gray CM, McCormick DA (2003) Electrophysiological classes of cat primary visual cortical neurons in vivo as revealed by quantitative analyses. J Neurophysiol 89:1541–1566.

Nowak LG, Azouz R, Sanchez-Vives MV, Gray CM, McCormick DA (2003) Electrophysiological classes of cat primary visual cortical neurons in vivo as revealed by quantitative analyses. J Neurophysiol 89:1541–1566.

O'Connor DH, Huber D, Svoboda K (2009) Reverse engineering the mouse brain. Nature 461:923–929.

Ohki K, Chung S, Ch'ng YH, Kara P, Reid RC (2005) Functional imaging with cellular resolution reveals precise micro-architecture in visual cortex. Nature 433:597–603.

Ohki K, Chung S, Ch'ng YH, Kara P, Reid RC (2005) Functional imaging with cellular resolution reveals precise micro-architecture in visual cortex. Nature 433:597–603.

Ohki K, Chung S, Kara P, Hübener M, Bonhoeffer T, Reid RC (2006) Highly ordered arrangement of single neurons in orientation pinwheels. Nature 442:925–928.

Ohzawa I, Sclar G, Freeman RD (1982) Contrast gain control in the cat visual cortex. Nature 298:266–268.

Ohzawa I, Sclar G, Freeman RD (1985) Contrast gain control in the cat's visual system. J Neurophysiol 54:651–667.

Olivas ND, Quintanar-Zilinskas V, Nenadic Z, Xu X (2012) Laminar circuit organization and response modulation in mouse visual cortex. Front Neural Circuits 6:70.

Olsen SR, Bortone DS, Adesnik H, Scanziani M (2012) Gain control by layer six in cortical circuits of vision. Nature 0:1–8.

Olshausen BA, Field DJ (1996) Natural image statistics and efficient coding. Network 7:333–339.

Olshausen BA, Field DJ (1997) Sparse coding with an overcomplete basis set: a strategy employed by V1? Vision Res 37:3311–3325.

Olshausen BA, Field DJ (2004) Sparse coding of sensory inputs. Curr Opin Neurobiol 14:481–487.

Ozeki H, Finn IM, Schaffer ES, Miller KD, Ferster D (2009) Inhibitory stabilization of the cortical network underlies visual surround suppression. Neuron 62:578–592.

Pelli DG (1997) The VideoToolbox software for visual psychophysics: transforming numbers into movies. Spatial Vision 10:437–442.

Piscopo DM, El-Danaf RN, Huberman AD, Niell CM (2013) Diverse visual features encoded in mouse lateral geniculate nucleus. J Neurosci 33:4642–4656.

Priebe N, Ferster D (2012) Mechanisms of neuronal computation in mammalian visual cortex. Neuron 75:194–208.

Priebe NJ, Lampl I, Ferster D (2010) Mechanisms of direction selectivity in cat primary visual cortex as revealed by visual adaptation. J Neurophysiol 104:2615–2623.

Priebe NJ, Mechler F, Carandini M, Ferster D (2004) The contribution of spike threshold to the dichotomy of cortical simple and complex cells. Nat Neurosci 7:1113–1122.

Reich DS, Mechler F, Victor JD (2001) Temporal coding of contrast in primary visual cortex: when, what, and why. J Neurophysiol 85:1039–1050.

Reig R, Gallego R, Nowak LG, Sanchez-Vives MV (2006) Impact of cortical network activity on short-term synaptic depression. Cereb Cortex 16:688–695.

Rockhill RL, Daly FJ, MacNeil MA, Brown SP, Masland RH (2002) The diversity of ganglion cells in a mammalian retina. J Neurosci 22:3831–3843.

Rothman DL, Sibson NR, Hyder F, Shen J, Behar KL, Shulman RG (1999) In vivo nuclear magnetic resonance spectroscopy studies of the relationship between the glutamate-glutamine neurotransmitter cycle and functional neuroenergetics. Philos Trans R Soc Lond, B, Biol Sci 354:1165–1177.

Rudolph M, Destexhe A (2003) A fast-conducting, stochastic integrative mode for neocortical neurons in vivo. J Neurosci 23:2466–2476.

Sadagopan S, Ferster D (2012) Feedforward origins of response variability underlying contrast invariant orientation tuning in cat visual cortex. Neuron 74:911–923.

Sanchez-Vives MV, Nowak LG, McCormick DA (2000) Membrane mechanisms underlying contrast adaptation in cat area 17 in vivo. J Neurosci 20:4267–4285.

Sanchez-Vives MV, Nowak LG, McCormick DA (2000b) Cellular mechanisms of long-lasting adaptation in visual cortical neurons in vitro. J Neurosci 20:4286–4299.

Saul AB, Cynader MS (1989) Adaptation in single units in visual cortex: The tuning of aftereffects in the spatial domain. Visual Neurosci 2:593.

Schmitzer-Torbert N, Jackson J, Henze D, Harris K, Redish AD (2005) Quantitative measures of cluster quality for use in extracellular recordings. Neuroscience 131:1–11.

Scholl B, Tan AYY, Corey J, Priebe NJ (2013) Emergence of Orientation Selectivity in the Mammalian Visual Pathway. J Neurosci 33:10616–10624.

Schreiber S, Samengo I, Herz AVM (2008) Two Distinct Mechanisms Shape the Reliability of Neural Responses. J Neurophysiol 101:2239–2251.

Schuett S, Bonhoeffer T, Hübener M (2002) Mapping retinotopic structure in mouse visual cortex with optical imaging. J Neurosci 22:6549–6559.

Schummers J, Mariño J, Sur M (2002) Synaptic integration by V1 neurons depends on location within the orientation map. Neuron 36:969–978.

Schüz A, Palm G (1989) Density of neurons and synapses in the cerebral cortex of the mouse. J Comp Neurol 286:442–455.

Sclar G, Lennie P, DePriest DD (1989) Contrast adaptation in striate cortex of macaque. Vision Res 29:747–755.

Sekuler R, Pantle A (1967) A model for after-effects of seen movement. Vision Res 7:427–439.

Sengpiel F, Bonhoeffer T (2002) Orientation specificity of contrast adaptation in visual cortical pinwheel centres and iso-orientation domains. Eur J Neurosci 15:876–886.

Shapley R, Hugh Perry V (1986) Cat and monkey retinal ganglion cells and their visual functional roles. Trends Neurosci 9:229–235.

Shou T, Li X, Zhou Y, Hu B (1996) Adaptation of visually evoked responses of relay cells in the dorsal lateral geniculate nucleus of the cat following prolonged exposure to drifting gratings. Visual Neurosci 13:605–613.

Sibson NR, Dhankhar A, Mason GF, Rothman DL, Behar KL, Shulman RG (1998) Stoichiometric coupling of brain glucose metabolism and glutamatergic neuronal activity. Proc Natl Acad Sci USA 95:316–321.

Simoncelli EP, Olshausen BA (2001) Natural image statistics and neural representation. Annu Rev Neurosci 24:1193–1216.

Skottun B, De Valois R, Grosof D, Movshon J, Albrecht D, Bonds A (1991) Classifying simple and complex cells on the basis of response modulation. Vision Res 31:1078–1086.

Sohya K, Kameyama K, Yanagawa Y, Obata K, Tsumoto T (2007) GABAergic neurons are less selective to stimulus orientation than excitatory neurons in layer II/III of visual cortex, as revealed by in vivo functional Ca2+ imaging in transgenic mice. J Neurosci 27:2145–2149.

Solomon SG, Lee BB, Sun H (2006) Suppressive surrounds and contrast gain in magnocellular-pathway retinal ganglion cells of macaque. J Neurosci 26:8715–8726.

Solomon SG, Peirce JW, Dhruv NT, Lennie P (2004) Profound contrast adaptation early in the visual pathway. Neuron 42:155–162.

Soma S, Shimegi S, Suematsu N, Sato H (2013) Cholinergic modulation of response gain in the rat primary visual cortex. Sci Rep 3:1138.

Spruston N, Johnston D (2008) Out of control in the dendrites. Nat Neurosci 11:733–734.

Stanisor L, van der Togt C, Pennartz CMA, Roelfsema PR (2013) A unified selection signal for attention and reward in primary visual cortex. Proc Natl Acad Sci USA 110:9136–9141.

Stosiek C, Garaschuk O, Holthoff K, Konnerth A (2003) In vivo two-photon calcium imaging of neuronal networks. Proc Natl Acad Sci USA 100:7319–7324.

Stroud AC, LeDue EE, Crowder NA (2012) Orientation specificity of contrast adaptation in mouse primary visual cortex. J Neurophysiol 108:1381–1391.

Swift DJ, Smith RA (1982) An action spectrum for spatial-frequency adaptation. Vision Res 22:235–246.

Tan AYY, Brown BD, Scholl B, Mohanty D, Priebe NJ (2011) Orientation selectivity of synaptic input to neurons in mouse and cat primary visual cortex. J Neurosci 31:12339–12350.

Teich AF, Qian N (2003) Learning and adaptation in a recurrent model of V1 orientation selectivity. J Neurophysiol 89:2086–2100.

Truchard AM, Ohzawa I, Freeman RD (2000) Contrast gain control in the visual cortex: monocular versus binocular mechanisms. J Neurosci 20:3017–3032.

Ullman S, Schechtman G (1982) Adaptation and Gain Normalization. Proceedings of the Royal Society B: Biological Sciences 216:299–313.

Van Hooser SD, Heimel JAF, Chung S, Nelson SB, Toth LJ (2005) Orientation selectivity without orientation maps in visual cortex of a highly visual mammal. J Neurosci 25:19–28.

Varela JA, Sen K, Gibson J, Fost J, Abbott LF, Nelson SB (1997) A quantitative description of short-term plasticity at excitatory synapses in layer 2/3 of rat primary visual cortex. J Neurosci 17:7926–7940.

Vautin RG, Berkley MA (1977) Responses of single cells in cat visual cortex to prolonged stimulus movement: neural correlates of visual aftereffects. J Neurophysiol 40:1051–1065.

Vidyasagar TR (1990) Pattern adaptation in cat visual cortex is a co-operative phenomenon. Neuroscience 36:175–179.

Vinje WE, Gallant JL (2000) Sparse coding and decorrelation in primary visual cortex during natural vision. Science 287:1273–1276.

Vogelstein JT, Packer AM, Machado TA, Sippy T, Babadi B, Yuste R, Paninski L (2010) Fast nonnegative deconvolution for spike train inference from population calcium imaging. J Neurophysiol 104:3691–3704.

Völgyi B, Chheda S, Bloomfield SA (2009) Tracer coupling patterns of the ganglion cell subtypes in the mouse retina. J Comp Neurol 512:664–687.

Wang X-J, Liu Y, Sanchez-Vives MV, McCormick DA (2003) Adaptation and temporal decorrelation by single neurons in the primary visual cortex. J Neurophysiol 89:3279–3293.

Wang Y, Celebrini S, Trotter Y, Barone P (2008) Visuo-auditory interactions in the primary visual cortex of the behaving monkey: Electrophysiological evidence. BMC Neurosci 9:79.

Wässle H (2004) Parallel processing in the mammalian retina. Nature Rev Neurosci 5:747–757.

Wiesel TN, Hubel DH (1966) Spatial and chromatic interactions in the lateral geniculate body of the rhesus monkey. J Neurophysiol 29:1115–1156.

Williams SR, Mitchell SJ (2008) Direct measurement of somatic voltage clamp errors in central neurons. Nat Neurosci 11:790–798.

Wilson NR, Runyan CA, Wang FL, Sur M (2012) Division and subtraction by distinct cortical inhibitory networks in vivo. Nature 488:343–348.

Winston JS (2004) fMRI-Adaptation reveals dissociable neural representations of identity and expression in face perception. J Neurophysiol 92:1830–1839.

Yao H, Shi L, Han F, Gao H, Dan Y (2007) Rapid learning in cortical coding of visual scenes. Nat Neurosci 10:772–778.

Zaghloul KA, Boahen K, Demb JB (2005) Contrast adaptation in subthreshold and spiking responses of mammalian Y-type retinal ganglion cells. J Neurosci 25:860–868.